2006

Electrodeposition of CoCu Nanostructures

Yutong Li
Louisiana State University and Agricultural and Mechanical College, yli6@lsu.edu

ELECTRODEPOSITION OF CoCu NANOSTRUCTURES

A Dissertation

Submitted to the Graduate Faculty of the
Louisiana State University and
Agricultural and Mechanical College
in partial fulfillment of the
requirements for the degree of
Doctor of Philosophy

in

The Department of Chemical Engineering

by
Yutong Li
B.S., Hebei Univeristy of Science and Technology, 1996
M.S., Beijing University of Chemical and Technology, 1999
M.S., Louisiana State University, 2004
August 2006

To my loving parents,

AKNOWLEGEMENTS

I sincerely thank my graduate advisor Dr. E. J. Podlaha for her insightful guidance, great patience and continuous inspiration, which made this study possible.

I thank Professor Dr. Armando B. Corripio, Ralph W. Pike, James J. Spivey for accepting my invitation to be on my graduate committee.

My sincere thanks also go to Dr. David. P. Young and Dr. M. Moldovan in LSU Physics Department for magnetoresistance measurements, Ruili Fan, Wen Dai and Dr. W. Wang in LSU Mechanical Engineering Department for UV lithography, Dr. X. Xie in LSU Geology Department for WDS analysis and SEM micrographs, Mrs. M. Henk in LSU Biological Sciences Department for TEM, Mr. Ling at CAMD for his help in the x-ray exposures.

I would also like to acknowledge my colleagues in the Electrochemical Engineering lab, Dr. Q. Huang, Mrs. Despina Davis, Mr. Rohit Mishra, Mr. M. Guan and all the coworkes for the helpful discussions.

This work was financially supported by National Science Foundation.

TABLE OF CONTENTS

LIST OF TABLES

LIST OF FIGURES

ABSTRACT

Electrodeposition is a key component in the microelectronic industry because it has the following advantages: low cost, easy operation and the capability to deposit into irregular geometries such as recessed and curved areas. In this dissertation, CoCu alloys were investigated to fabricate multilayers, microdevices and microposts. All of these multilayer structures were composed of nanometric copper and cobalt-rich layers in order to obtain magnetoresistance, a phenomenon where the resistance of multilayer structures decreases with increases of external magnetic field.

An investigation was carried out in order to evaluate appropriate plating conditions during multilayered thin film deposition, with the aim to obtain higher magnetoresistance at lower magnetic field. The effects of layer size, pH, bilayer number, seed layer and nickel component on the magnetoresistance of multilayered thin films were experimentally explored. A magnetoresistance of 5 % was obtained with the saturation field of less than 3000 Oe on the multilayered thin films by a conventional pulse method. An alternative electrodeposition process, which is referred to as pulse train in this dissertation, was first applied to study its effect on magnetoresistance of multilayered thin films. A pulse train control deposition of the cobalt layer during the fabrication of CoCu/Cu multilayers can improve magnetoresistance over the conventional square-wave pulse. A maximum 7-8 % magnetoresistance was obtained.

The conditions that resulted in the best GMR in thin films were employed to fabricate a multilayered microdevice by combining UV lithography and electrodeposition. The geometric effects of the microdevices on their magnetoresistance

were investigated in detail. The pulse train control method was also employed to improve the magnetoresistance of the microdevices.

High aspect ratio CoCu/Cu multilayered microstructures were also electrodeposited. A single sulfate electrolyte with sodium citrate was employed to successfully fabricate 500 μm tall microposts prepared by x-ray lithography. A giant magnetoresistance of 4 % was demonstrated in a single 500 μm tall micropost. It is the first demonstration of GMR in a micropost exceeding a 10 μm. A detailed investigation of the effects of the layer thickness, plating potentials, nickel component and the pulse train method on the magnetoresistance of microposts was performed.

CHAPTER 1. INTRODUCTION

Giant magnetoresistance multilayers (GMR) are comprised of alternating nanometric layers of ferromagnetic materials (i.e. Fe, Co, Ni) and nonferromagnetic materials (i.e. Cu, Au, Cr). Magnetoresistance is characterized by a decrease in resistance with an increase of the applied external magnetic field. Giant magnetoresistance usually refers to a large value, greater than 1 %, in a field of the order of 10000 Oe. In a zero applied magnetic field, an antiferromagnetic exchange coupling across the nonferromagnetic layer results in the magnetization vectors of the ferromagnetic layer arranging antiparallel to each other. In this situation spin-dependent electron scattering makes the resistivity high. In an external magnetic field strong enough for saturation, all magnetizations are parallel. This reduces the spin-dependent scattering and therefore the resistivity becomes small.

Vapor phase fabrication methods (i.e. sputtering, molecular beam epitaxy) have been the method of choice to fabricate multilayers with high GMR values greater than 65 %.[1] However, these methods have severe limitations when depositing on irregularly shaped substrates and deep recesses. In these geometries electrodeposition finds a niche because this method can readily deposit into recessed and irregularly shaped geometries due to the inherent nature of the electrolyte, filling voids around the electrode.

Multilayers can be electrodeposited from a single electrolyte, containing an excess concentration of the less noble reactant species. In the model system examined here, CoCu, Co is less noble than Cu. The current or potential is pulsed between a high and low value to generate the layers. At a low current density or more positive potential, the noble element (Cu) is deposited as an unalloyed layer, but its deposition current is

limited by the low ion concentration. While at high current density or more negative potential, the less noble elements are deposited as an alloyed layer. The nature of the deposit is influenced by many factors such as electrolyte component composition, concentration, pH, agitation, current density or potential difference between cathode and anode.[2,3]

Although it is possible to plate GMR multilayers by the electrodeposition method, the values do not compete with the highest ones reported for physical vapor techniques, but are nonetheless high enough for commercial applications. Based on present products, the applications for GMR sensors include positioning of pneumatic cylinders, robotics, speed and position identification of bearings, transmission gear speed sensing, vehicle detection for traffic, position sensing for shock abs control, and read heads. Since many of these applications are integrated as microdevices, electrodeposition may be the fabrication method of choice, not only because of its low cost but also because its ability to provide the possibility to plate multilayer thin film into micropatterned features. The first significant GMR in electrodeposited superlattices was reported by the Bristol group in 1993 when Alper *et al*.[4] obtained over 15 % GMR in a fields of up to 8000 Oe at room temperature in multilayers consisting of alternating layers of Cu and a ferromagnetic CoNiCu alloy. Although Bird *et al.*[5] found 55 % GMR in their electrodeposited Co/Cu system, it has not been possible to reproduce it, and most researchers since that time have obtained GMR less than 30 %. The lack of comparable GMR values has been associated with non-discrete layering, rough interface, growth inhomogeneity, and lack of crystallinity.[6-8] A key problem in electrodeposition is the dissolution of the less noble element by the more noble metal because of an inherent exchange reaction.[9,10]

Microdevices requiring high-aspect ratio structures can be fabricated by the Lithography, Galvanoformung, Abformung (LIGA) technology, German words for lithography, electroforming, and molding.[11] Different alloys and metal composites can be employed to adapt materials to a desired property for micro-electro-mechanical systems (MEMS) applications. Ehrfeld *et al.*[12] have summarized some metal-based materials in use or under development for the electrodeposition of LIGA products: Ni, Cu, and Ni-Co alloys have been used for mold inserts, Au for X-ray absorbers, Ni, Ni-Co, and Ni-P for micromechanics, Fe, and Ni-Fe for sensors and actuators, Cu, and Zn for sacrificial layers, Ag, Au, Cu and Zn for functional coatings, and Au, and Cu for electrical contacts. In our lab, NiW and NiW-γ-Al_2O_3[13], NiCu and NiCu-γ-Al_2O_3 alloys[14] have been successfully deposited into 500-μm deep recesses and the composition distribution of the micropost studied systematically. In this dissertation, CuCo alloys and multilayers are developed to introduce giant magnetoresistance (GMR) materials as MEMS components.

The primary challenges when plating into deep recesses is the control of the composition and the avoidance or minimization of the side reaction. For example, the concentration of hydroxyl ions (OH^-), a product of oxygen and water reduction, can accumulate at the electrode surface, resulting in a steep increase of local pH at the electrode surface, which may alter the metal reaction rates and subsequent deposit concentration. In addition, proton reduction further contributes to the pH rise. The worse case scenario is that if the increase in pH rises high enough to form insoluble species in the recess, the electrode surface becomes blocked and prevents further growth of the deposit. Hydrogen evolution also gives rise to a loss of current efficiency, lack of deposit uniformity and increased surface roughness. Pulse plating is one method to overcome this

problem that has been used with alloy deposition.[3,4] A long relaxation time follows a short plating time to allow hydroxyl ions and hydrogen to diffuse out and avoid the rise of local pH. However, during the relaxation time exchange reactions can occur, disrupting the composition. Adapting such a method to developed multilayer deposits into deep recesses has yet to be demonstrated and is one goal of the work here.

In this dissertation, CoCu/Cu multilayers are deposited as thin films with galvanostatic pulses. The magnetoresistance (MR) was characterized and a multilayered microdevice was fabricated by combining UV lithography and electrodeposition. A single citrate electrolyte was developed to electrodeposit micropost of CoCu/Cu multilayerers into 500-μm deep recesses in a pattern of 183×183 μm squares from sulfate-citrate electrolyte. To date, there are no examples of CoCu alloys, even unlayered, electrodeposited into deep recesses, outside of the work presented here.

In summary, Chapter 2 presents a brief literature review of GMR multilayer thin films. Regular pulse electrodeposition of multilayered thin films is presented in Chapter 3. The effects of pulse train deposition on magnetoresistance of thin films were investigated in Chapter 4. Microfabrication of a Co/Cu multilayered microdevice are presented in Chapter 5. In Chapter 6, electrodeposition of 500-μm tall Co/Cu multilayer micropost and their magnetoresistance behavior are discussed. A summary of the results is finally presented in Chapter 7. The unlayered CoCu thin film and deep recess alloy deposition are presented in Appendix A and Appendix B, respecitively.

1.1 References

1. S. S. P. Parkin, R. Bhadra and K. P. Roche, *Physical Review Letters*, **66**, 2152 (1991).

2. C. A. Ross, *Annual Review of Materials Science*, **24**,159 (1994).

3. Gyana R. Pattanaik, Dinesh K. Pandya, and Subhash C. Kashyap, *Journal of the Electrochemical Society*, **149** (7), C363 (2002).

4. M. Alper, K. Attenborough, R. Hart, S. J. Lane, D. S. Lashmore, C. Younes and W. Schwarzacher, *Applied Physical Letters*, **63**, 2144 (1993).

5. K. D. Bird and M. Schlesinger, *Journal of the Electrochemical Society*, **42**, L65 (1995).

6. Y. Ueda, N. Hataya, H. Zaman, *Journal of Magnetism and Magnetic Materials*, **156**, 350 (1996).

7. E. Chassaing, A. Morrone, and J. E. Schmidt, *Journal of the Electrochemical Society*, **146**, 1795 (1999).

8. S. K. J. Lenczowski, C. Schönenberger, M. A. M. Gijs, W. J. M. de Jonge, *Journal of Magnetism and Magnetic Materials*, **148**, 466 (1995).

9. L. Péter, A. Cziráki, L. Pogány, Z. Kupay, I. Bakonyi, M. Uhlemann, M. Herrich, B. Arnold, T. Bauer, and K. Wetzig, *Journal of the Electrochemical Society*, **148** (3), C168 (2001).

10. P. Nallet, E. Chassaing, M. G. Walls, and M. J. Hytch, *Journal of Applied Physics*, **79**, 6884 (1996).

11. E. W. Becker, W. Ehrfeld, P. Hagmann, A. Maner, D. Munchmeyer, *Microelectronic Engineering,* **4**,35 (1986).

12. W. Ehrfeld, M. Abraham, M. Lacher, H. Lehr, *Proceedings of Micro Electro Mechanical Systems, IEEE, Japan*, **86**, 404 (1994).

13. L. Namburi, Master Thesis, " Electrodepositon of NiW Alloys into Deep Recess," Louisiana State University (1999).

14. A. Panda, PhD Thesis, "*Electrodeposition of Nichel-Copper Alloys and Nickel-Copper-Alumina Nanocomposites into Deep Recess for MEMS"*, Louisiana State University, (2003).

CHAPTER 2. LITERATURE REVIEW

Giant magnetoresistance was first discovered in 1988 in Fe/Cr systems by Baibich *et al*.[1] Almost at the same time Binasch *et al.*[2] studied the exchange coupling of Fe/Cr/Fe sandwich films grown epitaxially on (110) GaAs and found that magnetoresistance was higher in the antiparallel state of iron magnetization than in the parallel state. This new form of MR is different from anisotropic magnetoresistance, AMR (a resistivity change that occurs in polycrystalline ferromagnets), which is dependent on the average angle between the current density flowing in each crystal and the magnetization. In contrast, GMR is the resistance change when the magnetic alignment of adjacent ferromagnetic layers separated by a non-magnetic spacer is smaller than a certain critical length. If current is flowing in-plane (CIP) to the multilayers then the critical length is the electron mean free path (a few nanometers), and if the current is flowing perpendicular to the plane (CPP) the critical length is the larger spin diffusion length (several tens of nanometers). Parkin *et al*.[3,4] examined GMR, in a sputtered polycrystalline Co/Cu system. It was found that saturation magnetoresistance is more than 65 % at 295 K, five times larger than the GMR in Fe/Cr system at the same temperature. Another great contribution of Parkin *et al*. is that they discovered that GMR oscillated when the thickness of the nonmagnetic layer was varied. These oscillations resulted from the change of exchange coupling with the thickness of the nonmagnetic layer.

Vacuum processes such as sputtering, and molecular beam epitaxy (MBE), is the common methods for GMR thin film fabrication.[5] There are a variety of systems that have been demonstrated for multilayer deposition, including different combinations of magnetic materials: Co, Ni, Fe, and nonmagnetic materials: Cu, Au, Ag and Cr.[6]

Electrodeposition is an alternative non-vacuum process with the advantage of requiring simple equipment, high deposition rate, operation at room temperature and pressure, and the ability to deposit into irregular geometries. In this research a similar Co/Cu multilayer system is examined as a model system because of the inherently large GMR obtained with physical vapor deposited methods.[3] It is most advantageous to electrodeposit each layer from a single electrolyte. The trade-off, however, is that the Co layer can never be completely pure elemental Co, but will contain a small amount of Cu. Thus, the model system adapted here is best represented as multilayers of a Co-rich alloy and Cu: CoCu/Cu.

2.1 Fundamentals of Electrodeposition

Electrodeposition refers to the electrochemical reduction of metal ions at a cathode surface from an electrolyte when current passes through a circuit composed of a conductive electrolyte, cathode and anode, as shown in Figure 2.1. The reaction can be represented as

$$M^{n+} + ne^{-} \Rightarrow M \tag{2.1}$$

where M^{n+} and M denote metal ions and metals, respectively, and n represents the number of electron transferred. For both Cu^{+2} and Co^{+2} ions n=2. In a driven cell, shown in Figure 2.1, cations migrate toward the cathode, anions toward the anode. Current is defined as the flow of positive charges and moves in a direction opposite to the electrons in the external circuit.

The thickness of deposited metals can be calculated by Faraday's law, which is shown in Equation 2.2,

$$thickness = \frac{itAM\varepsilon}{A\rho Fn} \tag{2.2}$$

where the thickness of metal deposited on substrate depends on the current density passed, i, the plating time, t, substrate area, A, molecular weight of metal, M, current efficiency, ε, density of the metal, ρ, and Faraday's constant, F (96485 Coulomb/eq).

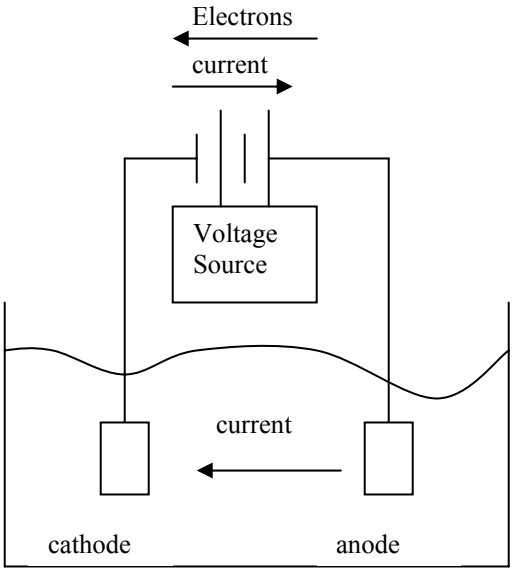

Figure 2-1 Cell Schematic

There are two methods to plate multilayers, from a dual-bath or single-bath. In dual-bath electrodeposition the substrate is transferred between two different electrolytes and a layer is deposited during each immersion while controlling the applied voltage or current. This method requires that the film is not exposed to the atmosphere to minimize corrosion at each sublayer interface. Single-bath electrodeposition uses one electrolyte to plate different materials by modulating current or potential. In either case, the reduction potentials for each reaction depend on the ion concentration and can be calculated by the Nernst equation

$$E_{rev} = E^0 + \frac{RT}{nF} \ln \frac{\prod_i a_{ox,i}^{s_{ox,i}}}{\prod_i a_{red,i}^{s_{red,i}}} \qquad 2.3$$

where E^0 is the standard equilibrium potential, R is a constant (8.314 J/mol.K), T, is the electrolyte temperature (K), $a_{ox,i}$ represents the activities of oxidized species i, a_{rev} are the activities of the reduced species, and s is the stoichiometry of the chemical reaction. The reversible potential is specific to each reaction. In the system employed here, Cu has a larger reversible potential than Co therefore, it is more noble than Co, and Cu is preferentially deposited if at comparable bulk concentrations than Co. The disparity in nobility can be problematic in obtaining a cobalt-rich alloy. To decrease the content of Cu in a Co alloy, a mass transport limit of Cu is created by lowering its bulk concentration relative to Co. Figure 2.2, shows the kinetic and mass transport control of Cu in a Co-Cu system. At point A the reduction of Cu is controlled by kinetics. But when the applied potential becomes more negative, the reaction rate is controlled by the Cu ion transport (pt B) and the copper reduction current now is called the limiting current. In order to deposit a pure copper layer, the applied current must remain below the copper limiting current. When the current is bigger than the copper limiting current, or the working electrode potential is larger than the cobalt equilibrium potential, the less noble cobalt begins to be deposited at C. But at the same time copper is also deposited in the cobalt layer as an impurity. The resulting magnetic layer is not pure cobalt, but a cobalt and copper alloy. However, because the copper concentration is very low in the electrolyte, copper reduction is under transport control, and thus the copper content in the alloy is very small.

The electrodeposition method can be classified as galvanostatic, constant current, and potentiostatic, constant potential. The advantage of galvanostatic control is that the layer thickness can be kept constant by controlling the total charge passed through the

substrate; the disadvantage is that during deposition the potential applied to the substrate varies so that the multilayer interface may not be sharp. In contrast, the potentiostatic method can make the interface sharper because the potential is constant for each layer deposition, but the layer thickness can vary. In fabricating the multilayer a pulse scheme is required as shown in Figure 2.3, pulsing either with current or potential.

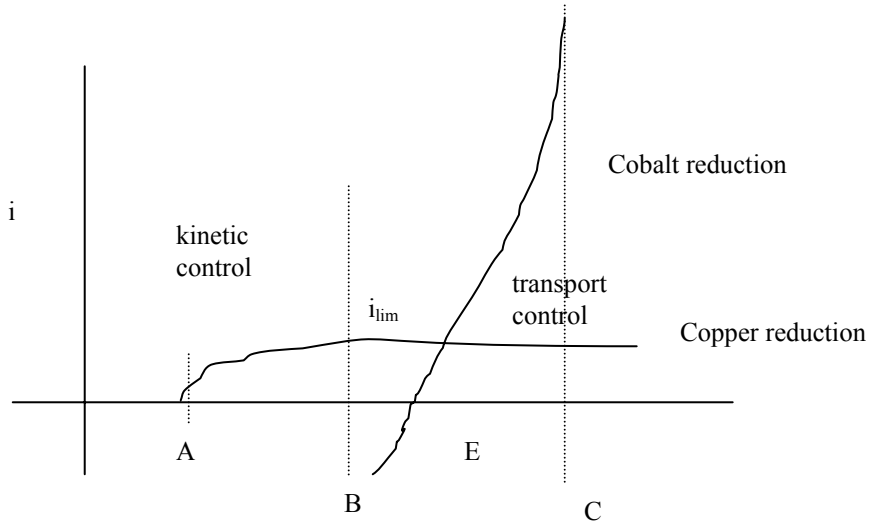

Figure 2-2 Sketch of kinetic control and transport control of copper reduction and kinetic control of cobalt reduction

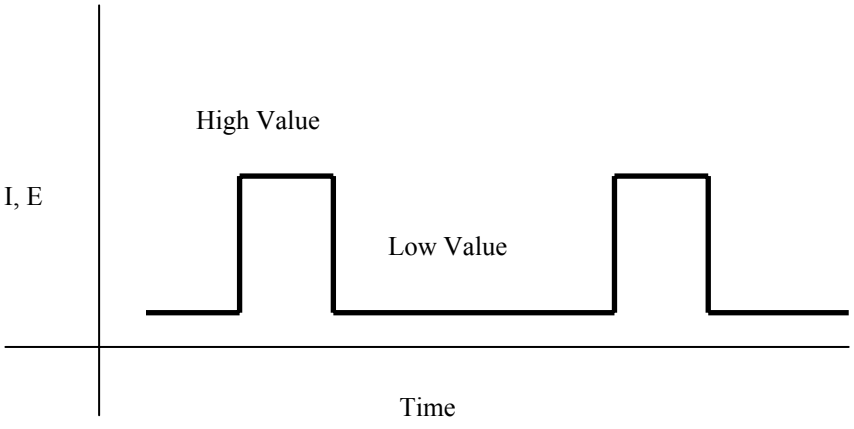

Figure 2-3 Schematic of pulse potential or current

2.2 Giant Magnetoresistance

2.2.1 Origin of GMR

The Mott model[7] can be used to qualitatively understand the origin of GMR, as illustrated in Figure 2.4. Mott proposed two main points. The first one is that electrical resistance is determined by up-spin and down-spin electron channels. Therefore, the electrical conduction occurs in parallel for the two spin channels. The second one is that in ferromagnetic metals the scattering rates of the up-spin and down-spin electrons are quite different, whatever the nature of the scattering centers. Here it is assumed that the scattering is strong for electrons with spin antiparallel to the magnetization direction and weak for electrons with spin parallel to the magnetization direction and it is also assumed that the mean free path is much longer than the layer thicknesses and net electric current flows in the plane of the layers.

Bottom panels in Figure 2.4 show the resistor network within the two-current series resistor model. Antiparallel coupling exist between magnetic layers through the non-magnetic layer. In a zero magnetic field, the magnetizations of neighboring magnetic layers are aligned antiparallel as shown in Figure 2.4(a), both the up-spin and down-spin electrons are scattered strongly within one of the ferromagnetic layers, resulting a high resistivity of the multilayer. When an external magnetic field is strong enough for saturation, the magnetizations change from antiparallel alignment to parallel alignment. In this case the up-spin electrons pass through the structure almost without scattering, whereas the down-spin electrons are scattered strongly within both ferromagnetic layers. Therefore, the total resistivity of the multilayer is low. In other words, both the existence of an interlayer exchange coupling leading to antiparallel alignment of magnetizations

and the changing direction of magnetization from antiparallel to parallel are two conditions for the appearance of GMR in a multilayer structure.

Various structures can exhibit similar changes in resistance with a magnetic field, in addition to the multilayers studied in this dissertation, these include: granular thin films, spin-valve structures with asymmetric magnetic layers, spin valves with an exchanged-biased layer, current perpendicular to plane (CPP) pillars, magnetic tunnel junctions (MTJ), colossal magnetoresistance (CMR) thin films and giant magnetoimpedance (GMI) films.[8]

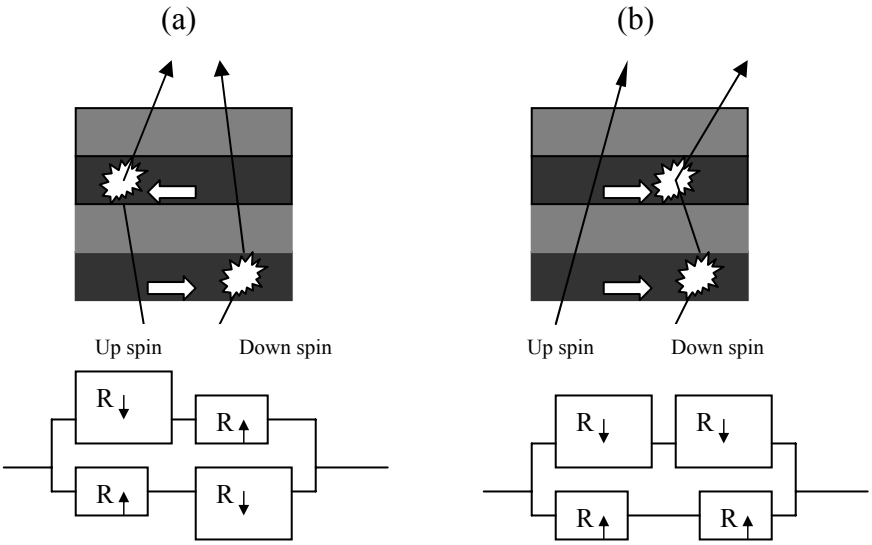

Figure 2-4 Schematic illustration of electron transport in a multilayer for antiparallel (a) and parallel (b) magnetization of the successive ferromagnetic layers; arrows indicate the magnetization directions, and solid lines are individual electron trajectories within the two spin channels.

The magnitude of the GMR value oscillates as the thickness of the nonferromagnetic spacer layers between the ferromagnetic layers is increased. It is caused by an oscillation in the sign of the interlayer exchange coupling between the ferromagnetic layers. The coupling can be antiferromagnetic and ferromagnetic such that the magnetic moments of successive ferromagnetic layers are either parallel

(ferromagnetic) or antiparallel (antiferromagnetic) in small magnetic fields. Oscillatory coupling was shown to be a very general property of almost all transition-metal magnetic multilayered systems in which the nonferromagnetic layer comprises one of the 3*d*, 4*d*, 5*d* transition metals or one of the noble metals.[9] The oscillation period was found to be just a few atomic layers, typically about 1 nm, but varying up to ~ 2 nm. Oscillation is easily observed in sputtering system, but rarely obtained in films produced by the electrodeposition method.

2.2.2 GMR Obtained by Electrodeposition

Numerous studies are available concerning CoCu alloys obtained by electrodeposition.[10-23] The nature of electrodeposits is determined by many factors including the electrolyte composition, additive, pH, temperature and agitation, the potential or current density. For example, Pattanaik *et al.*[11] reported that the deposition current density has a significant control over the composition and microstructure, and that the pH of the electrolyte affects the topography. AES (Auger Electron Spectroscopy) depth profiling analysis showed that the CuCo film is not homogeneous; the bulk of the film is richer in Co while the surface and the bottom of the film are Co-poor[12]. Although thermodynamics suggest Co and Cu are not miscible, electrodeposited CoCu alloys often form a solid solution with the alloy lattice parameter lying between that of pure copper and pure cobalt.

In Antón's study[10], it was shown that the lattice parameter follow Vegard's law when the compositions of Co in the alloy increase from 2 % to 25 %, i.e. a linear relation of lattice parameter with composition. Gónez *et al*.[17] also reported the presence of a solid solution in a granular alloy electrodeposited from citrate electrolytes. Pattanaik *et al.*[11]

plated CoCu alloys onto different substrates and measured GMR of the $Cu_{81}Co_{19}$ at room temperature with an applied magnetic field up to 10 kOe. The maximum GMR for the sample plated on n-Si with a copper seed layer is about 1 %, while the GMR for the sample deposited on Cu-coated Al_2O_3 substrate is ~0.6 %.

Alper *et al.*[24] is the first group to report that electrodeposited multilayers also exhibited significant GMR when they deposited CoNiCu/Cu multilayer on (100) textured polycrystalline Cu substrates. Subsequently other groups also studied electrodeposited multilayer GMR in different systems, electrolytes and different substrates. The largest room temperature GMR measured in the current in plane (CIP) mode is below 30 %[24-51]. Only one group[42] reported a magnitude of 55 % GMR at room temperature for electrodeposited Co/Cu multilayers. However no other investigators have been able to confirm this value. The lack of comparable GMR values has been associated with non-discrete layering, rough interface[13], growth inhomogeneity, and small grain size.[25-27]

Two important factors that influence the multilayer structure and subsequently the magnetic property of the multilayer are: *i.* inherent exchange reactions that occur just before depositing the more noble metal (i.e. Cu), and *ii.* purity of the two layers. Bradley and Landolt [20] investigated the exchange reaction between copper and cobalt under pulse-plating conditions. To their surprise, the exchange reaction was still observed at the pulse off times as long as 1600 s. The reason why the exchange reaction persisted so long was attributed to columnar growth of segregated phases. It was proposed that Cu deposited on solid Cu regions, instead of the cobalt-rich phase, during the exchange reaction. Therefore uncovered-cobalt was not protected even if the pulse off time was very long. Ueda *et al.*[27] correlated the GMR with the cobalt concentration in the copper layer. The

results show that the MR is affected significantly by the purity of the copper interlayer. For multilayer $[Co_{83}Cu_{17}15Å/Co_xCu_{100-x}13\ Å]_{50}$, ($Co_{83}Cu_{17}$ is a cobalt rich layer with thickness of 15 Å, Co_xCu_{100-x} is a copper rich alloy with thickness of 13 Å, and a bilayer number of 50) the MR decreased from 10 % to about 2 % when the cobalt concentration in the copper layer increased to 10 % , also consistent with Weihnacht *et al.*[51]

Myung *et al.*[26] used the sequential dual bath technique to plate Co/Cu GMR multilayers. In order to prevent cobalt dissolution and create sharp interfaces between the cobalt and copper layers, two kinds of copper plating solutions (an acid copper sulfate and a copper pyrophosphate electrolyte) were examined.. Also, two types of cobalt plating solutions were investigated for cobalt (acid cobalt sulfate and alkaline cobalt pyrophosphate). The acid copper sulfate solution with additives grew as bright nano-thick contiguous layers with a significant amount of cobalt dissolved during copper deposition. While alkaline copper pyrophosphate solution also produced nano-thick bright contiguous layers with a little amount of cobalt dissolved. Thus, copper pyrophosphate baths are superior to acid copper sulfate baths to produce distinct Co/Cu multilayers with higher GMR. The deposits plated from two different cobalt solutions showed a significant difference in properties. A maximum GMR of 2.5 % and sensitivity of 0.01 %/Oe were obtained with 5 nm thick Cu/4.5 nm thick Co layer deposited from sulfate bath. While a maximum GMR of 12 % and sensitivity of 0.052 %/Oe were obtained with 5 nm thick Cu/4.5 nm thick Co layer deposited from cobalt pyrophosphate baths. A mathematical model by Huang *et al.*[45-46] has shown that a composition gradient can develop at the interface exaggerated by displacement reactions. Jyoko *et al.*[47] proposed that adding CrO_3 in the electrolyte could inhibit the dissolution of Co during Cu

deposition, which can minimize the interfacial roughness of the multilayer and prevent the large composition gradient at the layer interfaces. They reported a GMR value of 18 % at room temperature and a field of 10 kOe for the multilayer prepared in the presence of CrO_3. They also found that the giant magnetoresistance of this kind of multilayer oscillates with the copper thickness.

The total thickness of the multilayer or the number of bilayer also influences GMR greatly. When the deposit grows, the surface roughness, surface morphology, crystallite size will change. Péter *et al*.[50] reported that GMR of CoCu/Cu multilayer decreased with increasing bilayer number. Transmission electron microscopy (TEM) study revealed that at the beginning of the deposition of the CoCu/Cu multilayer, nano-sized crystallites formed with hexagonal close-packed (hcp) and face-centered cubic (fcc) crystal structures. After this initial polycrystalline step, the size of crystallites increases and fcc superlattices form with increasing average Cu concentration for the first hundred periods. The increasing of average copper concentration is not homogeneous. This may explain why the GMR decreases with the increasing film thickness. Others[14] reported that loss of preferred orientation of the crystallites was observed during growth and was thought to be an important factor for the decline in magnetoresistance with bilayer number.

Additives, mostly organic compounds, are used to improve the brightness[52] enhance corrosion resistance[53] and anti-wearing properties,[54] improve morphology and microstructure.[55] Additives were also used in multilayer deposition to improve the surface quality or inhibit the cobalt dissolution during copper deposition by the exchange reaction and therefore change the magnetoresistance. Unfortunately, most results show

that additives have a negative effect on the magnetoresistive property. For example, Lenczowski *et al*.[25] reported that addition of thiourea and Triton X-100 had a catastrophic effect on the magnetoresistance of Cu/Co multilayer. Kelly *et al.*[19] studied the effects of additives sodium dodecyl sulfate (SDS) and saccharin during the pulsed deposition of CuCo alloys. They found that SDS enhances Co displacement by Cu during open circuit conditions, while saccharin impedes this process. Chassaing [32] observed that multilayers deposited from a basic electrolyte without additives show a magnetoresistance of 9 % at 4.2 K and a field of 12 kOe, while the multilayer deposited from the electrolyte containing SDS and saccharin has a magnetoresistance of 25 % at 4.2 K. EI-Rehim *et al.*[22] reported that the addition of boric acid tends to increase the percentage of cobalt in the deposited alloys. Péter *et al*.[33] reported that the addition of NaCl in the sulfate bath decreases the GMR value of the Co/Cu multilayer although the film morphology was improved. It was also reported that the use of saccharin in the electrolyte inhibits the columnar-growth morphology in the Cu/Ni multilayer, leading to a brighter surface with a much smaller roughness.[55]

A substrate requirement for electrodeposition is that it must be conductive. However, in order to avoid the short-circuit effect of the conductive substrate for GMR measurements, the thin film needs to be peeled from the substrate. Another choice is to make the substrate very thin so that the resistance of the substrate is larger than the film and therefore most of the current will pass through the thin film. Different substrates were used in the multilayer electrodeposition with different purposes. Some authors consider using the substrate with different crystal orientation to improve the preferred orientation of the multilayer. Usually the substrates used for this purpose include a single

crystal such as Cu[32,48] and Pt[47], polycrystalline Cu[32] and Ti.[50] For these substrates the film must be removed from them before measurement of magnetoresistance. An alternative is to measure GMR directly without removing it from the substrate. Such kind of substrates include: silicon wafer with a seed layer of copper,[43] GaAs,[35] indium-tin oxide (ITO),[27,44] and copper thin films vapor-deposited on glass plates[27].

In the vacuum method, the most common substrate used to grow multilayers is a silicon wafer with a seed layer. The seed layer usually is Cu having a thickness of 10-100 nm. Parkin *et al.*[4] found that an Fe buffer layer sputtered onto a Cu seed layer can inhibit the diffusion of Cu atom into the silicon wafer and therefore make the interface of the multilayer flatter and sharper.

It is known that the choice of substrate has a large effect on the microstructure and GMR of multilayers. Kasyutich *et al.*[35] employed the potentiostatic method to directly deposit CoNiCu/Cu multilayers on GaAs(111) and GaAs(001). Three differences were found for these multilayers. The first difference is that epitaxial growth occurred on GaAs(001), but not on GaAs(111). The second one is that superlattice satellite peaks were observed for the multilayers deposited on GaAs(001), but not observed for those grown on GaAs(111). Satellite peaks are subsidiary peaks surrounding the zero-order peak, with peak position determined by the periodicity (total thickness of the repeating layers) of the multilayer. The presence of higher order satellite peaks, and intensity of such satellite peaks, indicate superlattice formation and a multilayer structure. The second difference is that for the multilayer with 50 repeats of nominal thickness 3 nm CoNiCu/ 2 nm Cu grown on GaAs (001), a 12 % transverse GMR was found at 8000 Oe, but for the same multilayer deposited on GaAs (111), about 6 % transverse GMR was

observed at the same magnetic field. This difference was thought to result from the structural defects in the multilayer grown on GaAs(111) compared with the multilayer plated on GaAs(100). These structural defects resulted in ferromagnetic coupling, which prevent the direction of magnetization vectors of successive ferromagnetic layers from being antiparallel, and therefore decrease GMR.

Shima *et al.*[43] electrochemically deposited Co/Cu multilayers on Si(100) substrates covered with a 40 nm thick copper layer sputtered by electron-beam evaporation. The XRD analysis showed that the Cu seed layer and Co/Cu multilayer has a preferential orientation of (100). Satellite peaks were observed around the Cu (002) peak. About 3 % GMR was measured for the sample [Co (3.7ML)/Cu (17ML)] $_{100}$ at room temperature and at a magnetic field of 0.3 T where saturation was not achieved.

Chassaing *et al.*[43] directly deposited CoCu/Cu multilayers on indium-tin oxide (ITO) glass so that magnetoresistance can be measured without removing the film from the substrate. The deposited multilayer has a pronounced (111) preferred orientation. The largest GMR they obtained is about 18 % at 4.2 K and magnetic field of 6 kOe. They also associate the low GMR value with the strong preferred (111) orientation, as also reported by Schwarzacher and Lashmore.[5] Multilayers were also directly deposited on copper thin films vapor-deposited on glass by Ueda *et al.*[27] A similar GMR of 15 % at room temperature was reported at 15 kOe, without saturation.

The Nabiyouni *et al.*[36] plated Co-Ni-Cu/Cu multilayers on (111) and (100) oriented Cu single crystal substrates and found a preferred orientation in the (111) direction peak when the multilayer was plated onto the (111) Cu substrate, and the opposite preferred orientation for the (100) Cu substrate case. The maximum GMR was

15 % for the latter case, with oscillations as Cu thickness varied, but for the former case the maximum GMR was only 9 %, with no oscillations. Similar results were also reported by Lenczowski *et al*.[25]

Shima[49] studied the correlation between structural imperfection and GMR in electrodeposited CoCu/Cu multilayers, on Si(100) with a copper seed layer. They found that the reason of low GMR is that the columnar grains grow during multilayer deposition, which resulted from the strain-driven perturbations. Therefore the strong magnetostatic coupling between neighboring magnetic layers overwhelmed the antiferromagnetic coupling.

2.2.3 Deep Recess GMR

Nanowire and micropillar shapes require electrodeposition into deep recesses. In nanowire electrodeposition, a nanoporous membrane is used as a template with cylindrical pores. Metal is sputtered on the backside of the membrane so that it is conductive. Micropillars are deposited into a lithographically fabricated structure. In this case, the electrode is prepared with a photoresists of a defined shape.

High aspect ratio plating of multilayers has been achieved in nanowires.[56-66] For example, in Co/Cu multilayered nanowires 15 %,[56] and 20 %[57] CPP GMR were found at room temperature. In NiFe/Cu systems, 20 %[61] CPP GMR was found at room temperature and 80 % at 4.2 K. In CoNi/Cu system, 55 % CPP GMR at room temperature was found by Blondel *et al*.[59] At 77 K 115 % was reported by Evans *et al*. [64] in Co/Cu system.

One example of submicron (0.3 μm deep, diameter 0.1 μm) pillars of permalloy/Cu has been demonstrated by Duvail *et al*.[67] To the best of our knowledge, there is no

demonstration of a Co/Cu multilayer in a submicron, lithographic pattern, which is the first step for the fabrication of GMR microdevices.

2.3 References

1. M. N. Baibich, J. M. Broto, A. Fert, F. Nguyen Van Dau, F. Petroff, P.Etienne, G Creuzet, A. Friederich, and J. Chazelas, *Physical Review Letters*, **61**, 2472 (1988).

2. G. Binasch, P. Grünberg, F. Saurenbach, and W. Zinn, *Physical Review* B, **39**, 4828 (1989).

3. S. S. P.Parkin, R. Bhadra and K. P. Roche, *Physical Review Letters*, **66**, 2152 (1991).

4. S. S. P.Parkin, Z. G. Li and D. J. Smith, *Applied Physical Letters*, **58**, 2710 (1991).

5. W. Schwarzacher and D. S. Lashmore, *IEEE Transaction on Magnetics*. **32**(4), 3133 (1996).

6. N. Masuko, T. Osaka and Y. Ito, "*Electrochemical Technology: Innovation and New Developmemts"*, Kodansha Ltd., Gordon and Breach Science Publishers, **279** (1996).

7. H. Ehrenreich and F. Spaepen, *Solid State Physics*, **56**, 6 (2001).

8. S. Tumanski, "*Thin film magnetoresistivity sensors"*, Institute of Physics Publishing, Dirac House, Temple Back, Bristol BS1 6BE, UK,1-4 (2001).

9. S. S. P. Parkin, *Physical Review Letters,* **67**, 3598 (1997).

10. R. L. Antón, M. L. Fdez-Gubieda, A. García-Arribas, J. Herreros, M.Insausti, *Material Science and Engineering*, A**335**, 97 (2002).

11. G. R. Pattanaik, D. K. Pandya, and S C. Kashyap, *Journal of the Electrochemical Society*, **149**(7), C363 (2002).

12. T. Cohen-Hyams, W. D. Kaplan, D. Aurbach, Y. S. Cohen and J. Yahalom, *Journal of the Electrochemical Society*, **150**, (1) C28 (2003).

13. K. Miyazaki, S. Kainuma, K. Hisatake, T. Watanabe, N.Fukumuro, *Electrochimica Acta*, **44**, 3715 (1999).

14. R. López, J. Herreros, A. García-Arribas, J. M. Barandiarán, M. L. Fdez-Gubieda, *Journal of Magnetism and Magnetic Materials*, **196-197**, 54 (1999).

15. H. Errahmani, A. Berrada, G. Schemerber, A. Dinia, *Journal of Magnetism and Magnetic Materials*, **238**, 147 (2002).

16. W. Wang, F. Zhu, W. Lai, J. Wang, G. Yang, J. Zhu and Z. Zhang, Journal Physics. D: *Applied Physics,* **32**, 1995 (1999).

17. E. Gómez, A. Labarta, A. Llorente, E. Vallés, *Journal of Electroanalytical Chemistry*, **517**, 66 (2001).

18. A.Yamada, T. Houga, Y. Ueda, *Journal of Magnetism and Magnetic Materials,* **239**, 273 (2002).

19. J. J. Kelly, P. Kern, and D. Landolt, *Journal of the Electrochemical Society*, **147**, 3725 (2002).

20. P. E. Bradley, D. Landolt, *Electrochimica Acta*, **45**, 1077 (1999).

21. T. Cohen-Hyams, W. D. Kaplan, D. Aurbach, Y.S. Cohen, and J. Yahalom, *Journal of the Electrochemical Society*, **150**, C28 (2003).

22. S. S. Abd EI-Rehim, S. M. Abd EI-Wahab, S. M. Rashwan and Z. M. Anwar, *Journal of Chemical Technology and Biotechnology*, **75**, 237 (2000).

23. P. C. Andricacos, *Journal of the Electrochemical Society*, **142**, 1824 (1995).

24. M. Alper, K. Attenborough, R. Hart, S. J. Lane, D. S. Lashmore, C. Younes, and W. Schwarzacher, *Applied Physics Letters,* **63**, 2144 (1993).

25. S. K. J. Lenczowski, C. Schönenberger, M. A. M. Gijs, W. J. M. de Jonge, *Journal of Magnetism and Magnetic Materials,* **148**, 456 (1995).

26. N. V. Myung, B. Y. Yoo, M. Schwartz, and K. Nobe, *Electrochemical Society Proceedings*, **29**, 154 (2000).

27. Y. Ueda, N. Hataya, H. Zaman, *Journal of Magnetism and Magnetic Materials,* **156**, 350 (1996).

28. E. Gómez, A Labarta, A. Lorente, E. Vallés, *Surface and Coating Technology*, **153**, 261 (2002).

29. V. I. Nikitenko, V. S. Gornakov, L. M. Dedukh, A. F. Khapikov, T. P. Moffat, A. J. Shapiro, R. D. Shull, M. Shima, L. Salamanca-Riba, *Journal of Magnetism and Magnetic Materials*, **198-199**, 478 (1999).

30. M. Shima, L. Salamanca-Riba, T. P. Moffat, R. D. McMichael, *Journal of Magnetism and Magnetic Materials*, **198-199**, 54 (1999).

31. A. M. Shukh, D. H. Shin, and H. Hoffmann, *Applied Physics*, **76**, 6507 (1994).

32. E. Chassaing, *Journal of the Electrochemical Society*, **148**, C690 (2001).

33. L. Péter, Z. Kupay, Á. Cziráki, J. Pádár, J. Tóth, and I. Bakonyi, *Journal of Physical Chemistry*, **105**,10867 (2001).

34. M. Troyon, L. Wang, *Applied Surface Science*, **103**, 517 (1996).

35. O. I. Kasyutich, W. Schwarzacher, V. M. Fedosyuk, P. A. Laskarzhevskiy and A. I. Masliy, *Journal of the Electrochemical Society*, **147**, 2964 (2000).

36. G. Nabiyouni, W. Schwarzacher, *Journal of Magnetism and Magnetic Materials*, **156**, 355 (1996).

37. G. Nabiyouni, O. I. Kasyutich, S. Roy, and W. Schwarzacher, *Journal of the Electrochemical Society*, **149**, C218 (2002).

38. M. Alper and W. Schwarzacher, S. J. Lane, *Journal of the Electrochemical Society*, **144**, 2351 (1997).

39. Y. Jyoko, S. Kashiwabara, and Y. Hayashi, *Journal of the Electrochemical Society,* **144**, L5 (1997).

40. S. Z. Hua, D. S. Lashmore, L. H. Bennett, and R. Hart, *Journal of Applied Physics,* **76**, 6519 (1994).

41. L. Péter, A. Cziráki, L. Pogány, Z. Kupay, I. Bakonyi, M. Uhlemann, M. Herrich, B. Arnold, T. Bauer, and K. Wetzig, *Journal of the Electrochemical society*, **148**(3), C168 (2001).

42. K. D. Bird and M. Schlesinger, *Journal of the Electrochemical Society,* **142**, L99 (1995).

43. M. Shima, L. Salamanca-Riba, R. D. McMichael, and T. P. Moffat, *Journal of the Electrochemical Society*, **149**, 439 (2002).

44. E. Chassaing, A. Morrone, and J. E. Schmidt, *Journal of the Electrochemical Society*, **146**(5) 1794 (1999).

45. Q. Huang and E. J. Podlaha, in *Proceedings of the 7th International Symposium on Magnetic Materials, Processes and Devices,* 202nd Meeting of The Electrochemical Society, Salt Lake City, UT Oct. 22 (2002).

46. Q. Huang, D. P. Young, and E. J. Podlaha, *Journal of Applied Physics*, **94**, 1864 (2003).

47. Y. Jyoko, S. Kashiwabara, and Y.Hayashi, *Journal of the Electrochemical Society*, **144**, L5 (1997).

48. R. D. McMichael, U. Atzmony, C. Beauchamp, L. H. Bennett, L. J. Swartzendruber, D. S. Lashmore, and L. T. Romankiw, *Journal of Magnetism and Magnetic Materials,* **113**,149 (1992).

49. M. Shima, L. G. Salamanca-Riba, R. D. McMichael, and T. P. Moffat, *Journal of the Electrochemical Society*, **148**(8), C518 (2001).

50. L. Péter, Z. Kupay, Á. Cziráki, J. Pádár, J. Tóth, and I.Bakonyi, *Journal of Physical Chemistry*, **105**,10867 (2001).

51. V. Weihnacht, L. Péter, J. Tóth, J. Pádár, Zs. Kerner, C. M. Schneider and I. Bakonyi, *Journal of the Electrochemical Society*, **150**(8), C507 (2003).

52. W. Plieth, *Electrochimic Acta*, **37**, 2115 (1992).

53. M. Troyon and L. Wang, *Applied Surface Science*, **103**, 517 (1996).

54. Q. J. Xue and W. Zhang, *Journal of Physics D: Applied Physics*, **30**, 3301 (1997).

55. J. J. Kelley, P. Bradley, and D. Landolt, *Journal of the Electrochemical Society*, **147**, 2975 (2000).

56. L. Piraux, J. M. George, J. F. Despres, C. Leroy, E. Ferain, R. Legras, K. Ounadjela, and A. Fert, *Applied Physics Letters*, **65**, 2484 (1994).

57. T. Ohgai, X. Hoffer, A. Fábián, L. Gravier and J. Ansermet, *Journal of Materials Chemistry*, **13**, 2530 (2003)

58. A. Blondel, J. P. Meier, B. Doublin, J.-Ph. Ansermet, *Applied Physics Letters*, **65**, 3019 (1994)

59. A. Blondel, J. Meier, B. Doublin, J.-Ph. Ansermet, K. Attenborough, P. Evens, R. Hart, G. Nabiyouni, and W. Schwarzacher, *Journal of Magnetism and Magnetic Materials*, **148**, 317 (1995).

60. W. Schwarzacher, O. I. Kasyutich, P. R. Evans, M. G. Darbyshire, Y. Ge, V. M. Fedosyuk, F. Rousseaux, E. Cambril, and D. Decanini, *Journal of Magnetism and Magnetic Materials*, **198-199**, 185 (1999).

61. S. Dubois, C. Marchal, J. M. Beuken, and L, Piaux, *Applied Physics Letters*, **70** (3), 396 (1997).

62. T. Ohgai, X. Hoffer, A. Fábián, L. Gravier and J. Ansermet, *Journal of Materials Chemistry*, **13**, 2530 (2003).

63. J. P. Spallas, Y. Huai, S. Vernon, B. Fuchs, B. Law, and D. R. Kaina, *IEEE Transactions on Magnetics*, **32** (5), 4710 (1996).

64. L. Piraux, S. Duvail, K. Ounadjela, A. Fert, *Journal of Magnetism and Magnetic Materials*, **175**, 127 (1997).

65. P.R. Evans, G. Yi, and W. Schwarzacher, *Applied Physics Letters*, **76**, 481 (2000).

66. S. Dubois, C. Marchal, J. M. Beuken, and L. Piraux, *Applied Physics Letters* , **70**, 396 (1997).

67. G. P. Heydon, S. R. Hoon, A. N. Farley, S. L. Tomlinson, M. S. Valera, K. Attenborough, and W. Schwarzacher, *Journal Physics, D: Applied Physics*, **30**, 1083 (1997).

68. J. L. Duvail, S. Dubois, L. Piraux, A.Vavrès, A. Fert, D. Adan, M. Champagane, F. Rovsseaux, D. Decanini, *Journal of Applied Physics*, **84**, 4359 (1998).

CHAPTER 3. ELECTRODEPOSITION OF Co/Cu THIN FILMS

3.1 Introduction

Electrodeposited nanostructured multilayers is a cost effective alternative to vapor deposited methods and can provide a means to deposit multilayered materials into deep recesses and irregular substrates, in order to integrate them into MEMS devices. Specifically, when nanometric ferromagnetic layers, i.e. Co, are separated by a nonmagnetic layer, i.e. Cu, the material exhibits giant magnetoresistance (GMR), a large variation of the electrical resistance when a magnetic field is applied. Magnetoresistance (MR) can also occur without layering due to the intrinsic nature of the ferromagnetic material, however, the value is not more than a few percent at room temperature, ~ 2 % for Co.[1] Electrodeposited multilayered films[2-16] generally have lower MR or GMR than those obtained by vapor techniques.[17] The poorer performance has been associated with non-discrete layering, rough interfaces, growth inhomogenity, and small grain size.[12, 13]

The CoCu alloy and multilayer system is examined here as a model system because of the inherently large GMR obtained with physical vapor deposition methods. The nature of CoCu electrodeposits is determined by many factors, including the electrolyte composition, additive, pH, temperature, agitation and the potential or current density. GMR in layered electrodeposited Co/Cu or CoNi/Cu thin films has been reported, [4-12] and it is affected by both the copper[8, 9, 16] and cobalt layer thickness.[5, 6, 16] In addition, the composition of the Co-rich layer affects GMR[9] as well as the choice of the Cu deposition current.[18] The choice of substrate has a large effect on the microstructure and GMR of multilayer. Schwarzacher *et al*.[19] has suggested that due to the displacement reaction of Co by Cu(II) ions at the low current densities, the interfacial region of the

layers is not discrete and lowers GMR. A mathematical model by Huang *et al.*[20] has simulated the resulting composition transient that can develop at the interface. Jyoko *et al.*[21] proposed that adding CrO_3 in the electrolyte could inhibit the dissolution of Co during Cu deposition.

In this chapter, CoCu/Cu thick multilayer films were deposited onto silicon wafers and different parameters that are expected to influence their GMR were examined. The layer thickness, pH, bilayer number, seed layer and nickel component were investigated in detail. It has been shown[22] that thick electrodeposits of hundreds of bilayers result in a lowering of GMR. However, thick films are of interest to MEMS-type devices where the GMR sensor material can also act as structural support. The growth of thick films, larger than one micron, become more sensitive to the electrolyte constituents and the plating parameters compared to the substrate surface.

3.2 Experimental

3.2.1 Electrolyte

The electrolyte for thin film plating is listed in Table 3.1. Analytical grade reagents from Fisher were used in the preparation of the solutions in distilled-DI water. The pH value was adjusted to 3.0 with sulfuric acid and sodium hydroxide at room temperature and was measured using a Orion® Model 420A pH meter.

Table 3-1 Electrolyte Compositions for Thin Film Plating

Component	Concentration
Copper Sulfate	0.005 M
Cobalt Sulfate	0.5 M
Boric Acid	0.543 M

3.2.2 Substrate Preparation

A n-type Sb doped (100) silicon wafer was first sent to CAMD to sputter 100 nm Ti as an adhesion layer and a 20 nm Cu as seed layer. Then the silicon wafer was cut into a 2.5×2.5 cm square plate and subsequently cleaned by deionized water, acetone and 2 % H_2SO_4 before it was put into the sample holder. The total exposed area is 1.6 cm^2.

3.2.3 Cell Design and Operation

Figure 3.1 is a schematic of the experimental setup for multilayer deposition. A holder was used to contain the substrate. The holder has two cylindrical disks, which are held together using screws. The bottom disk has a copper plate recessed to seat the copper foil substrate. A copper wire soldered to the bottom of the recessed plate served as the cathode connection. The top disk has a 1.6 cm^2 exposed area that enables the electrolyte solution to reach the substrate. A piece of platinum mesh was used as the anode. For the polarization and experiments, a saturated calomel electrode (SCE) was placed next to the substrate surface as reference electrode.

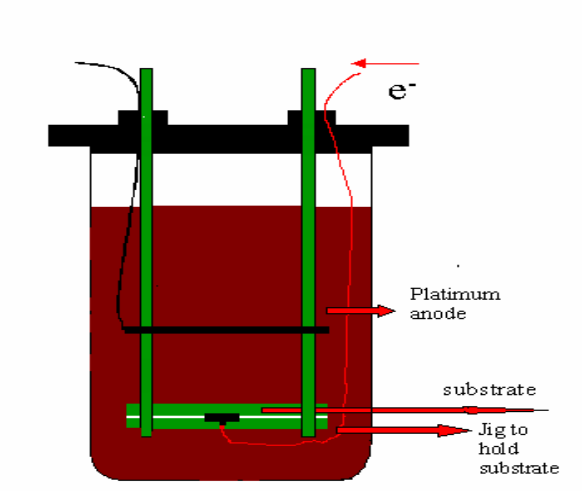

Figure 3-1 Schematic of the cell used for multilayer deposition

3.2.4 Deposition Process

Polarization curves were carried out with a Pine Instruments bipotentiostat, at a scan rate of 2 mV/s and the potential was corrected for ohmic drop, which is measured by impedance analysis with a Bas-Zahner IM6 Zahner® unit. All experiments were carried out at atmospheric pressure and at room temperature.

Constant current densities from –0.2 mA/cm^2 to –20 mA/cm^2 were applied to plate CuCo alloys on the stainless steel cathode in order to calculate the current efficiency during alloy deposition, the mass of the deposit film was obtained by weight. The quantity of charge, Q, passed was obtained by integration of the measured current over potential, $Q = \int IdE \cdot \frac{dt}{dE}$, The potential sweep rate, dE/dt, was 2 mV/s, and the mass of the deposited films was calculated from Faraday's law, shown in equation 2.2 .

$$m_{total} = \frac{QM_{Cu}M_{Co}}{nF(M_{Co}x_{Cu} + M_{Cu}x_{Co})} \tag{3.1}$$

In the present CoCu system the mass deposited was calculated in equation 3.1 where m_{total} is the mass of the deposit, for the alloy deposition, M_{Cu} and M_{Co} are the molecular weight of copper and cobalt respectively, x_{Cu} and x_{Co} are the weight fractions of Cu and Co. The partial current densities of Co (i_{Co}) and Cu (i_{Cu}) are the amounts of current contributing to each reduction reaction, while the difference from the total current is attributed to side reactions including H_2 evolution and O_2 reduction. The partial current densities, i_{Cu} and i_{Co} are defined as in equation 3.2 and 3.3

$$i_{Cu} = \frac{(-1000)(m_{total})(x_{Cu})(n_{Cu})(F)}{(60)(M_{Cu})(t)(A)} \qquad [=]\ mA/cm^2 \tag{3.2}$$

where A is the area of the electrode (A=1.6 cm^2). The side partial current density is defined as the difference between the total current density and the metal partial current current density.

$$i_{Co} = \frac{(-1000)(m_{total})(x_{Co})(n_{Co})(F)}{(60)(M_{Co})(t)(A)} \qquad [=]\ mA/cm^2 \tag{3.3}$$

$$i_{side} = i_{total} - (i_{Cu} + i_{Co}) \qquad [=]\ mA/cm^2 \tag{3.4}$$

and current efficiency, ε, is defined as the ratio of the metal rates over the total applied current density, i_{total}

$$\varepsilon = \frac{(i_{Cu} + i_{Co}) \times 100}{i_{total}} \tag{3.5}$$

where i_{total} is the total applied current density and ε is the current efficiency.

Multilayers were deposited onto n-type (100) silicon wafer with 100 nm Ti as adhesion layer and 20 nm Cu as seed layer by galvanostatic pulsing. Each pulse consisted of a low current density for the copper layer deposition, and a high current density for Cu-Co alloy layer deposition. The applied low current density was lower than the transport limiting current density observed in the polarization curve. The high current density was choosen to be sufficiently high so that the content of Cu in the Co rich layer was less than 10 wt. %. The total time that was needed was calculated as follows:

$$time_{total} = \frac{(t_{Cu} + t_{Co}) \times n_{bilayers}}{60} \qquad [=]\ \text{min} \tag{3.6}$$

where $n_{bilayers}$ is the number of the copper and cobalt bilayer, and t_{Cu} and t_{Co} is the time needed for plating one copper layer and one cobalt layer in seconds.

After deposition, the multilayers on the silicon wafer was quickly taken out from the electrolyte, rinsed with water and dried by kimwipes.

3.3 XRF, XRD and GMR Analysis

The composition of the CoCu thin films on the stainless steel was characterized by a Kevex Omicron energy-dispersive X-ray fluorescence analyzer (XRF).

X-ray powder diffraction data were obtained using a Bruker Advance D8 powder diffractometer equipped with a focusing Ge(111) incident beam monochromator (Cu Kα_1 radiation) with a Bragg-Bretano geometry. $2\theta/\theta$ diffractograms data were obtained at ambient temperature in the range of 2θ = 30-75° with a step range of 0.02° and a measuring time of 8 s per set.

For GMR measurements, the multilayers were cut into 7×4 mm^2 pieces and mounted into a GMR holder. The holder consisted of four platinum wires and was connected to the deposit in a straight line, as shown in Figure 3.2. When the magnetic field is parallel to the current in the film plane, the measured magnetoresistance is called longitudinal GMR. When the magnetic field is perpendicular to the current in the film plane, the magneto resistance is called transverse GMR. In the present works the in-plane transverse giant magnetoresistance (GMR) of the multilayers was measured at room temperature with a 9 T quantum design physical properties measurement system (PPMS), using the standard four-point probe ac technique at 27 Hz with an excitation current of 1 mA. The GMR is then defined according to $\Delta R/R=(R(H)-R(0))/R(0) \times 100$, where R(0) is the resistance at zero magnetic field, and R(H) is the resistance in external field H.

3.4 Electrolyte Characterization

Figure 3.3 shows the polarization curves obtained in a quiescent electrolyte. Regions where copper and cobalt are deposited are evident from the curves. The copper partial current density is apparent from the flat regions of the curve followed by the rise of the cobalt partial current densities at potentials more negative than –0.77 V. Copper ions are in a much lower electrolyte concentration compared to cobalt and thus it is expected that Cu reaches its limiting current density at low current densities of -0.34 mA/cm^2. In multilayer deposition, a current density of -0.2 mA/cm^2 was chosen since it is lower than the limiting current value. XRF analysis of the alloy deposited at this current density indicated that the thin film contained 99.6 % copper. The cobalt-rich layer was deposited under kinetic control at a current density of -20 mA/cm^2, the composition of the alloy was 95 % cobalt and 5 % copper. The current efficiency calculated according to Faraday's law was 50 % for copper deposition and 86 % for the cobalt-rich deposition. The plating time specified for the copper and cobalt-rich layer thicknesses were calculated based on these efficiencies.

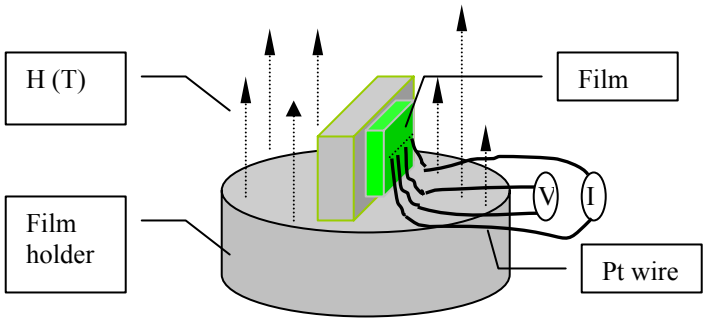

Figure 3-2 A schematic of the transverse GMR

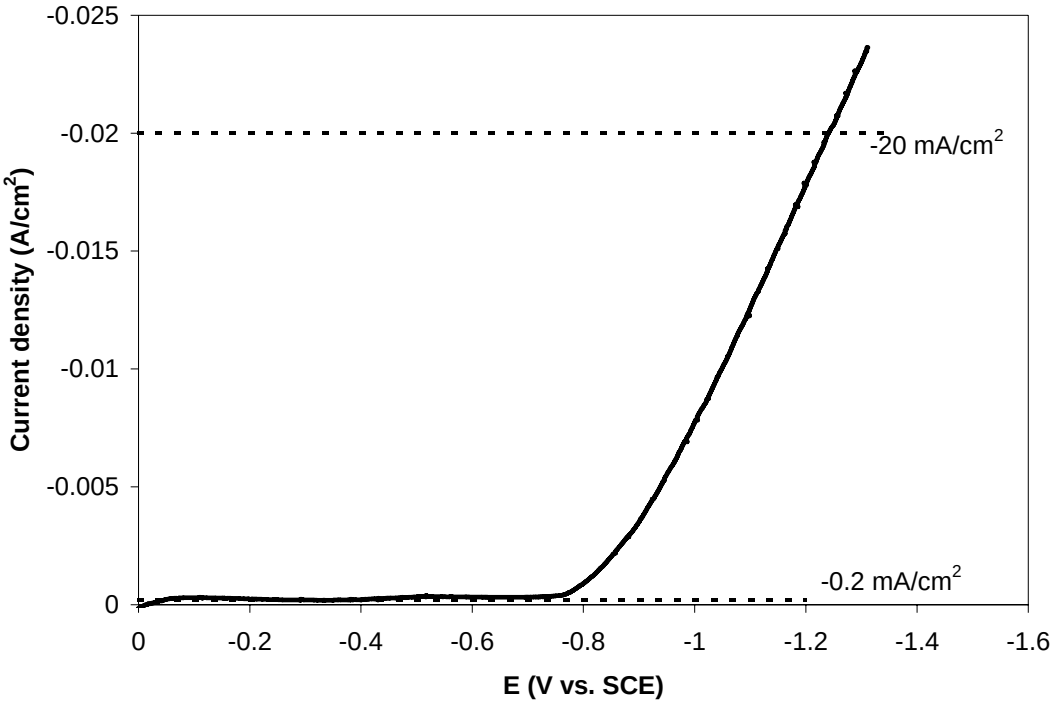

Figure 3-3 Polarization curve for quiescent electrolyte obtained at a scan rate of 2 mV/s

3.5 GMR

3.5.1 Cobalt and Copper Layer Thickness

It was well known that both cobalt and copper layer thickness play a significant role in the multilayer magnetoresistance behavior.[2] Clear evidence of oscillatory magnetoresistance with layer thickness has been found in the multilayers prepared by vacuum methods.[23, 24] However, electrodeposited multilayers have not always exhibited similar oscillatory behavior with layer thickness; the varying of the magnetoresistance with the layer thickness depended on the electrolyte and the specific plating process used. Some of electrodeposited multilayers show an oscillatory behavior with a change of copper layer thickness,[25 26] and some of them show a monotonous behavior.[27] These phenomena are attributed to the inherently different quality of the electrodeposited thin

films. Therefore, a systematic investigation of the layer thickness effect on the magnetoresistance was needed to determine the appropriate layer thickness for good magnetoresistance in our CoCu/Cu systems. Three series of multilayer samples with different copper and cobalt layer thickness were electrodeposited at a constant electrolyte pH of 3.0.

The first series of multilayer samples with thick cobalt layer thickness were deposited on silicon wafer substrates. The copper plating current density was -0.2 mA/cm^2 and the cobalt plating current density was -20 mA/cm^2. In this series of samples, the cobalt plating time was kept at 3 s and the copper plating time varied from 30, 40, 50, 60 to 70 s. The corresponding cobalt layer thickness was estimated to be about 19 nm by Faraday's law, taking into account the current efficiency. The copper layer thicknesses were calculated as 1.2, 1.5, 1.9, 2.3 and 2.7 nm based on the current efficiency of 50 % at -0.2 mA/cm^2. The plating bilayer number for these multilayer samples was 1000 and the total plating time for each sample was 21 hours and 47 min. The total multilayer thickness was in the range between 20 and 23 μm. At this layer thickness, the multilayer samples were easily peeled off the substrate and mounted onto a magnetoresistance characterization holder as shown in Figure 3.2.

The magnetoresistance results are shown in Figure 3.4. In Figure 3.4(a), the magnetoresistance of the multilayers at different layer sizes varied in the range of between -0.7 % and -3.2 % with saturation fields less than 5000 Oe. The maximum magnetoresistance exhibited an oscillatory-like behavior with the increase of copper layer thickness. (Figure 3.3(b))

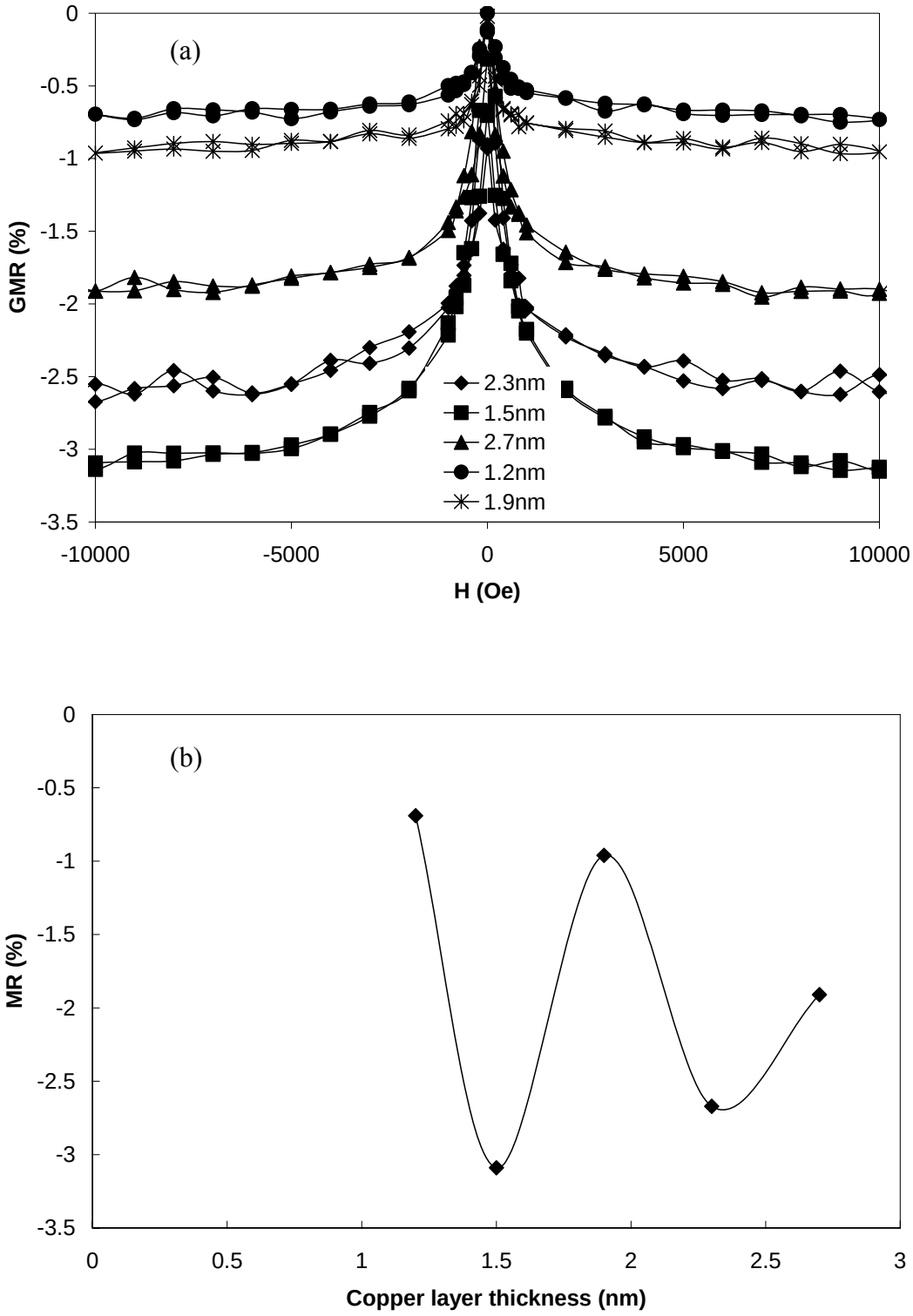

Figure 3-4 (a) Magnetoresistance of Co(19 nm)/Cu(x nm)$_{1000}$ (b) Maximum magnetoresistance for samples Co(19 nm)/Cu(x nm)$_{1000}$

The second series of multilayer samples were also plated onto the silicon wafer with the same current density. The cobalt plating time was decreased to 200 ms and the corresponding cobalt layer thickness was about 1.25 nm. The copper layer thickness varied from 1, 1.5, 2, 2.5, 3, 3.5 to 4 nm and the bilayer number was still kept at 1000. The total multilayer thickness is in the range between 2 to 5 μm. At these small layer thicknesses, it was hard to peel off the multilayer from the substrate and therefore they were directly mounted onto the measurement holder with a piece of silicon wafer together. The copper seed layer thickness was around 20 nm and therefore exhibits a larger resistance than those in the multilayer samples. Therefore, most of the current passed through the multilayer portion of the samples and a small amount of current passed through the seed layer during the measurement. In this case, the short-circuit influence of the copper seed layer on the magnetoresistance was neglected, although the true magnetoresistance value should be a little bit larger than the observed one.

Figure 3.5 is the magnetoresistance of the multilayer samples with variable Cu layer thickness Co(1.25 nm)/Cu(x nm)$_{1000}$. Figure 3.5 (a) indicated that the magetoresistance of the multilayers with smaller cobalt layer thickness also had a magnetoresistance value between -1 % and -4.8 % with a change of copper layer thickness. However, all of these samples were not saturated under the magnetic field of 10000 Oe. Therefore, the sensitivity of these multilayer samples is lower than that obtained with 19 nm cobalt layer thickness. Figure 3.5 (b) showed a different relation between maximum magnetoresistance value and copper layer thickness compared to Figure 3.3 (b). At smaller cobalt layer thickness, the magnetoresistance increases with an increase of the copper layer thickness.

(a)

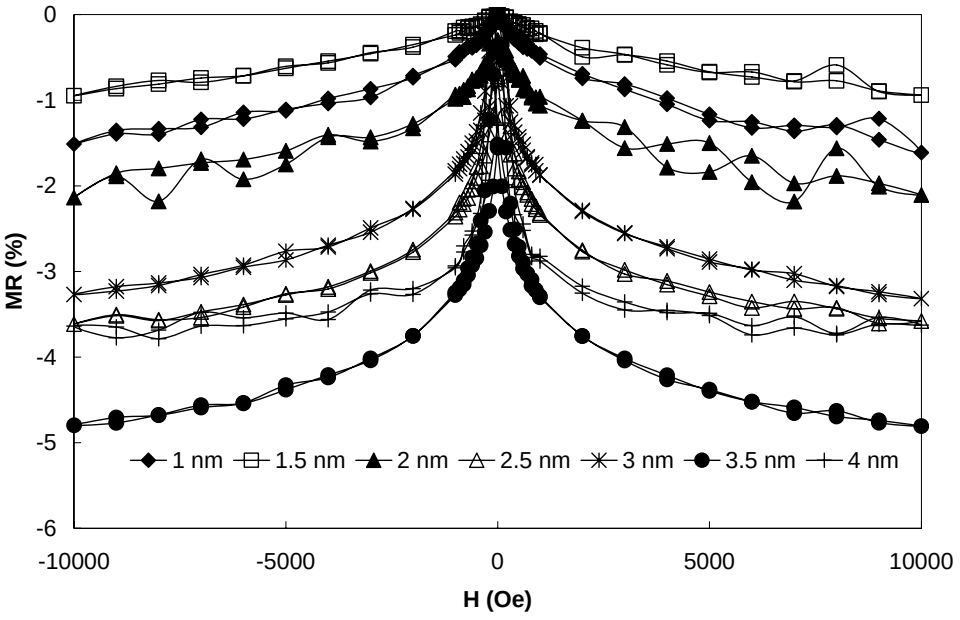

(b)

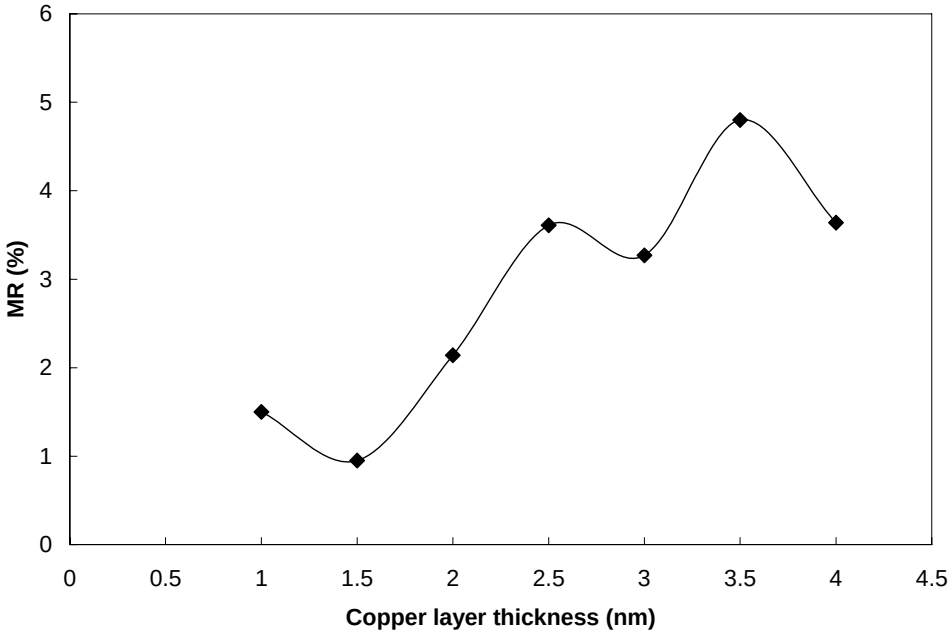

Figure 3-5 (a) Magnetoresistance of Co(1.25 nm)/Cu(x nm)$_{1000}$, (b) maximum magnetoresistance for samples Co(1.25 nm)/Cu(x nm)$_{1000}$

Another series of samples were deposited onto the silicon wafers at a middle cobalt layer thickness. The plating current density for the cobalt and copper layers were the same as those used before. The plating time for cobalt layer was controlled at 400 ms

and the corresponding copper layer thickness was 2.5 nm. The plating time for the copper layer was changed from 13, 26, 39, 52, 65, 78 to 91 s, the calculated copper layer thickness was 0.5, 1, 1.5, 2, 2.5, 3, 3.5, 4 nm. The bilayer numbers were 1000 for each sample, the same as those used in the previous experiments. The total sample thicknesses on the silicon wafer were between 3 and 7 μm.

The analysis results are shown in Figure 3.5. Compared to the other two series, this series of samples with cobalt layer thickness of 2.5 nm have larger magnetoresistance, ranging between -0.5 % and -5 %. The most significant result is that the sensitivity was improved. The saturation field was less than 3000 Oe for each sample, as shown in Figure 3.5 (a). Figure 3.5 (b) indicates that with the increase of the copper layer thickness, a maximum magnetoresistance of 5 % was obtained at a copper layer thickness of 3 nm and cobalt layer thickness of 2.5 nm. Characteristic GMR curves was observed for this sample at room temperature, as shown in Figure 3.6, which indicates a strong antiferomagnetic coupling between successive magnetic layers.[28,29] XRD was also employed to characterize this sample, the results are shown in Figure 3.7. The diffraction pattern show reflections of a fcc structure for copper with strong (111) intensity at 43.405^{o} and weak (100) intensity at 50.45^{o}, the diffraction peak for the silicon substrate was observed at 69.24^{o}. The corresponding FWHM for the three peaks are 0.361^{o}, 0.539^{o} and 0.089^{o}. Because the cobalt has the capability to absorb x rays, no diffraction peak for cobalt was obtained. The large ratio of the (111) diffraction intensity over (100) intensity indicated that the as-deposited CoCu/Cu multilayer in the present system exhibited a preferable growth of the (111) crystal structure, despite the fact that the silicon substrate

has a (100) structure. This suggested that the thin films didn't grow epitaxially, different from those deposited on copper foils.

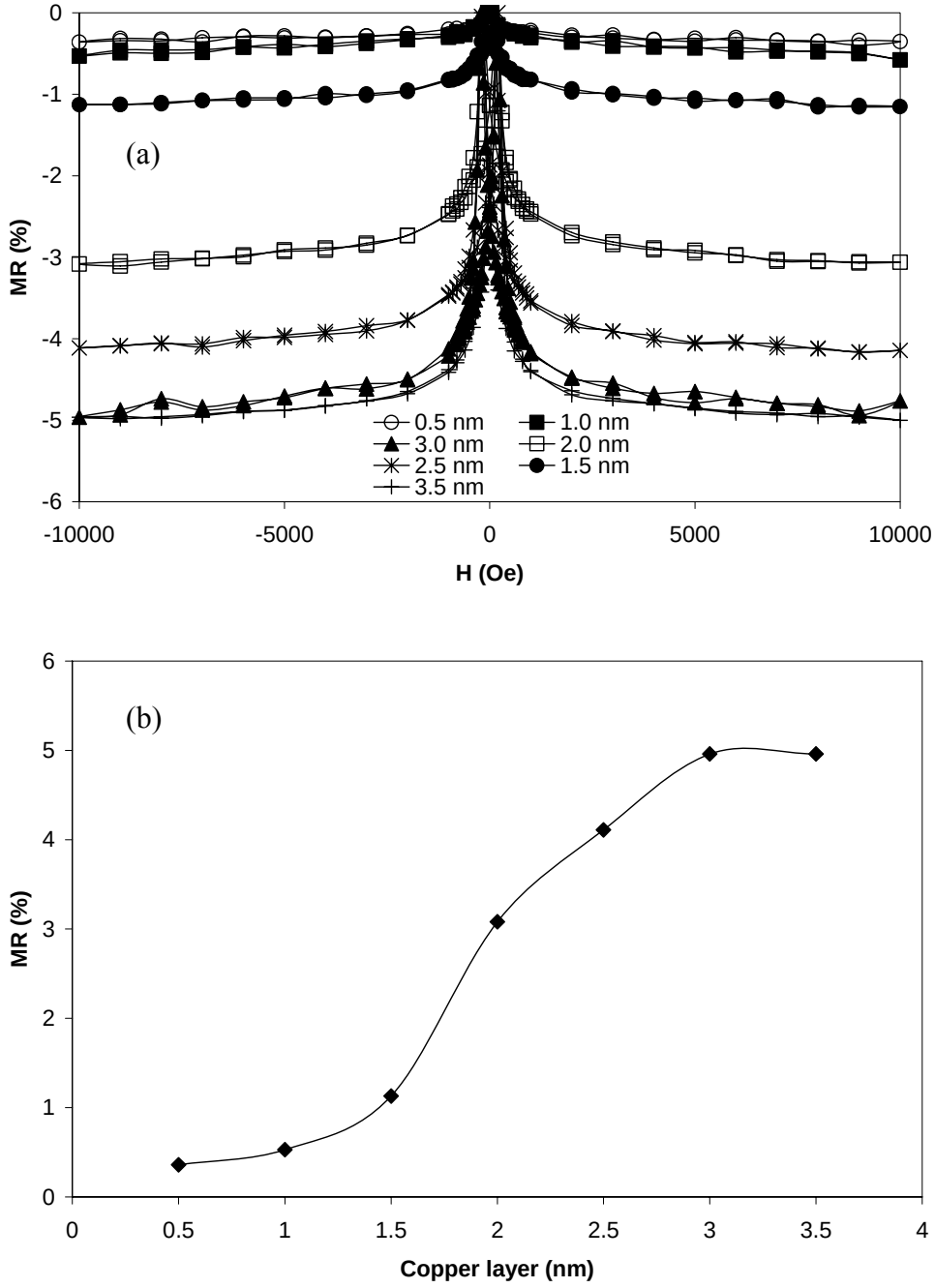

Figure 3-6 (a) Magnetoresistance of Co(2.5 nm)/Cu(x nm)$_{1000}$, (b) saturation magnetoresistance for samples Co(2.5 nm)/Cu(x nm)$_{1000}$

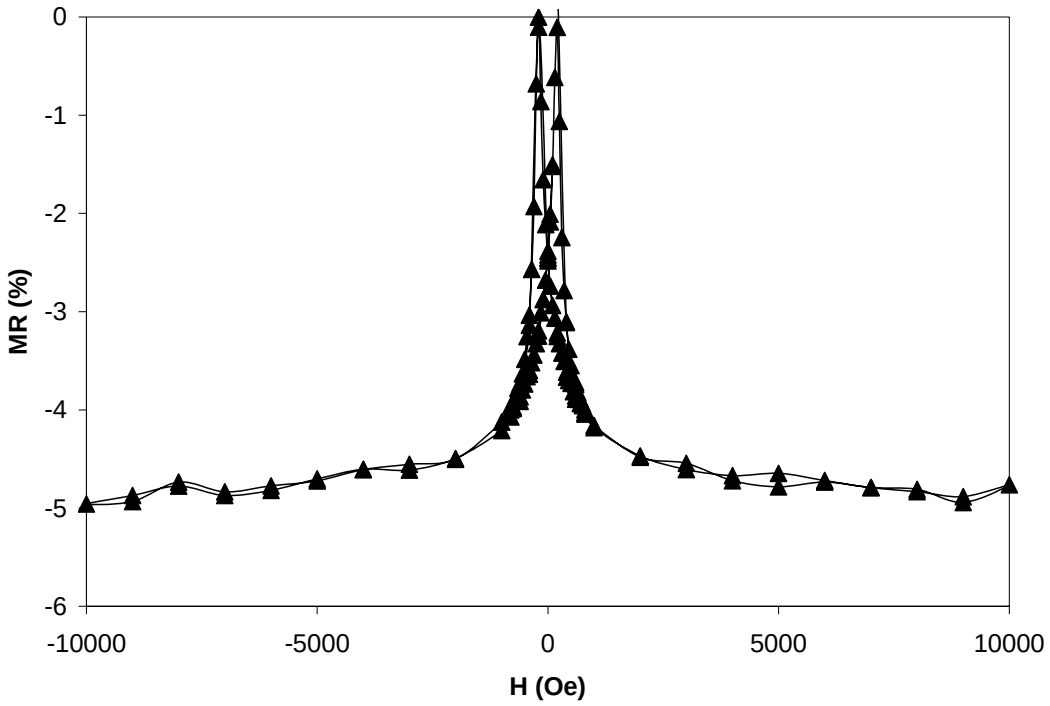

Figure 3-7 Magnetoresistance of Co(2.5 nm)/Cu(3 nm)$_{1000}$

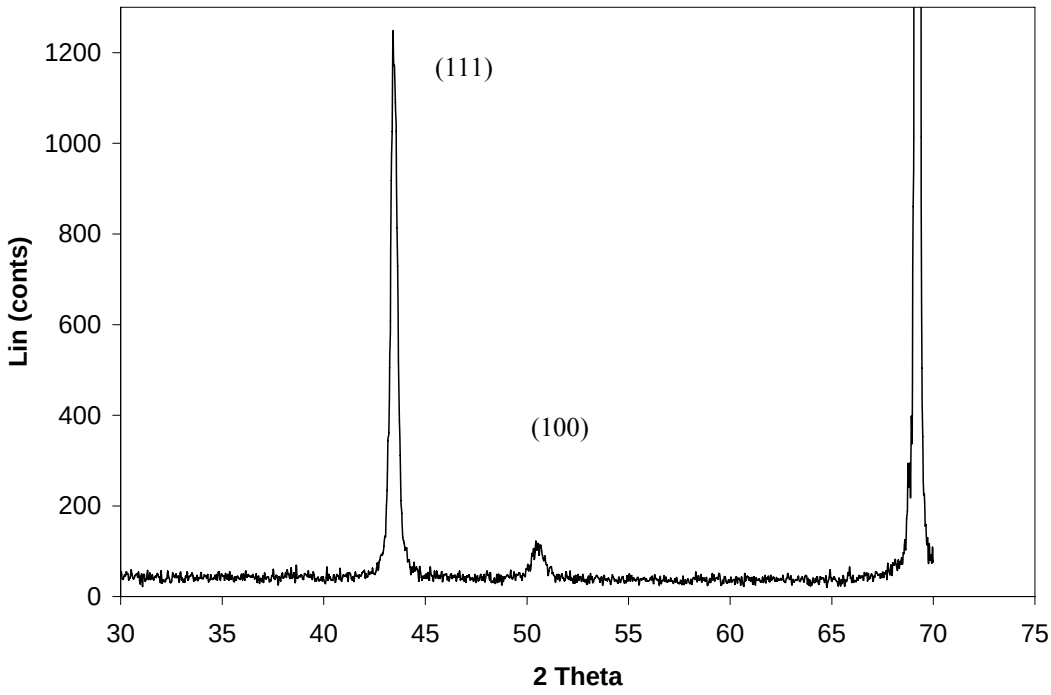

Figure 3-8 XRD of Co(2.5 nm)/Cu(3 nm)$_{1000}$

3.5.2 pH

It is known that the electrolyte pH is an important parameter that affects the GMR of electrodeposited multilayer thin films. CoNiCu/Cu multilayers deposited at an electrolyte pH of 1.8 exhibited better GMR property than those obtained at pH of 3.3.[19] In order to determine the most appropriate pH value to obtain better magnetoresistance, a series of CoCu/Cu multilayers were grown from the electrolyte with different pH, and then their magnetoresistance properties were investigated.

Figure 3.9 shows the results for the multilayer $[Co(2.5nm)/Cu(3\ nm)]_{1000}$ deposited at pH 2.8, 3.0, 3.2 and 3.4. Figure 3.9(a) shows the magnetoresistance behavior for each sample. The sensitivities are similar for all four samples. Figure 3.9(b) shows how the saturation magnetoresistance property changes with pH. The magnetoresistance varies in an oscillatory manner with the electrolyte pH. The large magnetoresistance value of 5 % was obtained at pH 3.0, and only 1.2 % and 2.5 % were obtained at higher electrolyte pH of 3.2 and 3.4. A magnetoresistance of 3.3 % was observed at the electrolyte pH of 2.8. When the pH was lower than 2.8, the quality of the thin film was poor because of the hydrogen evolution. A lot of holes were observed visually at the surface of the thin films. The electrolyte pH in the present system has a different influence on magnetoresitance property compared to the reported literature source where pH of 1.8 was better than pH of 3.3.[19] Therefore, lower pH is not always a favorable choice for electrodeposited multilayers. How the electrolyte pH influences the magnetoresistance depends on the electrolyte and the plating conditions used. The pH can affect the metal deposition mechanism, and change the hydrogen evolution rate.

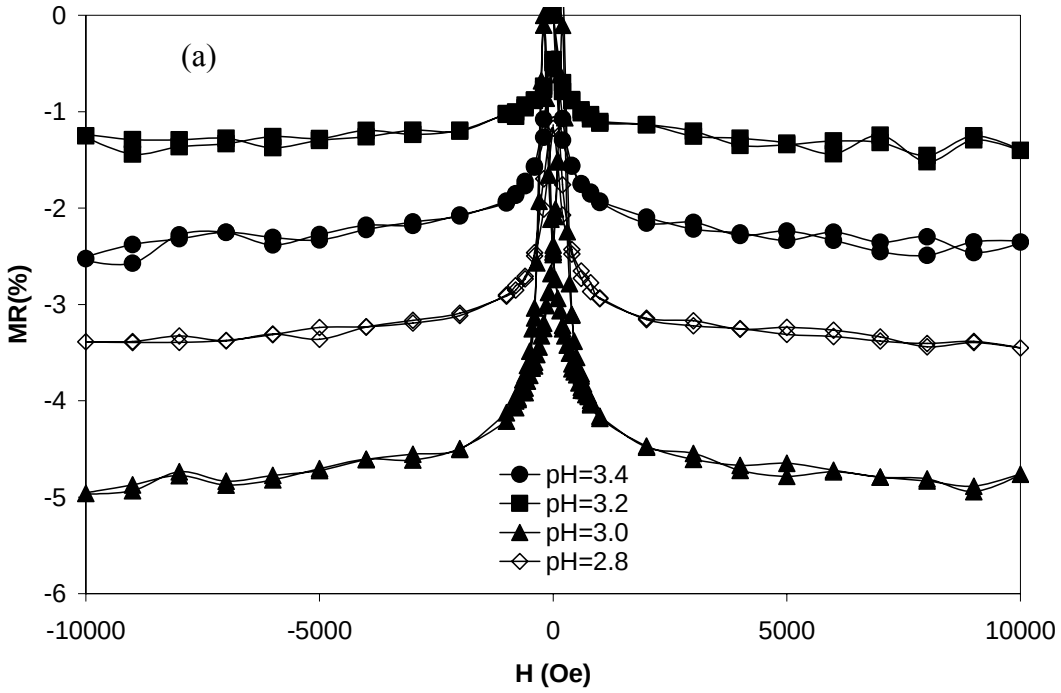

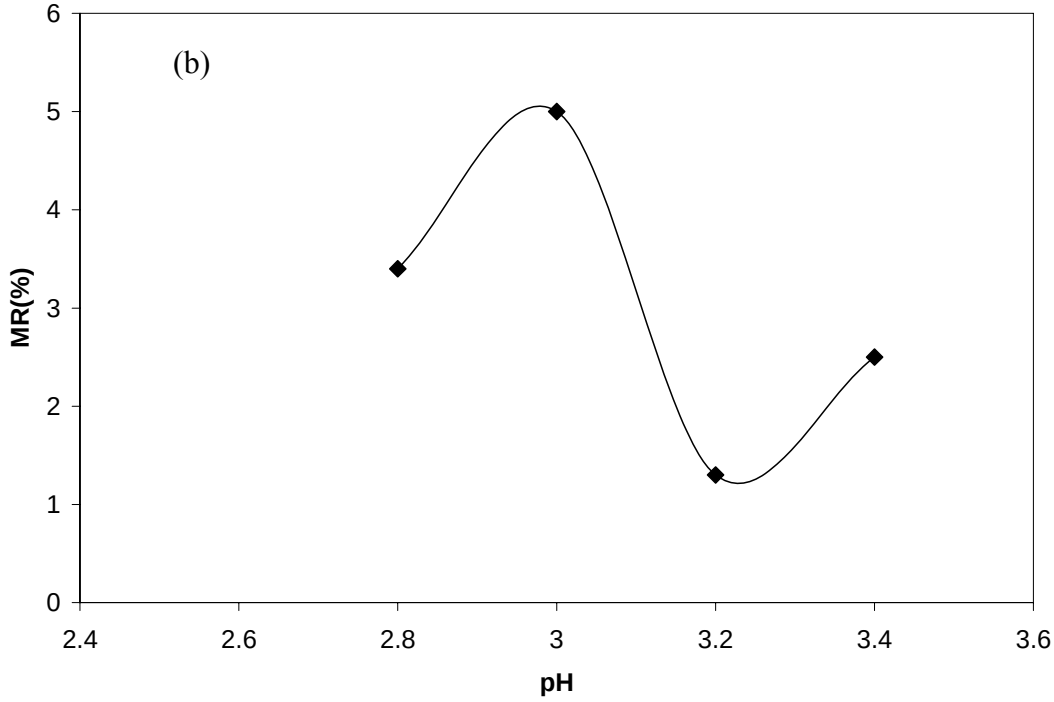

Figure 3-9 (a) Magnetoresistance of Co(2.5 nm)/Cu(3 nm)$_{1000}$ deposited at different pH (b) saturation magnetoresistance for samples Co(2.5 nm)/Cu(3 nm)$_{1000}$

3.5.3 Bilayer Number

The total thickness of the multilayer or the bilayer number plays an important role in the magnetoresistance behavior. The surface roughness, surface morphology, crystallite size will change with the growth of the multilayered thin films. It was assumed in the literaturethat GMR of CoCu/Cu multilayers decreased with increasing bilayer number because of the loss of interface structure and crystallographic orientation. Therefore, most of the electrodeposited multilayers in the literatures have been fabricated with a small bilayer number, especially for those thin films grown on silicon substrate.[3, 8, 10, 31] The typical bilayer numbers are 20, 50 or 100. In our study, we have focused on thicker thin films deposited onto silicon with larger bilayer numbers of 300, 500, 700 and 1000.

The results are shown in Figure 3.10. Figure 3.10(a) is the magnetoresistance behavior with a change of magnetic field; the magnetoresistance values were similar (-2.7 %) for the samples with bilayer numbers of 300, 500 and 700, and larger value of 5 % was obtained at bilayer number of 1000. Figure 3.10(b) is a plot of the saturation magnetoresistance value with the bilayer number. The magnetoresistance increases with an increase of bilayer number. This trend is inconsistent with the literature.[7,30] The reason for this phenomenon may be due to the change in quality of the thin films. At the start of deposition, the first few layers may not be continuous, since only a small amount of nuclei populate the surface. Experiments have confirmed that if the bilayer number was less than 300, the film surface looks visually poor, suggesting that the layers may not be ideally flat and continuous. When the nodules overlap and form a continuous film, multilayers are then formed. Thus there is a competition between the nucleation on Si

versus the ensuing metal. A larger bilayer number resulted in a better magnetoresistance property.

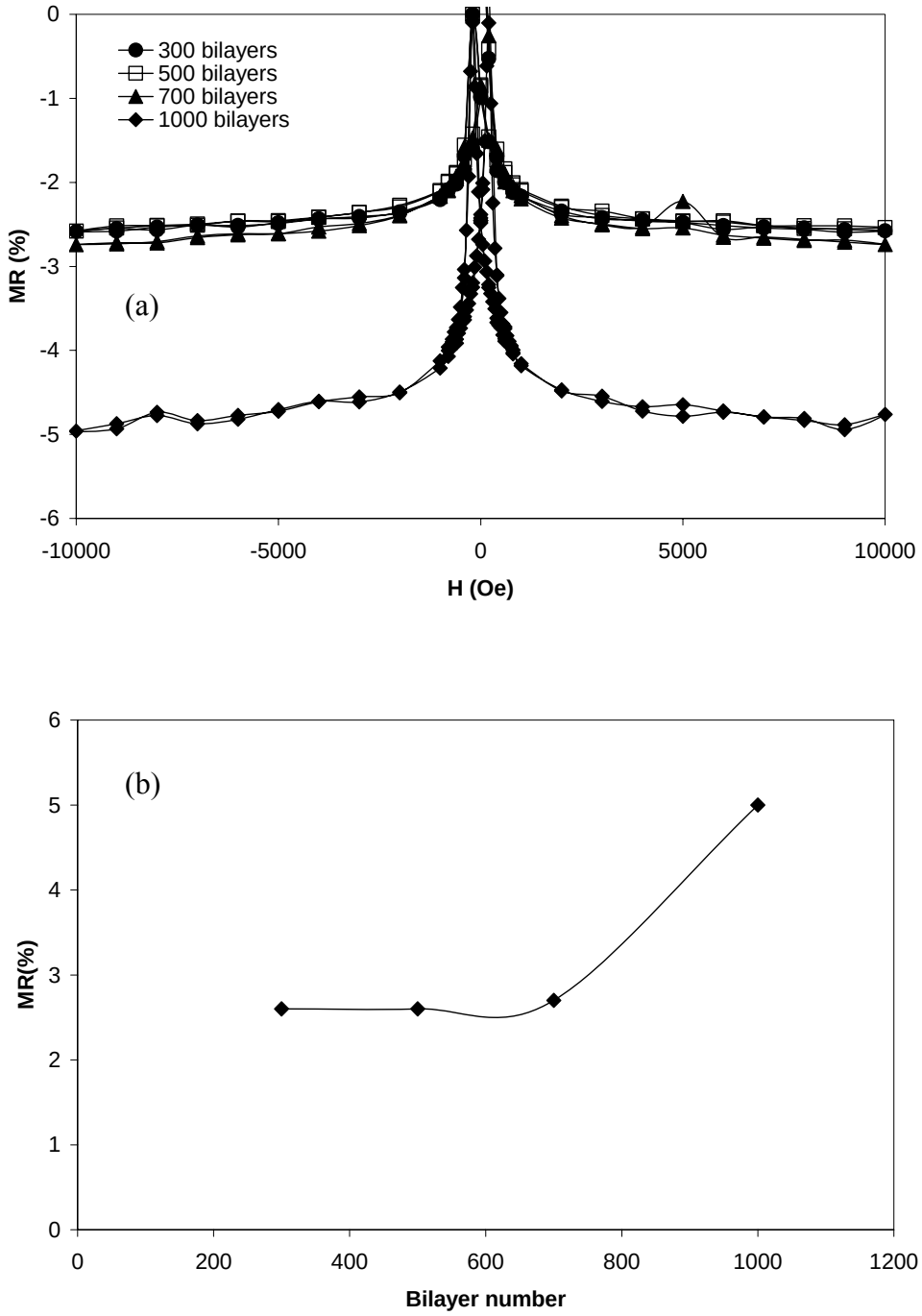

Figure 3-10 (a) Magnetoresistance of Co(2.5nm)/Cu(3nm)$_{1000}$ deposited at different bilayer numbers, (b) saturation magnetoresistance for samples Co(2.5 nm)/Cu(3nm)$_x$

3.5.4 Seed Layer

As discussed in Chapter 2, the choice of substrate has a significant effect on the microstructure and magnetoresistance property of multilayers. The silicon wafer[3,10,31] is a popular substrate because it provides the possibility to integrate the multilayers into semiconductor products. Direct electrodeposition of magnetoresistance multilayers on a silicon wafer without any seed layer is the first choice because this method avoids the extra sputtering process. However, to date, only one literature study[31] reported successful deposition of CoNi/Cu multilayers onto a silicon wafer with magnetoresistance value ove 10 %. Most of the multilayers were electrodeposited on silicon wafers with a 10-100 nm copper seed layer in order to obtain magnetoresistance. No literatures were published to compare the magnetoresistance difference between those thin films deposited onto silicon wafer with a Cu/Ti seed layer and without a Cu/Ti seed layer. In our experiments, we employed the same condition to deposit two thin films on these two different substrates.

The magnetoresistance characterization results are shown in Figure 3.11. Both the magnetoresistance value and sensitivity were improved when a copper seed layer was sputtered onto the silicon substrate before electrodeposition. The reason is attributed to two aspects. One is that the copper seed layer reduces the diffusion of the atoms into the silicon wafer as a barrier layer. A similar explanation was proposed by Parkin *et al.,*[33] who found that an Fe buffer layer sputtered onto a Cu seed layer can inhibit the diffusion of Cu atom into the silicon wafer and therefore make the interface of the multilayer flatter and sharper. Another aspect is that the nucleation process should be different on the copper seed layer and silicon wafer. This difference probably resulted in a change of the

the microstrucuture and further influenced the magnetoresistance behavior of the thin films.

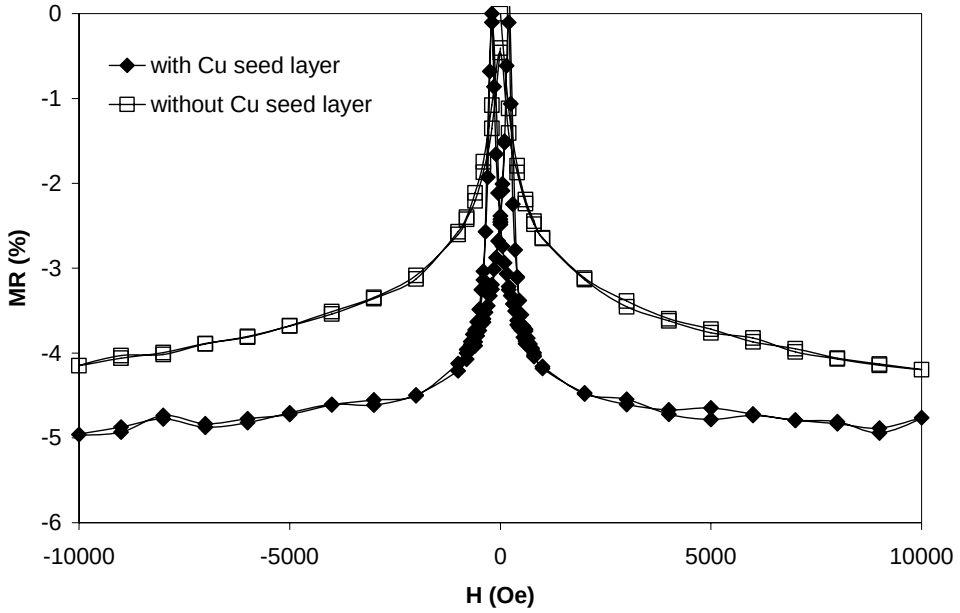

Figure 3-11 Magnetoresistance of Co(2.5 nm)/Cu(3 nm)$_{1000}$ deposited with and without the Cu seed layer

3.5.5 Nickel Addition to Electrolyte

Ni/Cu multilayers have been shown that they can be electrodeposited with a very well-defined layer structure.[34] However, this system was not expected to have a large magnetoresistance,[35] because of the low magnetic moment of Ni. In contrast, Co/Cu multilayers obtained from vacuum deposition methods had the largest reported magnetoresistance values,[23,36] but not in electrodeposited Co/Cu multilayers. In electrodeposition, one reason for the lower values maybe due to the problem of cobalt dissolution during the onset of copper deposition. One solution[18,25,32,37] to this problem is to add cobalt ions to the electrolytes used for Ni/Cu multilayer electrodeposition, with the aim to have well-defined structures as well as larger magnetoresitance than that obtained

with nickel alone. Although the concentration of the cobalt ions are usually smaller than that of the nickel ions, the magnetic layer consist of more cobalt elements because of the anomalous electrodeposition phenomena. Larger magnetoresistance in the range of 10 %-20 % was obtained for these CoNi/Cu multilayers.[25,32,37] Nabiyouni *et al*.[18] systematically investigated the effect of the ratio of cobalt and nickel in the magnetic layers on the magnetoresistance behavior. The amount of cobalt in the deposit was increased by increasing the cobalt ion concentration in the electrolyte with nickel sulphamate. A continuous increase of the magnetoresistance with the increase of Co-content was observed for the NiCu(3nm)/Cu(1nm) multilayers.

In our work, a different method was employed to study the nickel effect on the CoCu/Cu multilayers. Different concentrations of nickel ions were added into the cobalt-copper electrolyte. Nickel sulfate with concentrations of 0, 0.005, 0.01, 0.015, 0.02 and 0.03 M was used because one literature report[38] found that adding nickel sulfate to a sulfate electrolyte helped to inhibit the dissolution of cobalt and further enhance magnetoresistance. The plating time for the cobalt layer and copper deposition was kept at 400 ms and 78 s, the same as those parameters used previously. The cobalt-rich layer thickness may deviate slightly from the calculated value of 2.5 nm because of the addition of nickel. The composition of the magnetic layer should also vary with the different concentration of nickel sulfate.

The magnetoresistance characterization results for this series of samples are shown in Figure 3.12. Compared to the original thin films deposited without nickel, the entire series of multilayer samples obtained with nickel sulfate in the electrolyte exhibited a worse magnetoresistance behavior, (Figure 3.12(a)) while the saturation magnetic field

are similar for all of the six samples. The relation of magnetoresistance value with the concentration of nickel sulfate was summarized in Figure 3.12(b). At low concentration, the magnetoresistance varies around 1 %. Therefore, addition of nickel sulfate in the electrolyte has a negative effect on the magnetoresistance behavior.

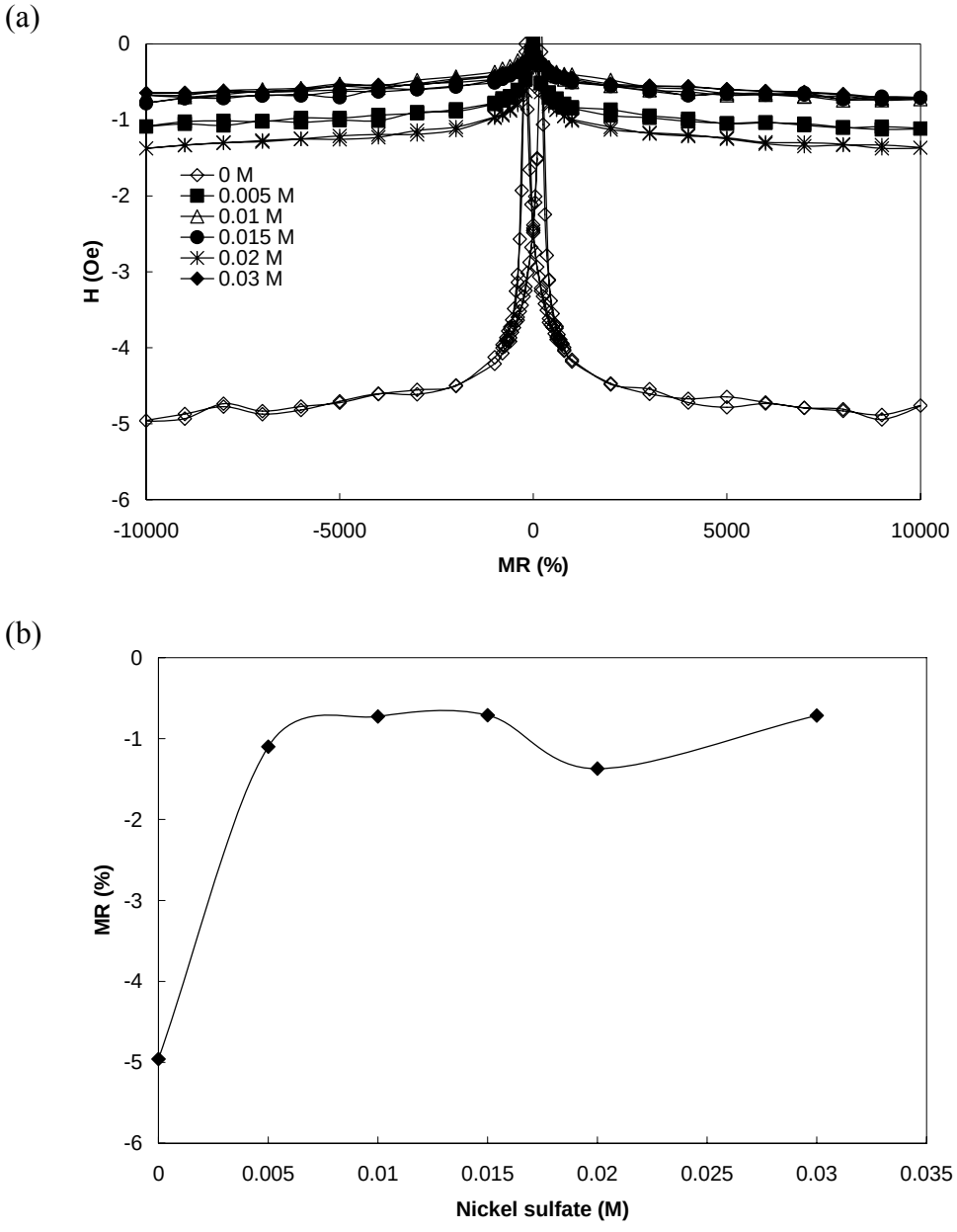

Figure 3-12 (a) Magnetoresistance of Co(2.5 nm)/Cu(3 nm)$_{1000}$ deposited in electrolyte with different concentration of $NiSO_4$, (b) saturation magnetoresistance of Co(2.5nm)/Cu(3nm)$_{1000}$ with different concentration of $NiSO_4$ in the electrolytes

To date, most of the CoNi/Cu multilayers were deposited in an electrolyte containing the nickel sulphamate. Some studies[39,40] reported that there was no displacement reaction between nickel and cobalt for NiCo/Cu multialyers deposited from a nickel sulphamate electrolyte, although one literature study[41] disagreed with this point by comparing a calculated and the measured composition in nickel-copper alloys.

A similar process was utilized to investigate the nickel sulphamate effect on magnetoresistance compared to deposits fabricated from a nickel sulfate electrolyte. The concentrations of the nickel sulphamate were 0, 0.005, 0.01, 0.015, 0.02 and 0.03 M. The measured magnetoresistance is shown in Figure 3.13. All of these samples deposited with nickel sulphamate didn't exhibit a saturated magnetoresistance behavior, therefore, the sensitivity of these samples decreased (Figure 3.13(a)) The magnetoresistance has an oscillatory trend with an increase of the nickel sulphamate in the electrolyte, and the magnetoresistance values become smaller than that of the original sample.(3.13(b)).

Comparing Figure 3.12 and Figure 3.13, it was notable that both the nickel sulfate and the nickel sulphamate didn't improve the magnetoresistance, which was inconsistent with some literature reports.[38] Additionally both kinds of nickel ions influence magnetoresistance of the thin films in different ways. Although magnetoresistance became worse for both systems, nickel sulphamate is better than the nickel sulfate for CoNi/Cu multilayers electrodeposition, the reason is likely due to the different magnetic layer composition and layer thicknesses, which resulted from the different electrodeposition process.

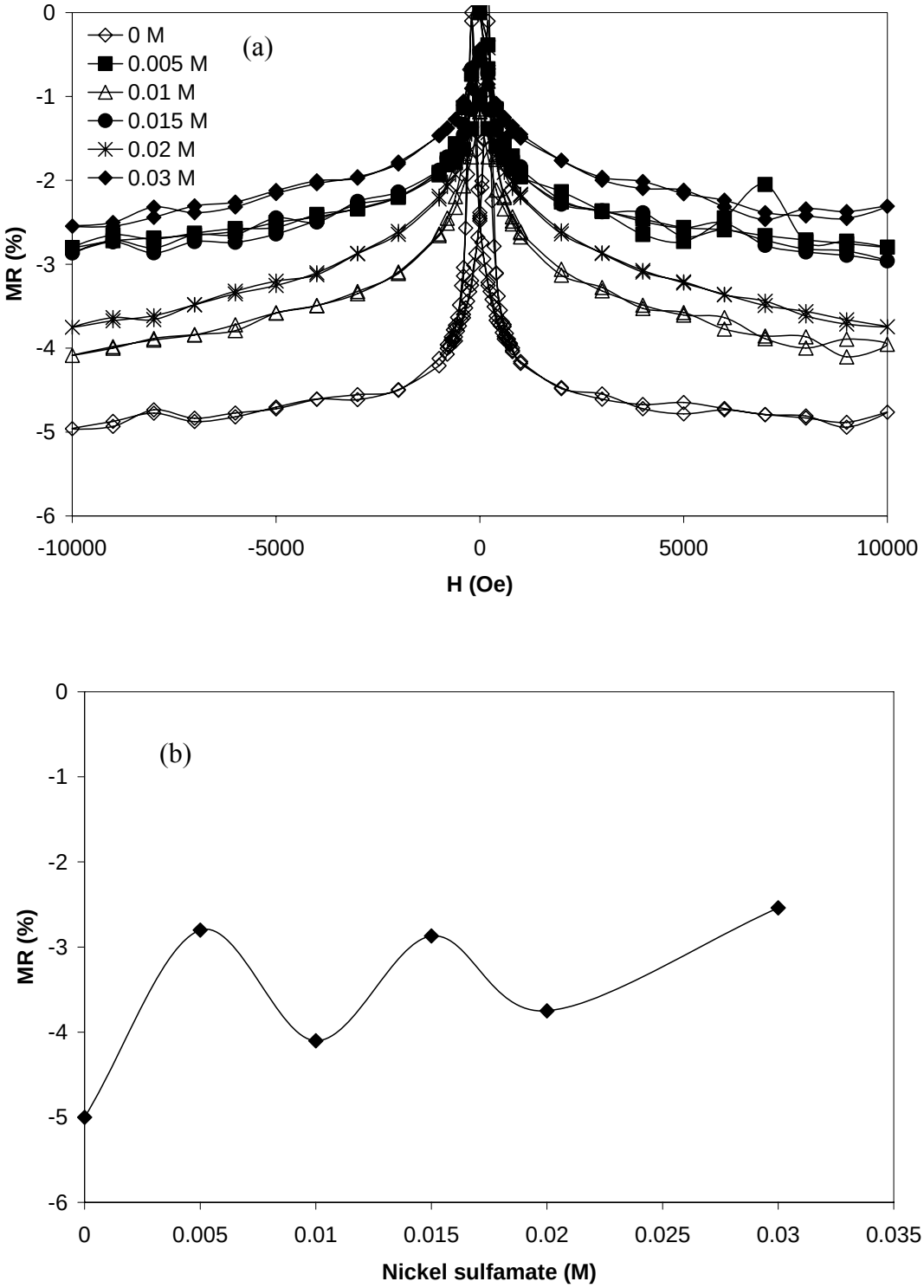

Figure 3-13 (a) Magnetoresistance of Co(2.5 nm)/Cu(3 nm)$_{1000}$ deposited in electrolyte with different concentration of nickel sulfamate, (b) maximum magnetoresistance of Co(2.5 nm)/Cu(3 nm)$_{1000}$ with different concentration of nickel sulfamate in the electrolytes

3.6 Summary

Magnetoresistance of eletrodeposited CoCu/Cu multilayers strongly depended on the cobalt and copper layer thickness, however, no clear oscillatory behavior between the magnetoresistance and the copper layer thickness has been found. The sensitivity of the multilayers at cobalt layer thickness of 2.5 nm was much better than those at 1.25 nm and 19 nm. Over 5 % magnetoresistance was observed for the multilayer with copper thickness of 3 nm and cobalt layer thickness of 2.5 nm. The electrolyte pH of 3.0 is the best value with regard to the magnetoresistance value and the thin film quality. Larger bilayer number was favorable because the total continuity of the thin film on the silicon wafers was improved. A seed layer on the silicon wafer was important to improve the nucleation and further to improve the magnetoresistance. The influence of nickel ions into the electrolyte on the magnetoresistance depended on the nickel source. Nickel sulphamate was better than nickel sulfate, however, the magnetoresistance of the multilayers was not improved by adding a small amount of either nickel sulfate or nickel sulphamate.

3.7 References

1. T. R. Mcguire, and R. I. Potter, *IEEE Transactions on Magnetics*, **11**, 1018 (1975).

2. W. Schwarzacher, and D. Lashmore, *IEEE Transactions on Magnetics*, **32**, 3133 (1996).

3. M. Shima, L. Salamanca-Riba, R. McMichael, andT. Moffat, *Journal of the Electrochemical Society*, **148**, C518 (2001).

4. E. Gomez, , A. Labarta, A.Llorente and E. Valles, **153**, 261 (2002).

5. M. Shima, L. Salamanca-Riba, T. Moffat and R. McMichael, *Journal of Magntism and Magnetic Materials*, **199**, 52 (1999).

6. E. Chassaing, , *Journal of the Electrochemical Society*, **148**, C690 (2001).
7. L. Peter, Z. Kupay, K. Cziraki, J. Padar, J. Toth, I. Bakonyi,. *Journal of Physical Chemistry B*, **105**, 10867 (2001).

8. O. Kasyutich, W. Schwarzacher, V. Fedosyuk, P. Laskarzhevskiy, and A. Masliy, *Journal of the Electrochemical Society*, **147,** 2964 (2000).

9. G. Nabiyouni and W. Schwarzacher, *Journal of Magnetism and Magnetic Materials*, **156,** 355 (1996).

10. S. Lenczowski, C. Schonenberger, M. Gijs, and W. Dejonge, *Journal of Magnetism and Magnetic Materials*, **148**, 455 (1995).

11. N. V. Myung, B. Y. Y., M. Schwartz, and K. Nobe. *Electrochemical Society Proceedings,* **154** (2000).

12. Y. Ueda, N. Hataya and H. Zaman, *Journal of Magnetism and Magnetic Materials*, **156**, 350 (1996).

13. E. Chassaing, A. Morrone and J. Schmidt, *Journal of the Electrochemical Society*, **146**, 1794 (1999).

14. M. Shima, L. Salamanca-Riba, R. McMichael and T. Moffat, *Journal of the Electrochemical Society*, **149**, C439 (2002).

15. A. M. Shukh, D. H. Shin and H. Hoffmann, *Journal of Applied Physics,* **76**, 6507 (1994).

16. V. Nikitenko, V. S Gornakov, L. M.Dedukh, A. F. Khapikov, T. P.Moffat, A. J. Shapiro, R.D. Shull, M. Shima, L. Salamanca-Riba,, *Journal of Magnetism and Magnetic Materials*, **199**, 477 (1999).

17. S. S. P. Parkin, *Annual Review of Materials Science*, **25**, 357 (1995).

18. G. Nabiyouni, W. Schwarzacher, Z. Rolik and I. Bakonyi, *Journal of Magnetism and Magnetic Materials*, **253**, 77 (2002).

19. M. Alper, W. Schwarzacher and S. Lane, *Journal of the Electrochemical Society,* **144**, 2346 (1997).

20. Q. Huang and E. Podlaha, *Journal of the Electrochemical Society*, **151**, C119 (2004).

21. Y. Jyoko, S. Kashiwabara and Y. Hayashi, *Journal of the Electrochemical Society,* **144**, L193 (1997).

22. E. Chassaing, *Journal of the Electrochemical Society*, **144**, L328 (1997).
23. S. S. P. Parkin, R. Bhadra, and K. P. Roche, *Physical Review Letters*, **66**, 2152 (1991).

24. D. Mosca, F. Petroff, A. Fert, P. A. Schroeder, W. P. Pratt, R. Laloee, *Journal of Magnetism and Magnetic Materials*, **94**, L1 (1991).

25. S. Hua, D. S. Lashmore, L. Salamancariba, W. Schwarzacher, L. J. Swartzenruber, R. D. Mcmichael, L. H. Bennett, R. Hart, *Journal of Applied Physics*, **76**, 6519 (1994).

26. D. Lashmore, S. Hua and Y. Zhang, *Abstracts of Papers of the American Chemical Society*, **208**, 184 (1994).

27. S. K. J. Lenczowski, C. Schonenberger, M. A. M. Gijs and W. J. M. Dejonge, *Journal of Magnetism and Magnetic Materials*, **148**, 455 (1995).

28. C. H. Marrows, N. Wiser, B. J. Hickey and T. P. A.Hase, *Journal of Physics-Condensed Matter,* **11**, 81 (1999).

29. C. H. Marrows and B. J. Hickey, *Physical Review B*, **59**, 463 (1999).

30. R. Lopez, J. Herreros, A. Garcia-Arribas, J. M. Barandiaran and M. L. Fdez-Gubieda, , *Journal of Magnetism and Magnetic Materials*, **197**, 53 (1999).

31. A. O'Keeffe, O. Kasyutich, W. Schwarzacher, L. de Oliveira and A. Pasa, *Applied Physics Letters*, **73**, 1002 (1998).

32. M. Alper, K. Attenborough, V. Baryshev, R. Hart, D. S. Lashmore, W. Schwarzacher, *Applied Physics Letters*, **63**, 2144 (1993).

33. S. S. P. Parkin, A. Mansour and G. P. Felcher, ‚*Applied Physics Letters*, **58**, 1473 (1991).

34. D. S. Lashmore and M. P. Dariel, *Journal of the Electrochemical Society*, **135**, 1218 (1988).

35. H. Itoh, J. Inoue and S. Maekawa, *Journal of Magnetism and Magnetic Materials*, **126**, 479 (1993).

36. S. S. P. Parkin, Z. G. Li and D. J. Smith, *Applied Physics Letters,* **58**, 2710 (1991).

37. R. Hart, P. Midgley, A. Wilkinson, and W. Schwarazcher, *Applied Physics Letters*, **67**, 1316 (1995).

38. J. Zhang, M. Moldovan, D. P.Young and E. J. Podlaha, *Journal of the Electrochemical Society*, **152**, C626 (2005).

39. S. Menezes, and D. P. Anderson, *Journal of the Electrochemical Society*, **137**, 440 (1990).

40. D. M. Tench and J. T. White, *Journal of the Electrochemical Society*, **137**, 3061 (1990).

41. P. Bradley, S. Roy and D. Landolt, *Journal of the Chemical Society-Faraday Transactions*, **92**, 4015 (1996).

CHAPTER 4. PULSE TRAIN DEPOSITION OF Co/Cu THIN FILMS

4.1 Introduction

Electrodeposition of magnetic multilayers as an alternative method to vacuum processes such as sputtering and molecular beam evaporation has been documented, as reviewed by Ross,[1] Schwarazher *et al*.[2] and Alper.[3] To date, GMR values from electrodeposited multilayers are still not comparable to those obtained by vacuum evaporation, which is ascribed to the different quality of the deposits. For example, GMR of electrodeposited multilayers are influenced by interfacial roughness, deposit crystallization, structural imperfection, layer composition, substrates preparation, electrolyte additives and preparation methods.[4-10] One common characteristic in the electrodeposition of multilayers is that the substrate has to be conductive. In order to measure GMR and avoid the current being shunted through the substrate, thin films can either be removed from the substrate [10, 11] or the multilayer deposit must be significantly thicker than the conductive regions of the substrate so that the multilayer resistance dominates. Typical GMR values obtained from electrodeposited Co/Cu multilayers onto silicon wafer are 5 %[12] and 14 %[6] at room temperature. The copper seed layer thickness is 40 nm and 20 nm, and the corresponding bilayer number is 100 and 50 so that the multilayer thickness is larger than the seed layer thickness.

Pulse plating has the capability to influence metallic crystallization by changing the competition between crystal growth and nucleation rate in single metal deposition.[13] Experimental results also verified that the crystallite size of a metal deposit can be decreased by pulsed deposition.[14-16] Recently Gupta *et al.*[17] reported that pulsed potential plating reduced the surface roughness of single copper or single cobalt deposits. They

also applied a pulsed potential train scheme, linking the two pulse formats to deposit smooth Co/Cu multilayers. However, there is a trade-off. A pulse deposition can also enhance the limiting current density of diffusion controlled species,[18,19] such as Cu, during the deposition of the Co rich layer. An increased amount of Cu in the magnetic layer is expected to decrease GMR.[20] In our work, the cobalt-rich layer current density or copper current density was pulsed during Co/Cu multilayer electrodeposition and the GMR characterized. To the best of our knowledge, the effect of pulse train deposition on magnetoresistance of Co/Cu multilayers has not been investigated and is presented here.

4.2 Experimental

Multilayered Co/Cu thin films were electrodeposited in a quiescent sulfate electrolyte containing 0.005 M CuSO4·5H_2O, 0.5 M $CoSO_4$·7H_2O, 0.543 M boric acid. Analytical grade reagents were used in the preparation of the solutions in distilled, de-ionized water. The pH value was adjusted to 3.0 with sulfuric acid and sodium hydroxide. A n-type (100) silicon wafer with a 100 nm Ti adhesion layer and a 20 nm Cu seed layer was employed as the cathode. The total exposed area is 1.6 cm^2. A platinum mesh was used as an anode.

Polarization curves were carried out with a Pine Instruments bipotentiostat, at a scan rate of 2 mV/s, and the potential was corrected for the ohmic drop, which is measured by impedance analysis with a Bas-Zahner IM6. A PINE bipotentiostat with an AMEL 5680 function generator were used to provide square current waveforms for regular pulsed deposition and an AMEL 7050 potentiostat/galvanostat were used to generate pulse train current.

Compositional characterization of the samples was performed by a Kevex Omicron energy-dispersive X-ray fluorescence analyzer (XRF) and a wavelength dispersive spectrometer (WDS) (Jeol JXA-733). The morphology of the deposits was obtained from a Scanning Electron Microscope (SEM) (Joel JSM-840A).

The magnetoresistance (MR) effect was measured with a 9T Quantum Design Physical Properties Measurement System (PPMS) using the standard four-point probe ac technique at 27 Hz with an excitation current of 1mA, according to [*R(H)-R(0)*]/*R(0)*, where *R(H)* is the resistance at an applied magnetic field *H*, and *R(0)* is the resistance when the external magnetic field is zero.

4.3 Results and Discussion

4.3.1 Electrolyte Characterization and Multilayer Deposition

The polarization curve has been shown in Figure 3-3. In multilayer deposition, a current density of -0.2 mA/cm^2 was chosen since it is lower than the limiting current value. The cobalt-rich layer was deposited under kinetic control at a current density of -20 mA/cm^2, The current efficiency calculated according to Faraday's law was 50 % for copper deposition and 86 % for the cobalt-rich deposition. The plating time specified for the copper and cobalt-rich layer thicknesses were calculated based on these efficiencies.

4.3.2 Regular Pulse

As discussed in Chapter 3, a series of multilayers with a constant cobalt-rich layer thickness of 2.5 nm and varying copper layer thickness were first plated with regular pulsed current. The bilayer number was 1000, ([Co(2.5 nm)/Cu(xx nm)$_{1000}$]). The plating time for cobalt-rich layer was constant at 400 ms and the plating time for the copper layer varied for different layer sizes. The magnetoresistance increased with an increase of the

copper layer thickness from 0.5 to 3.5 nm and reached a maximum value at a copper layer size of 3 nm, shown in Figure 3-6. At this layer size, the plating time was 78 s and the magnetoresistance was 5 % at a saturation field less than 3000 Oe, In Figure 3-7, the sensitivity at fields below 700 Oe was -0.006 %/Oe, indicative of quality multilayer quality and used as a basis for the pulse train examination.

4.3.3 Pulse Train

Since a maximum magnetoresistance was observed when the cobalt-rich thickness and copper layer thicknesses were equal, 2.5 and 3 nm respectively, these layer sizes were determined to evaluate the pulse train effect on magnetoresistance. In regular pulse deposition as shown in Figure 4-1(a), the plating time for 2.5 nm cobalt layers and 3 nm copper layers was 400 ms and 78 s, respectively. In pulse train control deposition, every single cobalt layer or copper layer was deposited by a pulse current while the copper or cobalt-rich layer was produced by constant current, as shown in Figure 4-1(b) and Figure 4-1(c). When the cobalt-rich layer was deposited by a series of pulses, the cycle number was: 1, 2, 4, 8, 10, and 20, keeping the total Co layer charge constant. Because the total plating time was maintained at 400 ms in order to obtain the 2.5 nm layer thickness, the corresponding on time for every cycle should vary from 400 ms, 200 ms, 100 ms, 50 ms to 20 ms while the off time was constant at 100 ms. Similarly, when the copper layer was produced by a series of pulses the corresponding on time for every cycle varied from 78, 13, 3, 1, 0.3, 0.1 and 0.05 s with corresponding cycle numbers of 1, 6, 26, 78, 260, 780, 1560, For the pulsed train copper layer, the off time for every cycle was also kept at 100 ms.

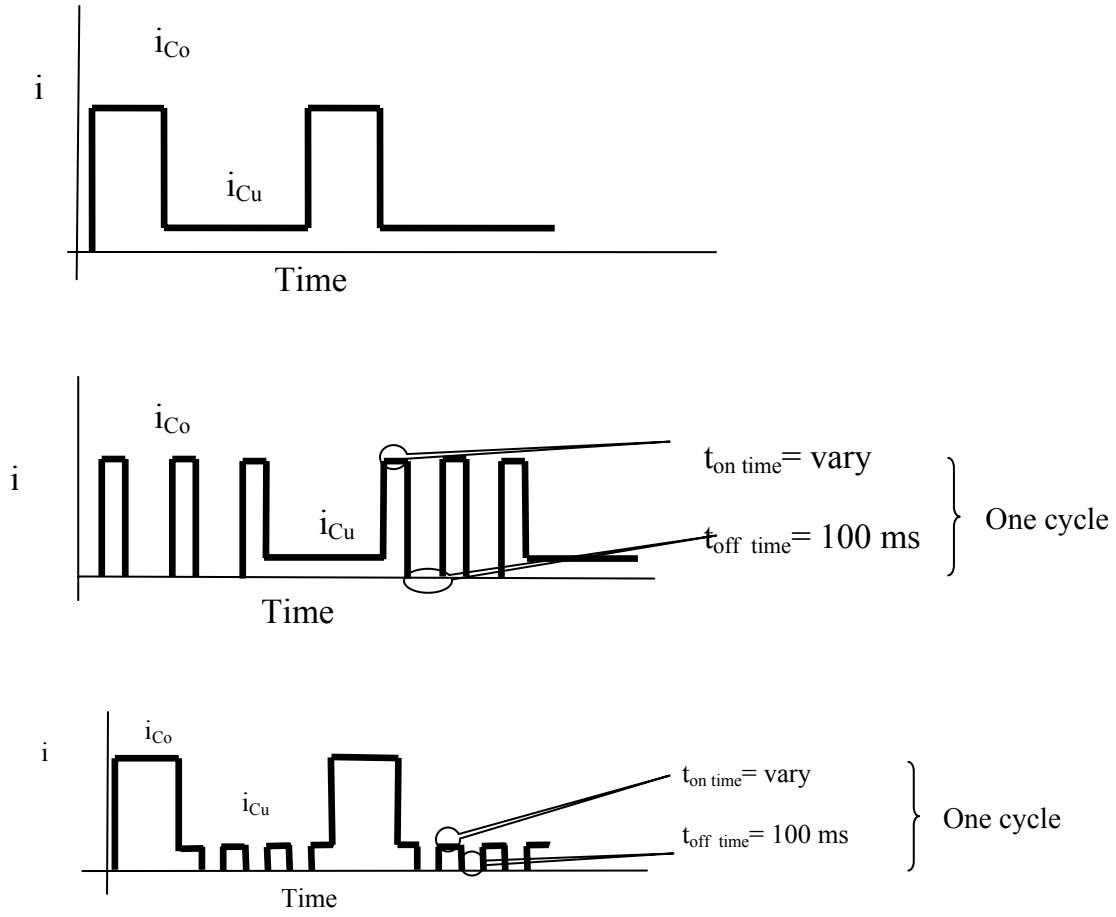

Figure 4-1 A sketch of (a) regular pulse deposition, (b) pulse train deposition on cobalt side, (c) pulse train deposition on copper side.

Figure 4-2 shows the magnetoresistance of $[Co(2.5\ nm)/Cu(3\ nm)]_{1000}$ when the cobalt layer was plated by a series of pulses with different cycle numbers, while the copper layer was deposited by a constant current. The magnetoresistance varied from 3.5 % to 7 % with saturation field between 2000-3000 Oe. In Figue 4-2 (b), the saturation GMR is expressed as a function of the duty cycle ($t_{on}/(t_{on} + t_{off})$). A maximum resistance value occurs in the data at a duty number of 0.333 (cycle number 8), an improvement over the regular pulse scheme. When the duty cycle number is smaller than this value, the magnetoresistance decreases and is less than the value obtained with the regular pulse.

(a)

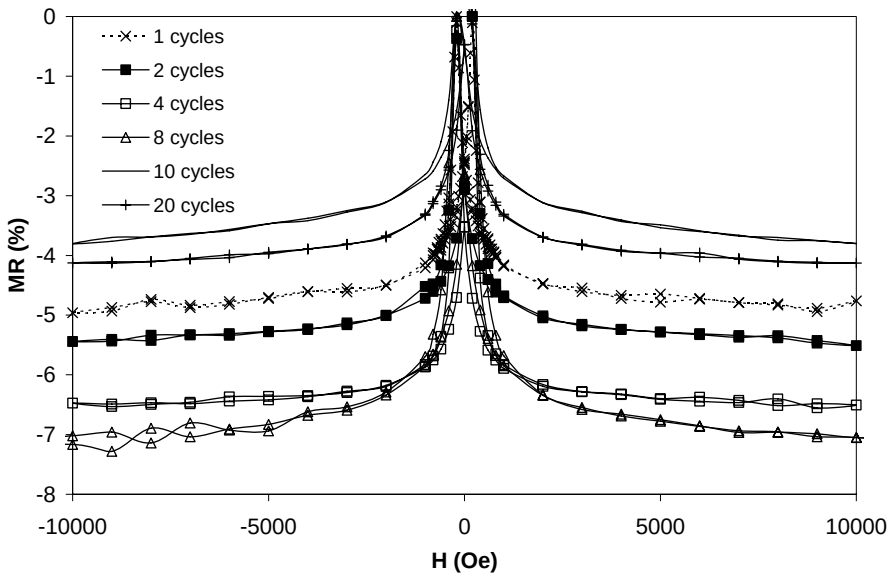

(b)

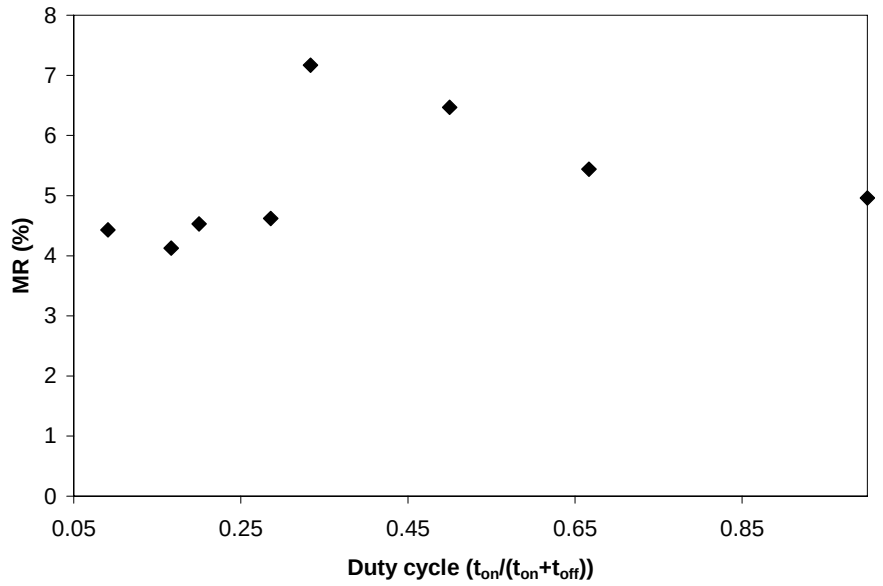

Figure 4-2 (a) Magnetoresistance of multilayers $[Cu(3\ nm)/Co(2.5\ nm)]_{1000}$ when cobalt layer was plated with pulse train current, (b) maximum magnetoresistance of multilayers $[Cu(3\ nm)/Co(2.5\ nm)]_{1000}$ with duty cycle when cobalt layer was plated with pulse train current.

Figure 4-3(a) is the magnetoresistance of $[Co(2.5\ nm)/Cu(3\ nm)]_{1000}$ when the copper layer was deposited by a series of pulses with different cycle numbers while the cobalt layer was plated with a constant current. The results showed that the

magnetoresistance varied slightly when the cycle number changed from 1, 6, 26, 78, 260, and 780 to 1560. All of the samples exhibited a magnetoresistance value in the range of 4.5- 5.0 % with a small change of saturation field. Similarly, the magnetoresistances of these multilayers were also plotted with duty cycle number as shown in Figure 4-3(b). The magnetoresistances were similar with a decrease of duty cycle.

Since the magnetoresistances of $[Co(2.5nm)/Cu(3nm)]_{1000}$ increased when the cobalt layer was plated by a series of pulses with a decrease of duty cycle in the range 1-0.333, SEM was carried out to investigate the morphology of deposits at 1 bilayer number and 1000 bilayer number, as shown in Figure 4-4 and Figure 4-5 for pulsed train Co layers. After deposition of 1 bilayer number, the density of the nodules decreased and the nodule size increased slightly with a decrease of duty cycle. However the nodule sizes were almost the same at every duty cycle after deposition of 1000 bilayers shown in Figure 4-5. These differences indicated that the pulse train currents had some effects on the morphology of the multilayers at the starting deposition though not a dramatic one.

(a)

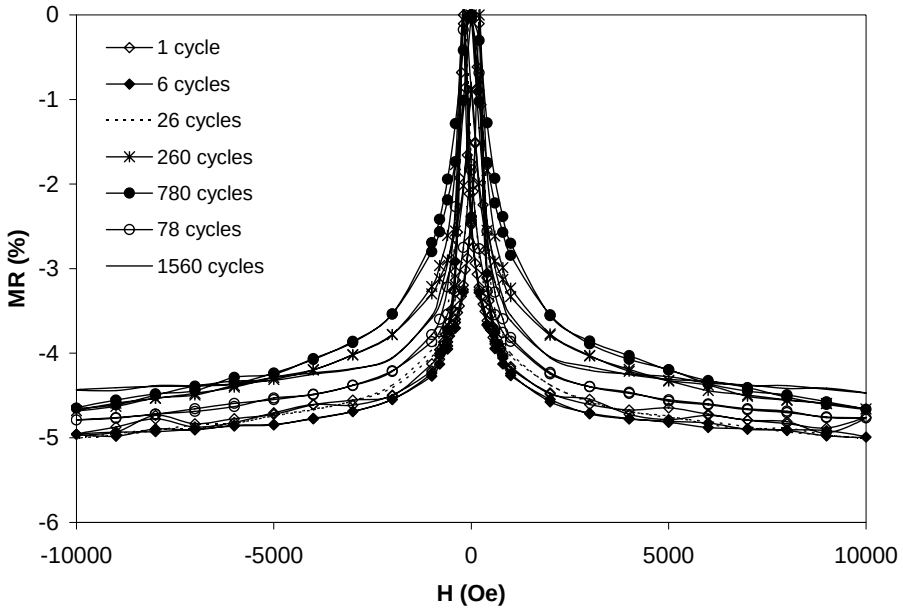

(b)

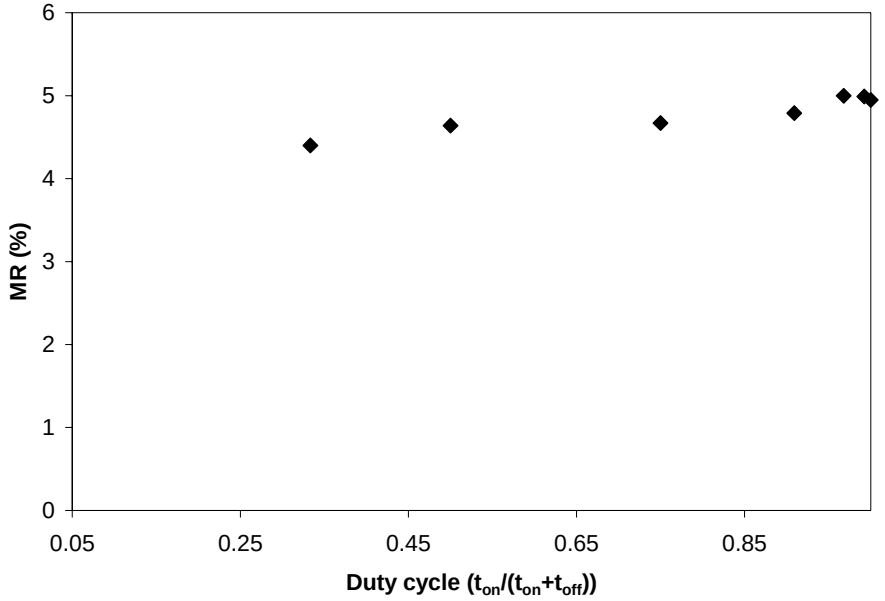

Figure 4-3 (a) Magnetoresistance of multilayers $[Cu(3\ nm)/Co(2.5\ nm)]_{1000}$ when copper layer was plated with pulse train current, (b) maximum magnetoresistance of multilayers $[Cu(3\ nm)/Co(2.5\ nm)]_{1000}$ with duty cycle when copper layer was plated with pulse train current.

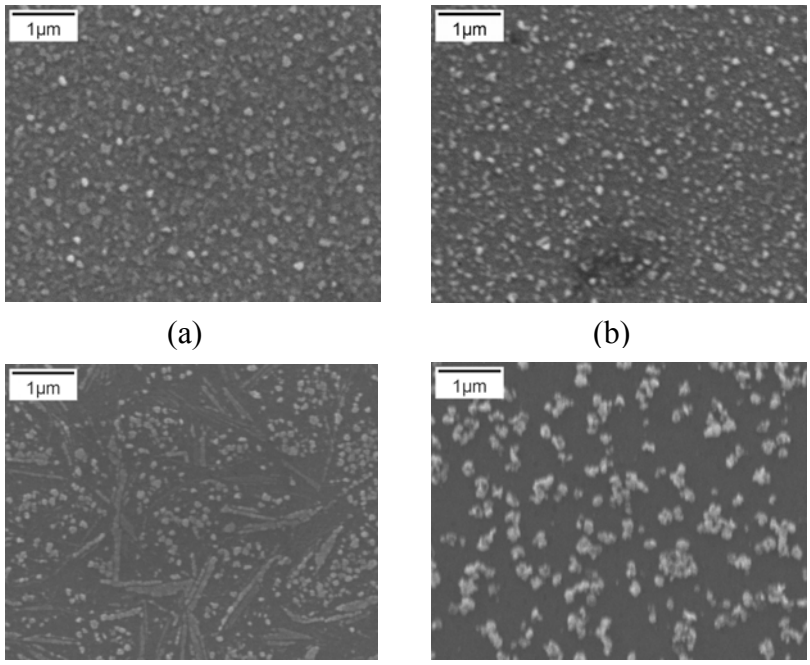

Figure 4-4 SEM of multilayer $[Cu(3\ nm)/Co(2.5\ nm)]_1$ at a duty cycle of (a) 1, (b) 0.666, (c) 0.5, (d) 0.333, cobalt layer was deposited by pulse train control.

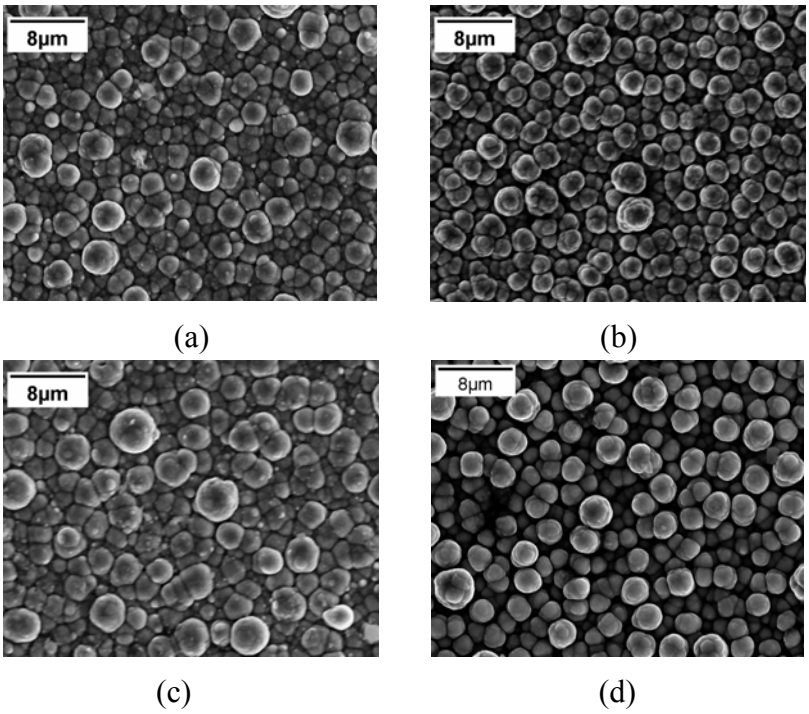

Figure 4-5 SEM of multilayer [Cu(3 nm)/Co(2.5 nm)]$_{1000}$ at a duty cycle of (a) 1, (b) 0.666, (c) 0.5, (d) 0.333, copper layer was deposited by pulse train control.

Cheh[19] solved on the electrodeposition diffusion controlled case of a single metal ion. He assumed that both the nonfaradaic component of the applied current and the migration of the metal ion were negligible and therefore the concentration of the metal ion is governed by Fick's second law of diffusion.

$$\frac{\partial C}{\partial t} = D\frac{\partial^2 C}{\partial^2 x^2} \tag{4.1}$$

with the following periodic boundary conditions

$$C=C_0 \qquad \text{for } t=0 \text{ and all } x \tag{4.2}$$

$$C=C_0 \qquad \text{for } t>0 \text{ and } x=\delta \tag{4.3}$$

$$D\left(\frac{\partial C}{\partial t}\right) = \frac{i}{nF} \quad \text{for } t>0 \text{ and } x=0 \tag{4.4}$$

The pulsed current density in Eq. 4.4 can be expressed as

$$i = i_p \text{ for } 0<t\leq t_1,\ t_2<t\leq t_3 \text{ etc.} \tag{4.5}$$

$$i = 0 \text{ for } 0<t\leq t_1,\ t_2<t\leq t_3 \text{ etc.} \tag{4.6}$$

where c is the concentration of metal ion, C_0 is its concentration in the bulk of the solution, D is the diffusion coefficient of the metal ion, δ is the thickness of the diffusion layer, n is the number of electrons transferred during the deposition process, F is the Faraday's constant, t is the time, and I is the applied current density. In the pulse deposition, the cyclic period is θ, the time when the current is on in period is θ, and the time when the current is off in the same period be θ_2. The cyclic period θ is given by

$$\theta = \theta_1 + \theta_2 = t_2 = (t_4 - t_2) = (t_6 - t_4), \text{ etc.} \tag{4.7}$$

where i_p is the pulsed current density, t_1, t_3, t_5 etc. are the times that describe the end of the "on" pulse, and t_2, t_4, t_6 etc. are the times that describe the end of the "off" or relaxation. The surface concentration of the metal ion is obtained by solving the equations from 4.1 to 4.7. The pulse limiting current is also obtained when the surface concentration is zero. The results showed that when a species is under mass transport control there is an increase in the limiting current density during the duration of the pulse, $(i_{p\text{-}c})_{\lim}$ compared to the dc counterpart, $(i_{d\text{-}c})_{\lim}$.

$$\frac{(i_{p-c})_{\lim}}{(i_{d-c})_{\lim}} = \left(1 - \frac{8}{\pi^2}\sum_{k=1}^{\infty}\frac{1}{(2k-1)^2}\frac{\exp\left[(2k-1)^2 a\theta_2\right]-1}{\exp\left[(2k-1)^2 a\theta\right]-1}\right)^{-1} \tag{4.8}$$

where $(i_{p\text{-}c})_{\lim}$ and $(i_{d\text{-}c})_{\lim}$ is the limiting current density for pulse plating and constant current plating, respectively. a is defined as $\pi^2 D/4\delta^2$, D is the diffusion coefficient of the metal ion, δ is the thickness of the steady state diffusion layer, θ_2 is the off time in one cycle period, θ is the total on time and off time in one cycle period. Similarly, Viswanathan *et al.*[21] developed a dimensionless equation for the calculation of the

limiting current density for intermittent potential. In order to reduce the number of linear equations to be solved, they also developed expressions for the average upper bound and lower bound limiting current density. This upper bound and lower bound method was used by Marlot *et al.*[22] to estimate the Mo content in the pulsed deposition of NiMo alloys.

Here, we employed equation 4.1 to calculate the pulse limiting current density by truncating the sum part to the term with a magnitude less than 10^{-15}. This is different from the numerical solution or asymptotic form adopted by Cheh. The diffusion layer thickness calculated from the steady state limiting current density was about 136 μm and the diffusion coefficient of the copper ions was assumed as 4.8×10^{-6} cm^2/s. The ratio of pulse limiting current density $(i_{p\text{-}c})_{\lim}$ over dc limiting current density $(i_{d\text{-}c})_{\lim}$ for the conditions in the electrolyte presented here is shown in Figure 4-6(a). The ratio of pulse limiting current density over dc limiting current density increase with a decrease in duty cycle. A ratio of 2.82 occurs at the duty cycle of 0.333 where the maximum magnetoresistance exists, suggesting a large increase in the Cu concentration in the Co-rich layer.

Overall composition analyses were measured by WDS on multilayers obtained by pulsed train control deposition of the cobalt layer, as shown in Figure 4-6(b). The overall copper deposit weight percentage increased with a decrease in duty cycle. This increase of copper composition is partly due to the increase of the pulse limiting current when the cobalt layer is deposited with a pulse train. The measured copper composition was compared to a calculated composition increased according to:

$$Cu(wt.\%) = \frac{(i_{Cu}.t_{Cu} + (i_{p-c})_{\lim}.t_{Co}).M_{Cu}}{(i_{Cu}.t_{Cu} + (i_{p-c})_{\lim}.t_{Co}).M_{Cu} + (i_{Co} - (i_{p-c})_{\lim}).t_{Co} * M_{Co}} \times 100 \qquad (4.9)$$

where i_{Cu} is the copper layer plating current density, t_{Cu} is the copper layer plating time, $(i_{p\text{-}c})_{lim}$ is the limiting current density for pulse plating, i_{Co} is the cobalt layer plating current density, t_{Co} is the cobalt layer plating time, M_{Cu} is copper molecular weight, M_{Co} is cobalt molecular weight.

Figure 4-6(b) shows that there is a close match between the measured and calculated values at large duty cycles in the range of 1 to 0.5, but deviates at duty cycles larger than 0.5. The mismatch can be attributed to the displacement reaction between cobalt deposit and copper ions during the relaxation time inherent to the pulse train deposition. Displacement reactions between Co and Cu have been widely reported.[2, 6, 23] Since the off time in every single cycle during the pulse train deposition was set constant as 100 ms with a variation of cycle number, a smaller duty cycle number corresponds to a longer total time for displacement to occur and more copper at the cobalt-rich layer interface. Therefore, there are two governing features affecting the increase of Cu in the multilayers during the pulse train deposition of the Co layers: i. increase of the Cu limiting current density during the Co-rich layer deposition resulting in more Cu within the layer and ii. longer time available for the displacement of Co by copper ions resulting in more Cu at the interfacial region. Therefore, although the pulse train deposition can improve magnetoresistance of multilayers at some duty cycles, it should be operated within suitable duty cycle range. The decrease in GMR occurs when there is a larger contribution from the displacement reactions with a concomitant increase in interfacial Cu concentration. The results presented here suggest that an increase in Cu within the Co-rich layer (not at the interface) can actually be beneficial.

(a)

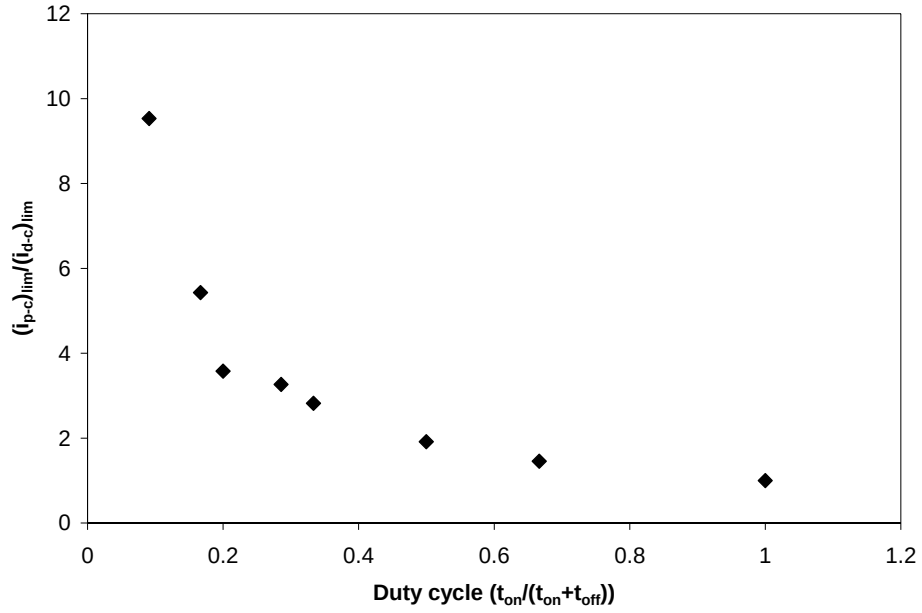

(b)

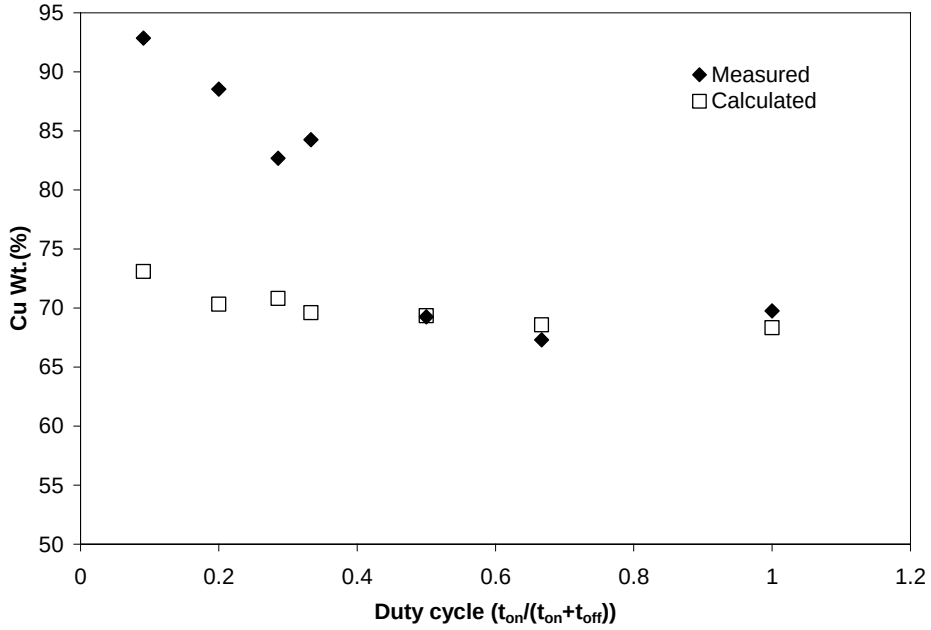

Figure 4-6 (a) Ratio of pulse train current limit over regular current limit when copper layer is plated by pulse train current, (b) measured and calculated overall copper component (weight percent) in multilayer $[Cu(3\ nm)/Co(2.5\ nm)]_{1000}$ when copper layer is plated by pulse train current.

4.4 Summary

A pulse train control deposition of the cobalt layer during the fabrication of

CoCu/Cu multilayers can improve magnetoresistance over the conventional square-wave pulse. A maximum 7-8 % magnetoresistance can be obtained with the decrease of duty cycle. Pulse train control deposition on copper layer has slight effect on magnetoresistance value. WDS analysis indicated that the copper concentration in the thin films increased with the decrease of duty cycle when cobalt layer was deposited with pulse train current. This increase resulted from the increase of pulse limiting current and the displacement reaction during the off time and was responsible for the decrease of magnetoresistance value of Co/Cu multilayers. The calculated overall copper concentration in the multilayer matched well with the measured concentration at large duty cycle number and mismatched at small duty cycle number, which can be ascribed to the displacement reaction between cobalt deposit and copper ion during the relaxation time.

4. 5 References

1. C. Ross, *Annual Review Materials*., **24**, 159 (1994).

2. W. Schwarzacher and D. Lashmore, *IEEE Transaction on Magnetics*, **32**, 3133 (1996).

3. M. Alper, in Nanostructured Magnetic Materials and Their Applications, D. Shi, B. Aktas., L. Pust, F. Mikailov, Editor, p. 111, Springer, Berlin (2002).

4. G. Nabiyouni and W. Schwarzacher, *Journal of Magnetism and Magnetic Materials*, **156**, 355 (1996).

5. O. Kasyutich, W. Schwarzacher, V. Fedosyuk, P. Laskarzhevskiy and A. Masliy, *Journal of the Electrochemical Society*, **147**, 2964 (2000).
6. S. Lenczowski, C. Schonenberger, M.Gijs, and W. Dejonge, *Journal of Magnetism and Magnetic Materials*, **148**, 455 (1995).

7. E. Chassaing, *Journal of the Electrochemical Society*, **148**, C690 (2001).

8. L. Peter, Z. Kupay, K. Cziraki, J. Padar, J. Toth, I. Bakonyi, *The Journal of Physical Chemistry B*, **105**, 10867 (2001).

9. A. Cziraki, M. Koteles, L. Peter, Z. Kupay, J. Padar, L. Pogany, I. Bakonyi, Uhlemann, M. Uhlemann, M. Herrich, B. Arnold, J. Thomas, H. D. Bauer, K. Wetzig, *Thin Solid Films*, **433,** 237 (2003).

10. Q. Liu, L. Peter, J. Toth, L. F. Kiss, A. Cziraki, I. Bakonyi, *Journal of Magnetism and Magnetic Materials*, **280**, 60 (2004).

11. Y. Jyoko, S. Kashiwabara and Y. Hayashi, *Journal of the Electrochemical Society*, **144**, L5 (1997).

12. M. Shima, L. Salamanca-Riba, R. McMichael and T. Moffat, *Journal of the Electrochemical Society*, **148**, C518 (2001).

13. J. Cl. Puippe, in Theory and Practice of Pulse Plating, Jean-Claude Puippe, F. Leaman, p. 17, American Electroplaters and Surface Finishers Society, Orlando (1987)

14. C. C.Wan, H. Y.Cheh and H. B. Linford, *Journal of Applied Electrochemistry*, **9**, 29 (1979).

15. G. W. Jernstedt, *Annual Proceedings of American Electroplaters and Surface Finishers Society*, **37**, 151 (1950).

16. A. Hickling and H. P.Rothbaum, *Trans. Inst. Metal Finishing*, **34**, 199 (1957).

17. D. Gupta, A. C. Nayak, D. Kaushik and R. K. Pandey, *Journal of Physical Chemestry Solids*, **66**, 861 (2005).

18. H. Y. Cheh, *Journal of the Electrochemistry Society*, **118**, 1132 (1971).

19. H. Y. Cheh, *Journal of the Electrochemistry Society*, **118**, 551 (1971).

20. J. Zhang, M. Moldovan, D. P. Young and E. J. Podlaha, *Journal of the Electrochemistry Society*, **152**, C626 (2005).

21. A. Marlot, P. Kern and D. Landolt, *Electrochimica Acta*, **48**, 29 (2002).

22. P. E. Bradley and D. Landolt, *Electrochimica Acta*, **45**, 1077 (1999).

CHAPTER 5. ELECTRODEPOSITION OF MICRODEVICE

5.1. Introduction

Giant Magnetoresistance(GMR) sensors have been widely applied from data storage system to displacement control devices[1, 2] and new electronic elements such as potentiometers[3], isolators[4] and gate components.[5] Zhang and Wang[6] has demonstrated a new serpentine microdevice that incorporates a giant magnetoresistance material. The advantage of this design is that the resistance of the thin film can be manipulated by changing the wire length and area. A similar serpentine shape was also used in spin valves to maximize the total magnetostriction by increasing the device length per die area.[7] Their design is used here and evaluated for different serpentine dimensions and plating parameters.

Vacuum fabrication such as sputtering[8-10] and molecular beam epitaxy[11-13] have been the main method to fabricate multilayers with high GMR values.[14] Electrodeposition is an alternative approach because of the advantage of low cost, room temperature operation and its capability to deposit into irregularly shaped substrates and deep recesses. However, electrodeposited multilayers with comparable GMR as those prepared by vacuum process still remain a challenge despite the plethora of research, as reviewed by Ross [15] and Schwarzacher.[16] Typical GMR values obtained from electrodeposited Co/Cu multilayers include (at their associated fields) 18 %[17](10 kOe), 16 %[18, 19](21 kOe),14 %[20](10 kOe),10 %[21](2 kOe) at room temperature. It has been widely observed in vapor deposited and electrodeposited films that the GMR varies with the non-magnetic spacer layer size and this behavior has been summarized in several reviews.[14, 16, 22] One special requirement for electrodeposition of multilayers is that the

substrate has to be conductive. In order to measure GMR and avoid the current being shunted through the substrate, thin films can either be removed from the substrate [17, 21] or the multilayer deposit must be significantly thicker than the conductive regions of the substrate so that the multilayer resistance dominates. Electrodeposition of multilayers onto silicon wafers makes it possible to combine electrodeposited multilayers with Si-based electronics for integrated sensors.

In this Chapter, the GMR behavior of Co/Cu multilayers directly electrodeposited into a serpentine geometry is presented and the influence of the line width, recess depth and bi-layer number and pulse train deposition is examined.

5.2. Experimental

5.2.1. Electrodeposition of Co/Cu Thin Films

A single sulfate electrolyte containing 0.5 M cobalt sulfate, 0.005 M copper sulfate and 0.543 M boric acid was employed to electrodeposit CoCu/Cu multilayers. The electrolyte was prepared with de-ionized (DI) water and its pH adjusted to 3.0 by dilute sulfuric acid. The substrate was n-type (100) silicon wafer sputtered with a 10 nm Ti adhesion layer and a 10 nm Cu conductive seed layer. The wafer was mounted into a holder for deposition. The holder was composed of two pieces of plastic which sandwiched the wafer and was sealed by two O-rings. The exposed area was 1.7 cm^2. A platinum mesh was used as anode, placed 40 mm paralled to the cathode surface. A square current wave pulse or a train of square wave current pulse was provided by a PINE bipotentiostat with an AMEL 5680 function generator. Deposition was processed in an unstirred electrolyte.

5.2.2 Microfabrication of the Silicon Pattern Substrate

Optical lithography (UV) was employed to fabricate the micro-serpentine device using AZ-1512 and SPR 220-7 photo resist. A detailed description of the 2-mask process was described in Table 5-1. A 100 nm Ti adhesion layer and 10 nm Cu seed layer were sputtered onto a n-type (100) silicon wafer. The AZ-1512 photoresist was spin-coated onto the Cu layer at 3000 rpm with a controlled thickness of 1.2 μm for 30 s, followed by a pre-bake process at 96 ^{0}C for 1 min. The photoresist was exposed for 20 s with the Oriel UV exposure station using the first mask (Figure 5-1) where the UV light can only go through the non-patterned area. The wavelength range of the exposure station is 220~450 nm and the light source is 1000 Watt Hg (Xe) lamp. The mask shown in Figure 5-1 contains 4 different size patterns; designed line width and gap were equal to each other with size of 200 μm, 150 μm, 100 μm, 50 μm, maintaining the constant total exposed area at 0.15 cm^2. The resist was developed by Microposit 454 developer for 1~2 min after exposure. The Cu seed layer and Ti seed layer was etched away by a copper etchant and 3 % HF, so that the short-circuit effect of the seed layer on GMR value can be reduced during the GMR measurement. The rest photoresist was stripped away by acetone for 3 min. The wafer was heated on a hotplate at 150 ^{0}C for 1 min, and then 7 μm or 18 μm SPR 220-7 photoresist was spun coated on the silicon substrate with a spin speed of 3000 rpm and followed by a prebake process at 90 ^{0}C for 100 s and at 115 ^{0}C for 100 s.

The photoresist was exposed for 30 s with Oriel UV exposure station using a second mask (Figure 5-2) where the UV light goes through the patterned area. Finally the exposed photoresist will be developed by solution MF 84 for 1~2 min and the

electrodeposition processes was carried out in the recessed areas. When the patterned thin films were finished plating, the remaining resist was striped by acetone and cleaned by DI water. Finally a silicon substrate with a patterned area covered by a conductive copper seed layer and a non patterned area covered by nonconductive photoresist layer was obtained. This silicon substrate was cut into 23×23 mm smaller piece and put into the jig holder as shown in chapter 3 for electrodeposition. The as-deposit sample will be taken out of the jig holder after the plating process is finished and put into acetone solution for stripping away the photoresist. Then the samples was cleaned by DI water and dried with kimwipes for characterization.

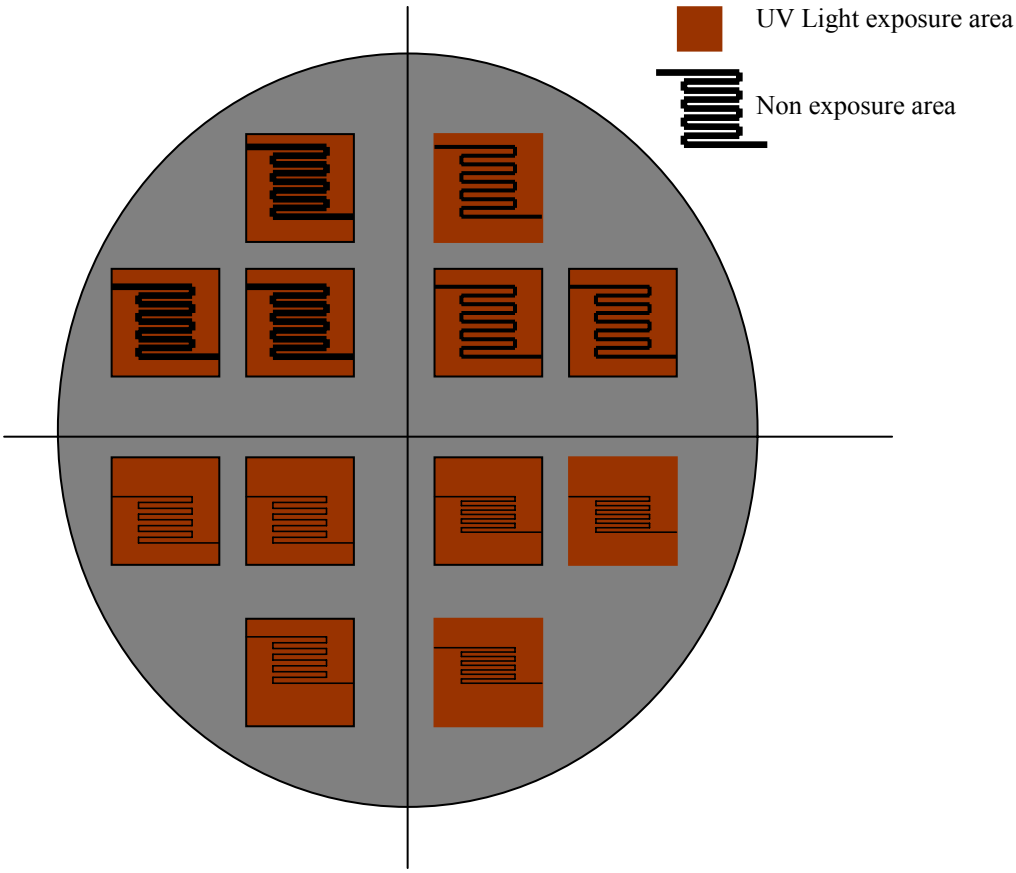

Figure 5-1 Mask 1 for UV lithography

Table 5-1 Step 1 for UV lithography process to fabricate substrate

		Surface cleaning: Blow by N2
	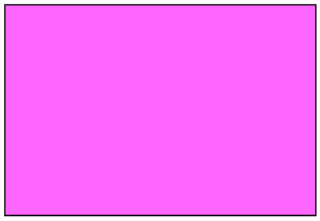	Evaporation Ti: 100A Evaporation Cu: 100A
		Singe: 1min, 115 °C on hotplate. Spin-coat photo resist (PR) AZ1512 Thickness: 1.2 um Spin speed: 3000 rpm Spin Time: 30 s Pre-bake PR hot plate, 96 °C, 1minute
		Expose Equipment: Quintel UL7000TL Mask Aligner/ Exposure System. Exposure time: 20 s
	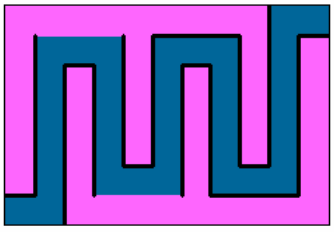	Develop exposed PR Developer: 354 Time: 1~2 min

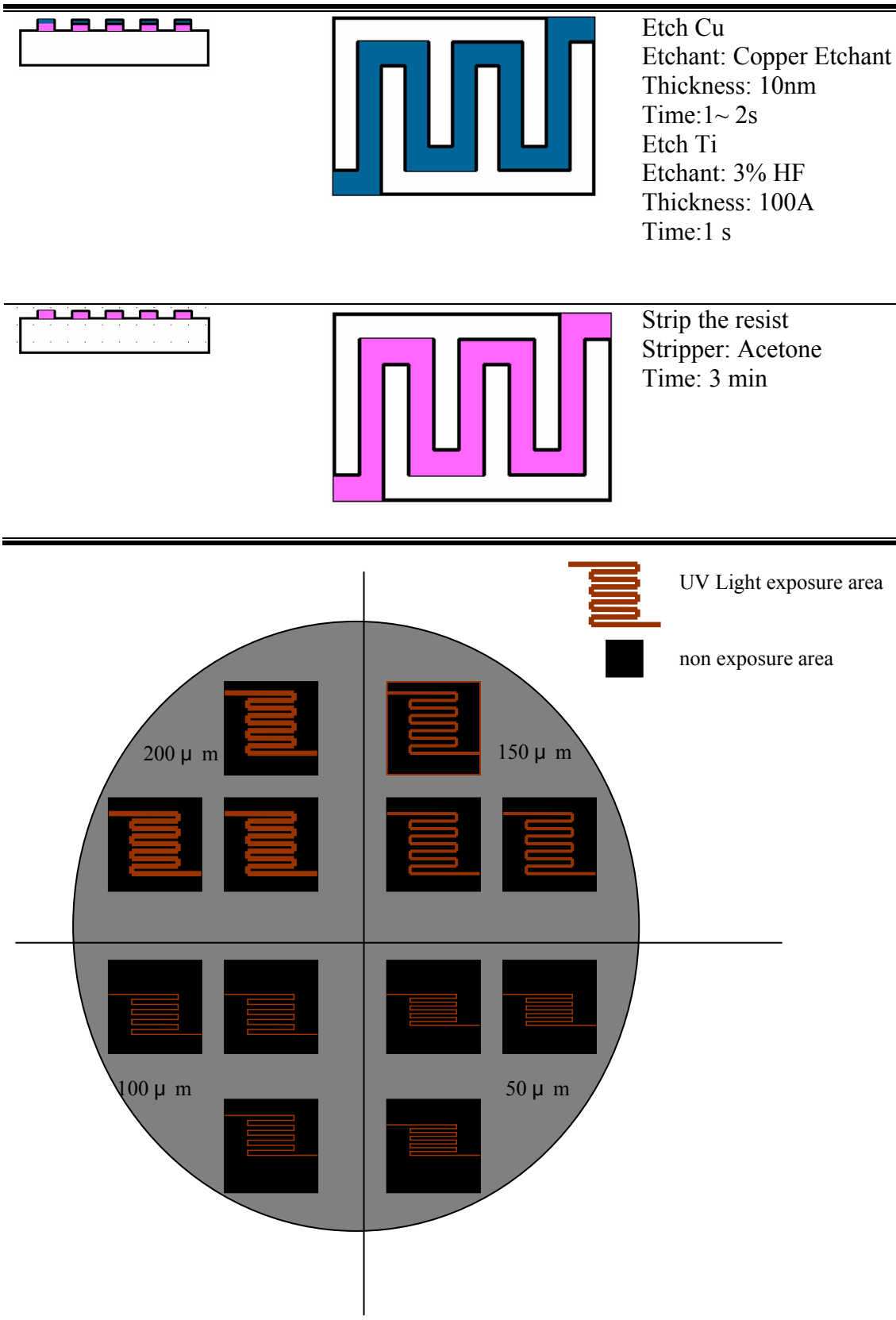

Figure 5-2 Mask 2 For UV lithography

Table 5-2 Step 2 for UV lithography process to fabricate substrate

		Singe: hotplate, 150 °C, 1 min. PR (SPR220-7) application PR: SPR 220-7 Thickness: 7 um Spin speed: 3000 rpm
		Expose Equipment: Quintel UL7000TL Mask Aligner/ Exposure System. Exposure time: 30 s
	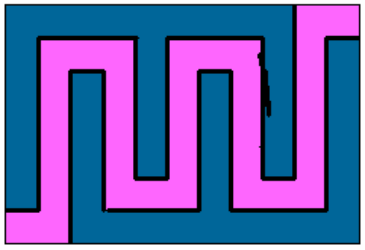	Develop exposed PR Developer: MF 84 Time: 1~2 min Rinse: DI water for 1~2 min Blow up by N2 Post Bake: Oven Bake 90 °C, 45~60 min

5.2.3. Characterization

The morphology of the deposits were obtained from a Scanning Electron Microscope (SEM) (Joel JSM-840A).Compositional characterization of the samples was performed by a Kevex Omicron energy-dispersive X-ray fluorescence analyzer (XRF) and the magnetoresistance (MR) effect was measured with a 9 T Quantum Design Physical Properties Measurement System (PPMS) using the standard four-point probe ac technique at 27 Hz with an excitation current of 1 mA. During measurement, two probes are at one end of the patterned thin film and other two probes are at another end. The contact scheme is shown in Figure 5-3(a). The current is perpendicular to the magnetic

field at the long length area and parallel to the magnetic field at the short length area because of the serpentine shape of the thin film wire. Therefore, the GMR of the patterned thin film is the combination of transverse and longitudinal magnetoresistance. Magnetoresistance was calculated according to the equation [R(H)-R(0)]/R(0)×R(0).

(a)

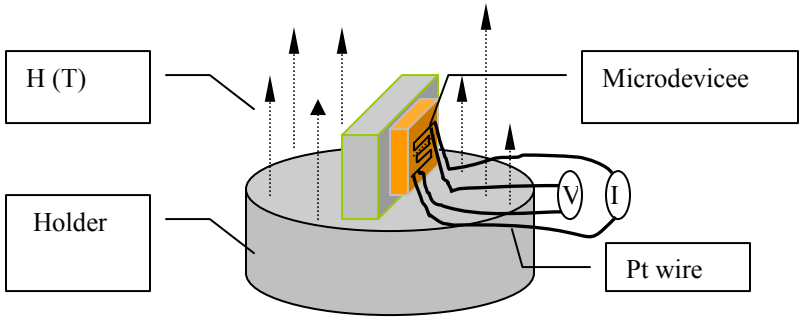

(b)

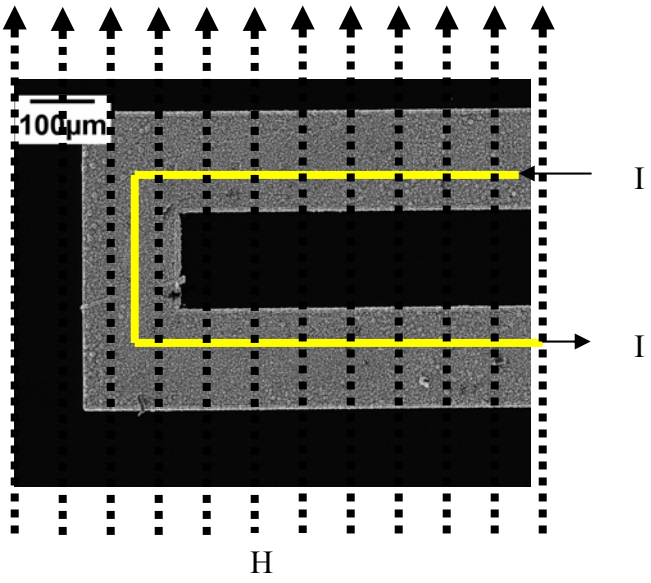

Figure 5-3 (a) Magnetoresistance measument for microdevice, (b) Combining transverse and longitudinal magnetoresistance

5.3 Results and Discussion

5.3.1. Regular Pulse Electrodeposition of GMR Sensors

The plating conditions for electrodeposition of GMR sensors were the same as those used for thin films deposition, as discussed in Chapter 3. The copper plating current

density for copper and cobalt were -0.2 mA/cm^2 and -20 mA/cm^2. The copper and cobalt layer thicknesses were determined as 3 and 2.5 nm with plating time of 78 s and 400 ms. Because a magetoresistance of 5 % with a saturation field less than 3000 Oe was obtained, as shown in Figure 3-7. GMR micro-sensors with different line widths of 200 μm, 150 μm, 100 μm, and 50 μm were fabricated with these plating current density and layer thicknesses. (Separation distance is the same as the line widths) Figure 5-4, 5-5 and 5-6 are the SEM of the samples with different line width and gap widths as follows: (a) 200 μm, (b) 150 μm, (c) 100 μm, and (d) 50 μm. The patterned thin film can be electrodeposited showing good continuity can be obtained by combination of galvanostatic deposition and UV lithography. Figure 5-5 and 5-6 shows higher SEM magnification of the samples with different line widths. Surface morphology is different at the edge of the line and middle of the line. The deposit is rougher at the edges compared to the middle, due to the slight non-uniformity of the current distribution.

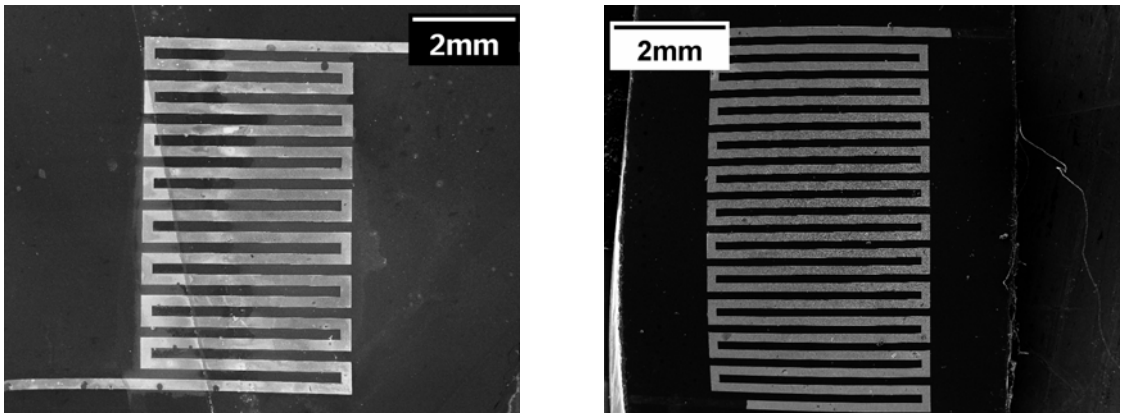

(a) (b)

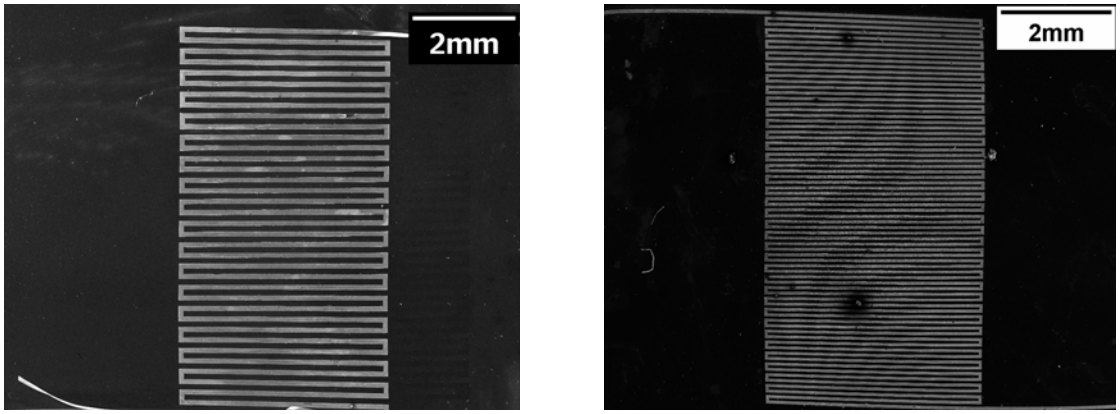

(c) (d)

Figure 5-4 SEM of patterned thin film $[Co(3\ nm)/Cu(2.5\ nm)]_{1000}$ with a line width of (a) 200 μm, (b) 150 μm, (c) 100 μm, (d) 50 μm with magnification 12×.

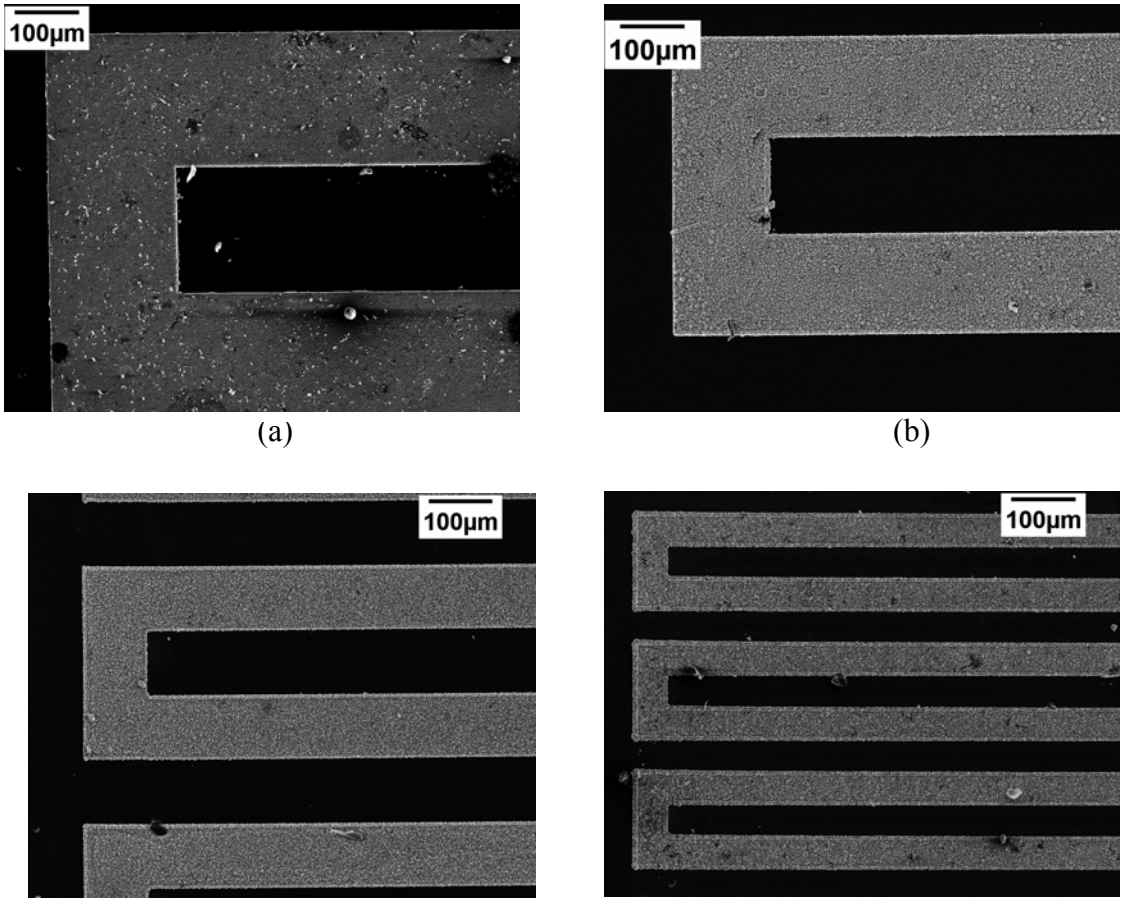

(a) (b)

(c) (d)

Figure 5-5 SEM of patterned thin film $[Co(3\ nm)/Cu(2.5\ nm)]_{1000}$ with a line width of (a) 200 μm, (b) 150 μm, (c) 100 μm, (d) 50 μm with magnification 150×

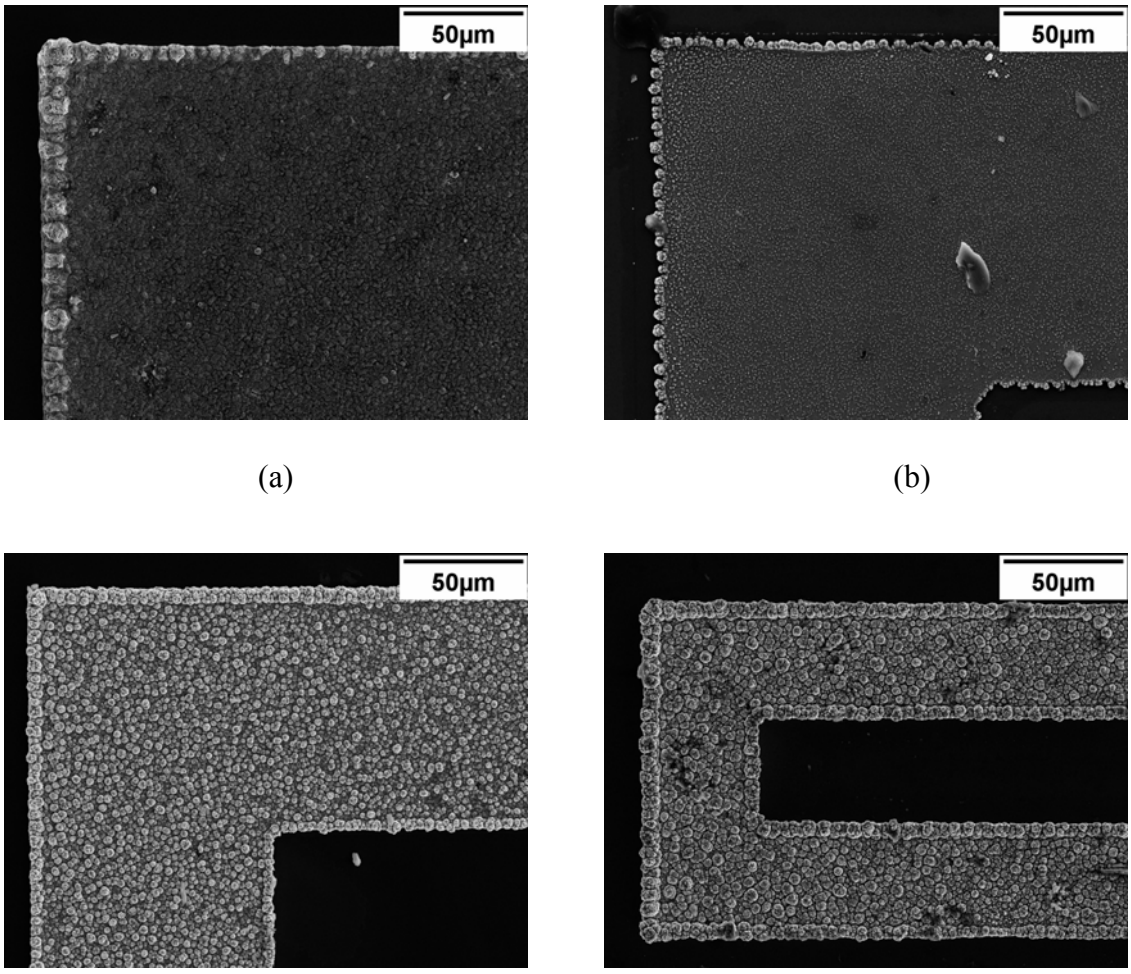

Figure 5-6 SEM of patterned thin film $[Co(3\ nm)/Cu(2.5\ nm)]_{1000}$ with a line width of (a) 200 μm, (b) 150 μm, (c) 100 μm, (d) 50 μm with magnification 550×

The effect of wire width on magnetoresistance of the microdevices was examined with two more patterned samples having bigger line widths of 290 μm and 805 μm (width is equal to gap). All of the six patterned samples were measured with the PPMS systems for magnetoresistance, the results are shown in Figure 5-7 (a) and (b). Compared to the thin film structures, the serpentine wires have four different magnetoresistance characters; the first is that there is a magnetoresistance change between 1-2 %, at fields below 10000 Oe. This value is significantly lower than that obtained for the thin film (5

%) Similarly, Matsuyama *et al.*[23] also observed that magnetoresistance of a spin valve prepared by sputtering decreased after patterning, The second observation is that magnetoresistance of the patterned samples didn't achieve saturation in contrast with the thin film structures. The third characteristic is that all magnetoresistance in serpentine structures didn't exhibit a parabolic shape, which is observed in the thin film samples. In addition, the pattern width also has an effect on GMR behavior, the GMR behavior becomes worse with the decrease of pattern width, magnetoresistance decreased sharply when the line width becomes 50 μm. The Last difference is that the resistances of the patterned serpentine thin films were significantly increased. The resistance of the patterned serpentine thin films with line width of 805 μm, 290 μm, 200 μm, 150 μm, 100 μm, and 50 μm are 50, 230, 300, 600, 1000 and 1900 times larger than that of the non patterned thin films with similar measured area. The increase of resistance makes it easier to test and therefore provide more applications possibility in GMR sensing.

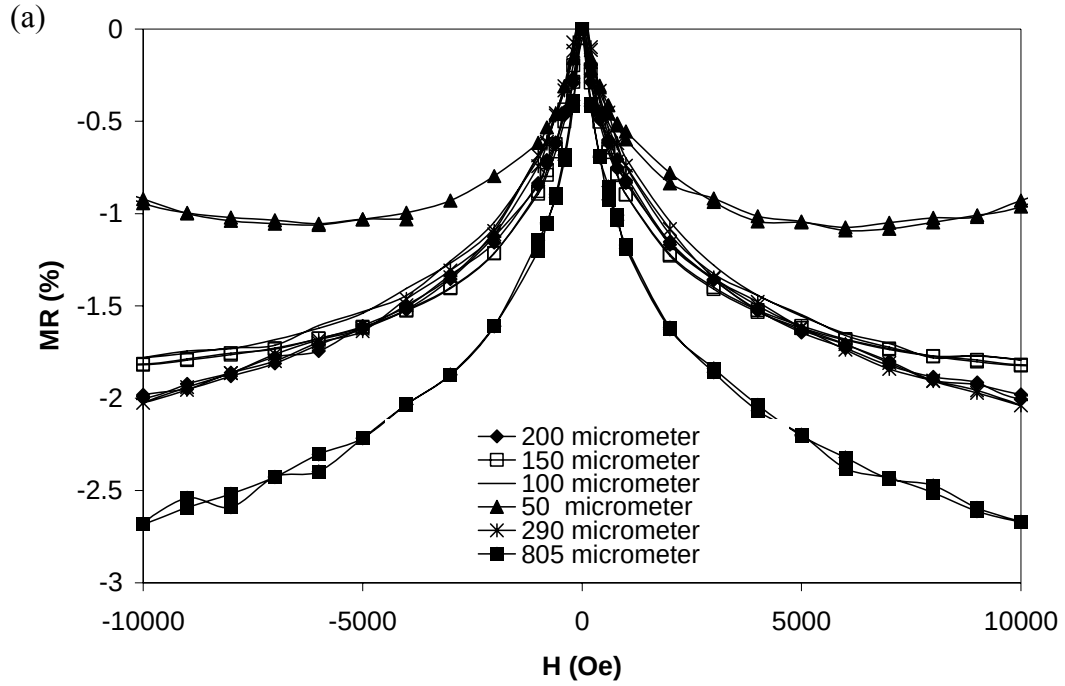

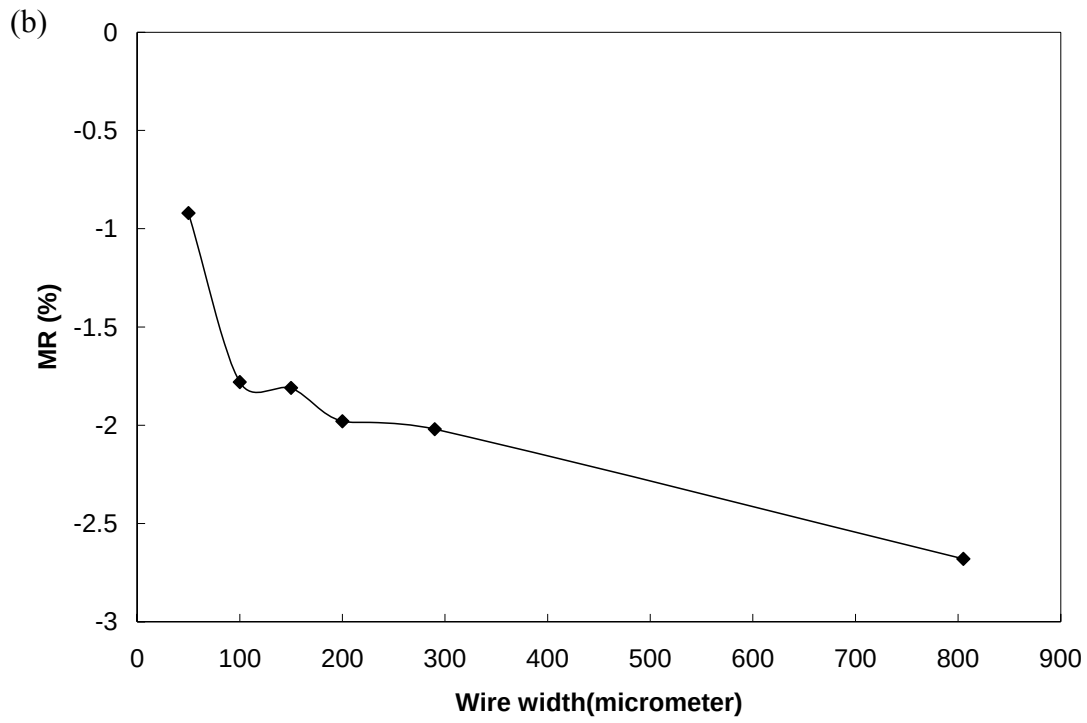

Figure 5-7 (a)Magnetoresistance of patterned thin film $[Co(3nm)/Cu(2.5nm)]_{1000}$ with variable line width, (b) maximum magnetoresistance of patterned thin film $[Co(3 nm)/Cu(2.5 nm)]_{1000}$ vary

The influence of recess depth from the patterned substrate was also investigated. Figure 5-8 is the magneroresistance of two samples with recess depth of 18 μm and 7 μm, respectively. The line width of the patterned substrate was 150 μm, the copper layer thickness was 3 nm and the cobalt layer thickness was 2.5 nm, bilayer number for both samples was 1000. A magnetoresistance of 1.8 % and 2 % were observed from the samples plated on the substrate with a recess depth of 18 μm and 7 μm, respectively. There was no large difference in magnetoresistance. Therefore, the recess depth had little effect on magnetoresistance of the deposit, even though the current distribution was expected to be a little different in these two different recess depths according to the research done by Dinan *et al.*[24]

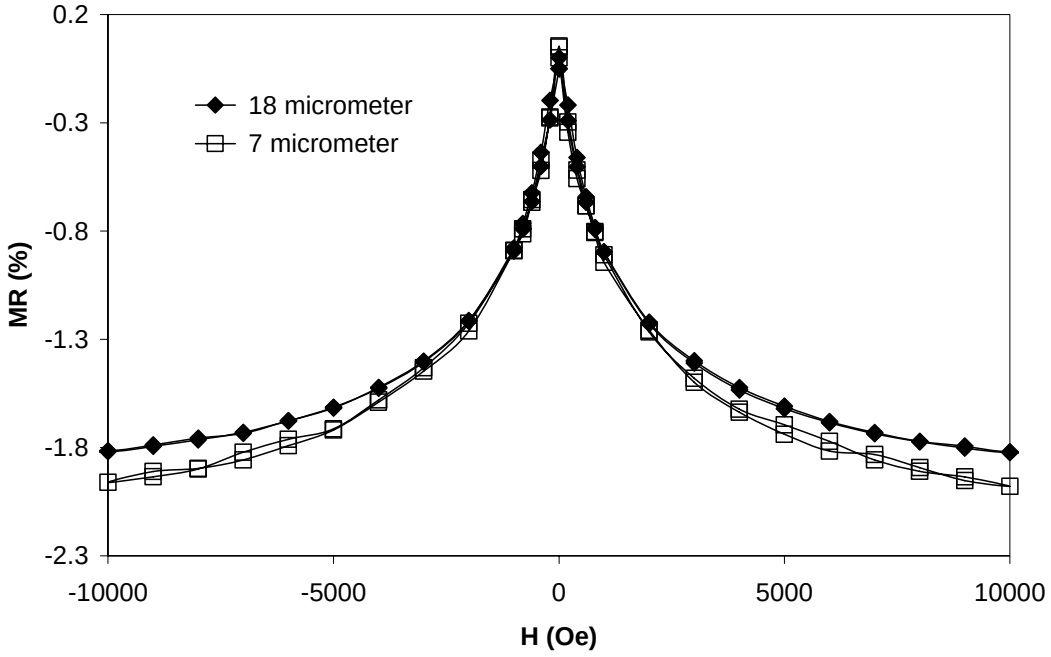

Figure 5-8 Magnetoresistance of patterned thin film $[Co(3nm)/Cu(2.5nm)]_{1000}$ with variable substrate recess depth

The effect of bilayer number on magnetoresistance was studied on the patterned thin film with a line width of 150 μm and recess depth of 18 μm. Figure 5-9 shows the magetoresistance of four samples with different bilayer numbers: 1000, 500, 300 and 100. The magnetoresistance of the micro-device with the smallest bilayer number, 100, is worse and the magnetoresistance of the sample with largerr bilayer number is better. This phenomenon is different from electrodeposited thin films in the previous reports[25, 26] which reported that as the bilayer number increases the magnetoresistance value decreases. This phenomenon can be ascribed to the competition between the shunting effect of the seed layer and the multilayer material.

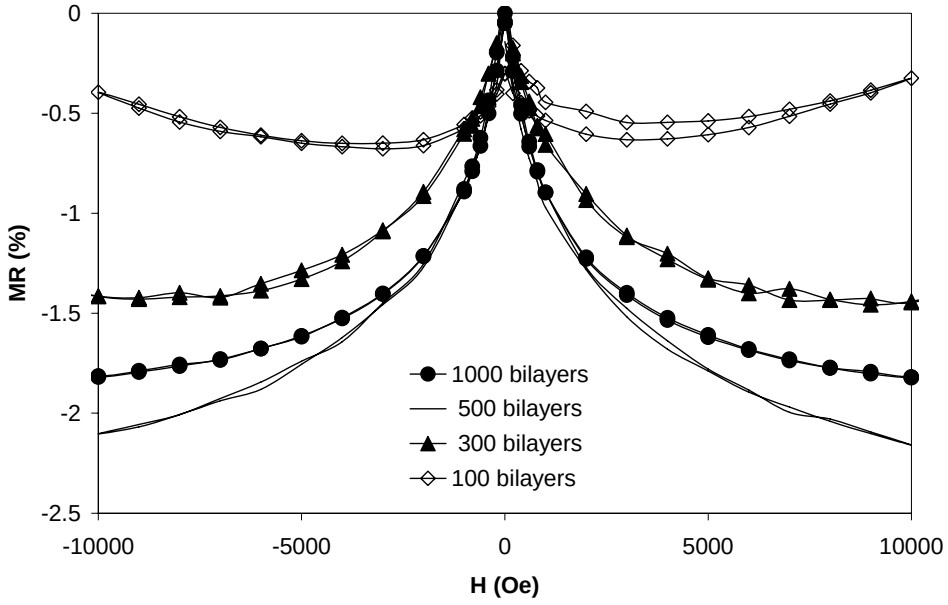

Figure 5-9 Magnetoresistance of patterned thin film $[Co(3nm)/Cu(2.5nm)]_x$ with variable bilayer number

5.3.2 Pulse Train Deposition of Microdevice

In Chapter 3 we already demonstrated that pulse train deposition can enhance magnetoresistance of thin films when the cobalt layer was deposited by a series of pulses with a cycle number below to 8. A similar method was also applied to microdevice deposition. The copper plating current density was kept -0.2 mA/cm^2 with 78 s plating time, the cobalt plating density was -20 mA/cm^2 with 100 ms off time, the plating on time varied from 100 ms to 50 ms, therefore the corresponding cycle number is 4 and 8. The magnetoresistance of different samples were shown in Figure 5-10. When no pulse train deposition was applied (cycle number is 1), the magnetoresistance was about 2 %, when the cycle number was increased to 4, the magnetoresistance value was enhanced to 2.2 %. When the cycle number was continually increased to 8, the largest magnetoresistance of 2.7 % was obtained. Therefore, the pulse train method also can improve the

magnetoresistance property at certain cycle values, which is similar as those observed in thin film deposition.

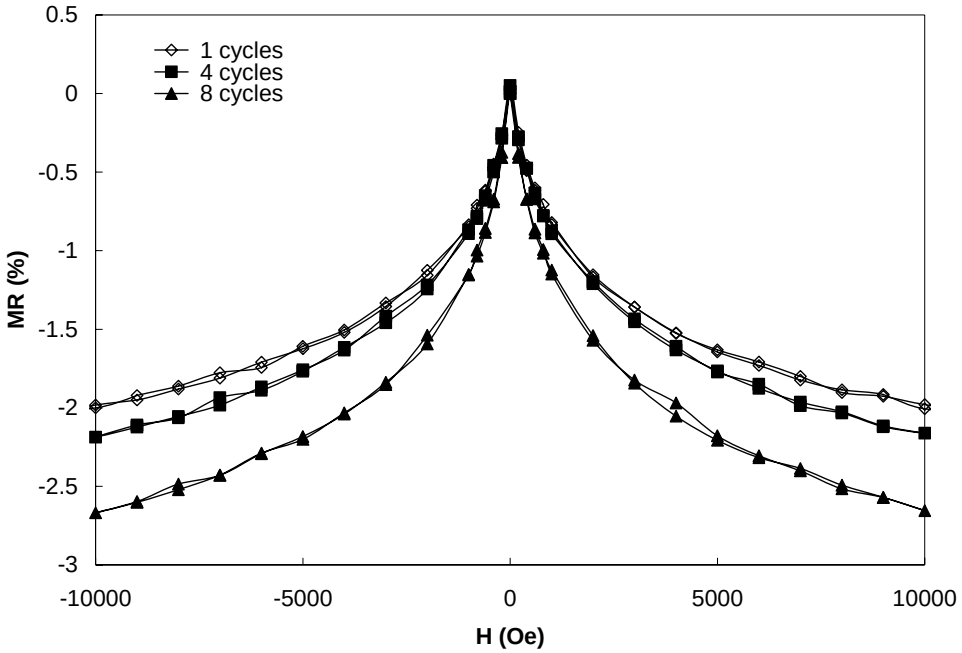

Figure 5-10 Magnetoresistance of microdevice plated by pulse train method

5.4 Summary

A GMR sensor substrate patterned by a lithography technique and serpentine thin film micro-deviced were deposited, the sensor magnetoresistance was improved with the enlargement of line width, and the increase of bilayer number also benefited the magnetoresistance property. The thickness of the photoresist has little effect on the magnetoresistance property of the microdevice. Pulse train deposition method also improved magnetoresistance of microdevice at some special cycle number.

5.5 References

1. M. Miller, P. Lubitz, G. A. Prinz, J. J. Krebs, A. S. Edelstein, S. F. Cheng, F. G. Parsons, *IEEE Transactions on Magnetics*, **33**, 3388 (1997).

2. P. Freitas, J. L. Costa, N. Almeida, L.V. Melo, F. Silva, J. Bernardo, C. Santos,

Journal of Applied Physics, **85**, 5459 (1999).

3. W. Clemens, H. A. M.VandenBerg, G. Rupp, W. Schelter, M. Vieth, J. Wecker, *Journal of Applied Physics*, **81**, 4310 (1997).

4. T. Hermann, W. Black, and S. Hui, *IEEE Transactions on Magnetics*, **33**, 4029 (1997).

5. M. Hassoun, W. Black, E. Lee, R. Geiger and A. Hurst, *IEEE Transactions on Magnetics*, **33**, 3307 (1997).

6. H. Zhang, and W. Wang, *Microsystem Technologies-Micro-and Nanosystems-Information Storage and Processing Systems*, **9**, 436 (2003).

7. T. J.Gafron, S. E. Russek, and S. L. Burkett, *Journal of Vacuum Science and Technology a-Vacuum Surfaces and Films,* **19**, 1195 (2001).

8. S. S. P. Parkin, R. Bhadra and K. P. O. Roche, *Physical Review Letters*, **66**, 2152 (1991).

9. S. S. P. Parkin, Z. G. Li, and D. J. Smith, *Applied Physics Letters*, **58**, 2710 (1991).

10. S. S. P. Parkin, A. Modak and D. J. Smith, *Physical Review B*, **47**, 9136 (1993).

11. M. J. Hall, B. J. Hickey, M. A. Howson, M. J. Walker, J. Xu, D. Greig, N. Wiser, *Physical Review B*, **47**, 12785 (1993).

12. E. Avdi, B. J.Hickey, D. Greig, M. A. Howson, M. J. Hall, J. Xu, M. J.Walker, N.Wiser, P. Degroot, *Journal of Applied Physics*, **73**, 5521 (1993).

13. K.Wellock, J. Caro and B. J. Hickey, *Journal of Magnetism and Magnetic Materials*, **199**, 27 (1999).

14. S. S. P. Parkin, *Annual Review of Materials Science*, **25**, 357 (1995).

15. C. Ross, *Annual Review of Materials Science*, **24**, 159 (1994).

16. W. Schwarzacher and D. Lashmore, *IEEE Transactions on Magnetics*, **32**, 3133 (1996).

17. Y. Jyoko, S. Kashiwabara, and Y. Hayashi, *Journal of the Electrochemical Society*, **144**, L5 (1997).

18. Y. Ueda, T. Houga, H. Zaman, and A.Yamada, *Journal of Solid State Chemistry* **147**, 274 (1999).

19. A.Yamada, T. Houga and Y. Ueda, *Journal of Magnetism and Magnetic Materials*, **239**, 272 (2002).

20. S. Lenczowski, C. Schonenberger, M. Gijs, and W. Dejonge, *Journal of Magnetism and Magnetic Materials*, **148**, 455 (1995).

21. Q. Liu, L. Peter, J. Toth, L. F. Kiss, A. Cziraki, I. Bakonyi, *Journal of Magnetism and Magnetic Materials*, **280**, 60 (2004).

22. S. S. P. Parkin, *Materials Letters*, **20**, 1 (1994).

23. K. Matsuyama, H. Asada, S. Ikeda and K. Taniguchi, *IEEE Transactions on Magnetics*, **33**, 3283 (1997).

24. T. Dinan, M. Matlosz, and D. Landolt, *Journal of the Electrochemical Society*, **138**, 2947 (1991).

25. L. Peter, A. Cziraki, L. Pogany, Z. Kupay, I.Bakonyi, M. Uhlemann, M. Herrich, B. Arnold, T. Bauer, K. Wetzig, *Journal of the Electrochemical Society*, **148**, C168 (2001).

26. Cziraki, A. M. Koteles, L. Peter, Z. Kupay, J. Padar, L. Pogany, I . Bakonyi, M.Uhlemann, M. Herrich, B. Arnold, J. Thomas, H. D. Bauer, K. Wetzig, *Thin Solid Films*, **424**, 229 (2003).

CHAPTER 6. ELECTRODEPOSITION OF Co/Cu MULTILAYERED MICROPOST

6.1 Introduction

Giant magnetoresistance (GMR) has been extensively studied in multilayered thin films with the current-in-plane (CIP) configuration as widely reviewed.[1,2] GMR measured when the current is perpendicular to the multilayer plane (CPP) is a challenge in a thin film due to the extremely small values of resistance, although it has been done with the use of a SQUID with Nb contacts for precision measurement of low voltages generated in Ag/Co multilayers.[3] Even though Pratt *et al.*[3] has observed a 3-10 fold increase in the CPP GMR compared to the CIP GMR, the measurement in thin films are restricted to liquid He temperatures to provide the superconducting quality of the contacts. There have also been theoretical arguments for a greater GMR in the CPP mode compared to CIP.[4, 5] Another alternative approach to the CPP GMR effect is to decrease the cross sectional area of the film and therefore increase the measured resistance. Nanowires is one obvious choice and a wide variety of studies have been carried out to demonstrate GMR in the CPP mode.[1,6,7] The electrodeposition of multilayers into nanoporous templates is straightforward, however, if the magnetic properties of an array of nanowires are measured within the template, then dipolar interactions between the wires may occur, and play a more dominant role in high porosity templates, such as in alumina. On the other hand, the magnetic measurement of a single wire can be cumbersome at the nanoscale. Pillar-like structures prepared by lithographic and microfabrication techniques is another structure conducive to CPP GMR. Because of the small cross sectional area, the resistance is on the order of a milliohm and can be measured by a conventional voltmeter. The advantage of these structures is that

temperature-dependent CPP GMR can be investigated, including room temperature, and they can be easily integrated into Micro-Electro-Mechanical systems (MEMS).

Gijs *et al*.[8] employed optical lithography to fabricate a pattern of vacuum sputtered Fe/Cr multilayers. The pillars were formed by removing a part of the multilayer through reactive ion etching. The samples had a height of 0.4-0.7 μm and a width ranging between 3 to 10 μm. At 4.2 K, a magnetoresistance of 108 % for multilayers [Fe(3 nm)/Cr(1 nm)]$_{100}$ was observed, four times larger than the corresponding CIP GMR. The magnetoresistance decreased slightly at temperatures lower than 60 K, but decreased strongly at higher temperature. A 14 % magnetoresistance remained at room temperature, though still about two times larger than the corresponding CIP GMR. Subsequently, MBE prepared Co/Cu[9,10] multilayered pillars were also made by a similar etching technique. In the [Co(1.2 nm)/Cu(1.1 nm)]$_{180}$ multilayers, above 90 % CPP GMR at low temperature and 56 % at room temperature were reported by Gijs *et al*.[9] Spallas *et al.*[11,12] sputtered a Co/Cu multilayer GMR and then used electron-beam lithography to create a pattern through which they dry etched the multilayer; a 13 % CPP GMR was achieved for the pillars with a diameter of 0.4 μm and height of 0.09 μm. Another important factor is that when the aspect ratio (height/diameter) is lower than 1, the magnetoresistance is a combination of CPP and CIP GMR. In the cited microfabricated pillar structures, the aspect ratio of Fe/Cr[8] and Co/Cu[9,10] pillars made by Gijs *et al.* were less than 0.3. The CPP sensor obtained by Spallas *et al.* [11,12] presented an aspect ratio of about 0.2. Here, microposts with an aspect ratio of 2.7 are fabricated by electrodeposition into a lithographically prepared recessed substrate and their GMR characterized. No metal etching step is required.

To date, there are few studies[13,14] that demonstrate electrodeposition of magnetic multilayers into a patterned structure. Schwarzacher *et al*.[13] electrodeposited an array of 1 μm diameter Ni-Cu/Cu dots into a resist template patterned by x-ray lithography and TEM analysis confirmed the multilayered structure with columnar growth. Duvail *et al.*[14] used the electrodeposition method to fabricate NiFe/Cu multilayered nanopillars with a height of 0.3 μm and diameter of 0.1 μm, (aspect ratio of 3), but the single pillar only exhibit 0.3 % MR at a temperature of 4.2 K. To the best of our knowledge, electrodeposited Co/Cu mulilayered microposts with heights of several hundreds of micrometers, and their CPP GMR behavior, have not been reported outside of the work presented here.

6.2 Experimental

6.2.1 Electrolyte

The electrolyte used for plating micro-posts is listed in Table 6-1. The electrolyte is similar to that used for thin film plating with the following changes: (1) sodium citrate is added to the electrolyte; and (2) a larger quantity of cobalt sulfate was used. Analytical grade reagents from Fisher were used in the preparation of the solutions in distilled-DI water. The pH value was adjusted to 6.0 in the same fashion as previously mentioned**.**

Table 6-1 Compositions of electrolyte used for deep recess plating

Component	Concentration / M
Copper Sulfate	0.005
Cobalt Sulfate	0.75
Boric Acid	0.543
Sodium Citrate	0.1
Triton X-100	0.4g/L

6.2.2 Substrate Preparation

The substrate for deep recess electrodeposition consists of four different layers: Cu, CuO, layer of bonding solution, and polymethylmethacrylate (PMMA). Each step in the process of substrate preparation is described below. A square copper plate 5 cm × 5 cm × 0.08 cm was used as a substrate (cathode). It was pretreated by washing with soap, soaking in 10 % H_2SO_4 for 2 minutes, and then degreasing by rinsing in acetone. The copper plates were oxidized in *Cu-oxidizing* solution at 95° C until a uniform black oxide layer was formed on the copper plate. The composition of the solution is listed in Table 6-2. Subsequently, it was placed in water and dried in air.

A 500 μm thick PMMA photoresist, the same size as the copper substrate, was adhered onto the copper substrate by using a *bonding* solution, see Table 6.2. The substrate was then subjected to a pressure resulting from stacking books on the top of the substrate. Figure 6.1 shows a schematic of the substrate preparation.

Table 6-2 Solutions for substrate preparation

Copper oxidizing solution		**Bonding solution**	
$NaClO_2$	54.26 g/l	MethylMethacrylate	17 g
NaOH	68.00 g/l	Powdered PMMA	1 g
Na_2CO_3	11.44 g/l	Benzoyl Peroxide	0.3 g
NaCl	4.67 g/l	Dimethyl Aniline	0.2 g
Developer solution		**Rinse solution**	
Diethylene glycol butyl ether	600 ml	Diethylene glycol butyl ether	800 ml
Morpholine	200 ml	Water	200 ml
2-minoethanol	50 ml		
water	150 ml		
Copper oxide etch solution			
Potassium chloride	0.5 M		
Hydrochloric acid	0.5 M		

The prepared substrate was sent to the Center for Advanced Microstructures and Devices for x-ray lithography. The exposure parameters used at CAMD for the two different masks used are given in Table 6-3. The photoresist was patterned by exposure to x-ray radiation through a mask having the desired pattern. In this case, the mask is a glass plate with a gold pattern, transparent in some regions and opaque where covered with gold, the transparent region is 183 x 183 micron squares. Since PMMA is a positive photoresist, the radiation causes chain scission of the exposed part of the resist enabling it to dissolve in a developing solution.

The exposed regions were dissolved away by using a *developer* solution, *pre-rinse* and *rinse* solutions. Their compositions are given in Table 6-2. The developing process consisted of four cycles of sonication, each consisting of: developing in *developer* solution for 10 min, rinsing in *pre-rinse* solution, which is an old rinse solution for 2 min, and rinsing in *rinse* solution for 1 hr. The substrate was then etched in *CuO-etch* solution for 2 min or until the copper oxide is completely removed. The constituents of the etch solution is also provided in Table 6-2. Thus, the holes or squares are open to the copper substrate creating a deep recess for electrodeposition. The final substrate was used as a Deep Recess Electrode (DRE).

6.2.3 Cell Design and Operation

The Deep Recess Electrode (DRE) was placed into a jig to hold it in place during electrodeposition. The jig used here for the deep recess electrode is larger than that used for the thin films electrodeposition in chapter 3. A Pt sheet that is placed approximately 1 cm above the jig served as the anode, see Figure 6-2. A mixer with a rate of 20 rpm was

applied to the electrolyte to keep the ion concentrations uniform everywhere in the container.

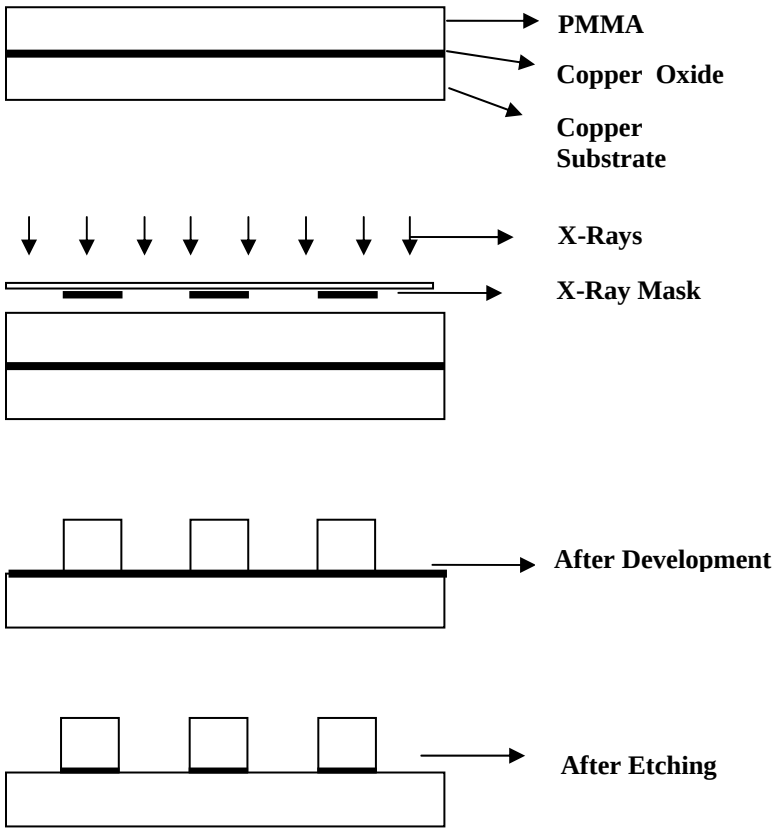

Figure 6-1 Schematic of recessed substrate preparation with x-ray exposure at CAMD

Table 6-3 Exposure parameters

Parameter	Quantity
Ring Energy	1.3 GeV
Filter	14 μm Al
He Pressure	25 torr
Scan Length	0.4 inches
Dose at the counter	9100 mA.min
Bottom Dose	3500 joules/cm^3

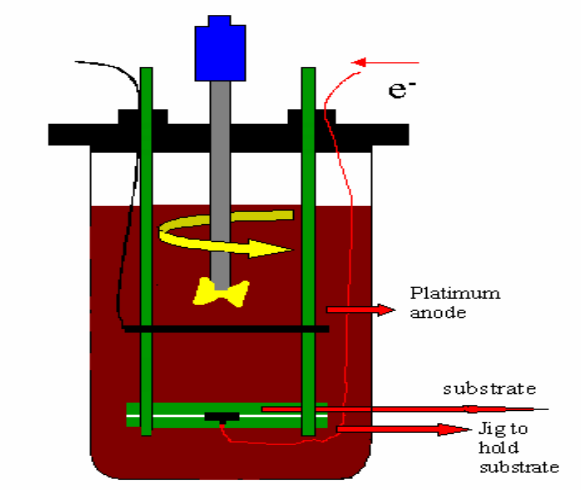

Figure 6-2 Schematic of experimental set up

6.2.4 Experimental Procedure

Deep recess plating was achieved using a pulse plating techniques. Pulse plating was carried out using an EG&G Princeton Applied Research Potentiostat/Galvanostat, Model 363 and an EG&G Parc Universal Programmer Model function generator. Polarization curves were carried out with a Pine Instruments bipotentiostat, at a scan rate of 5 mV/s. Multilayered microposts were deposited by both potentiostatic and galvanostatic pulsing. In potentiastaic pulsing, -0.5 V or -0.6 V vs. SCE was used for the coper layer plating, and -1.5 V or -1.7 V vs. SCE was applied for the cobalt layer plating. In galvanostatic pulsing, -0.2 mA/cm^2 was employed for the copper layer plating, which is lower than the copper plating limitting curent density. A value of -50 mA/cm^2 was used for the cobalt layer deposition. All experiments were carried out at atmospheric pressure and at room temperature. After the deposition into the recesses was complete, the sample was placed in acetone to dissolve away the PMMA. A part of this sample was cut using a diamond saw and mounted in epoxy in a way so that the length of the post is available for analysis. The cast was polished using 2000 and 4000 silicon carbon papers, and then

micropolished using microgrit papers, diamond and aluminium oxide pastes in order to obtain a 0.3 micron finishing.

6.2.4 SEM and TEM

The morphology of the deposits was obtained from a Scanning Electron Microscope (SEM) (Joel JSM-840A). The preparation of multilayered microposts for SEM included cross sectional cutting, epoxy resin mounting and polishing, followed by selective etching with a concentrated $K_2Cr_2O_7$ solution.[15] The posts were analyzed using a Superprobe 733-electron microprobe (JEOL company) with wavelength dispersive x-ray spectrometer for chemical composition of Cu and Co along the length of the micropost.

Nanosize layers within the micropost was examined with a Transmission Electron Microscope (TEM JEM-100CX operated at 80 kV). The micropost samples were first moved into a centrifuge tube and rinsed with water and acetone several times, and then they were infiltrated and embedded with L. R. white embedding resin, hard grade. Aluminum weigh boats were used as top and bottom of the mold A hotbaking process at 60 ^{o}C followed to polymerize resin, then the sample was cut into triangle shape with a saw and sectioned with a MT 5000 Vltramicrotome, as shown in Figure 6-3. Then those thin slices of micropost samples were moved into a grid for TEM characterization.

6.2.5 GMR

The CPP GMR measurements were made on a single, representative micropost at a room temperature, according to $[R(H)-R(0)]/R(0)$, where $R(H)$ is the resistance at an applied magnetic field H, and $R(0)$ is the resistance when the external magnetic field is zero. A four point measurement was carried out in a physical properties measurement

system (PPMS). The excitation current was 0.1 mA at 27 Hz between the four outer contacts so that the heat produced was negligible; the direction of the electric current was perpendicular to the magnetic field (transverse), as shown in Figure 6-4(a) or the direction of the electric current was parallel to the magnetic field (longitudinal), as shown in Figure 6-4(b).

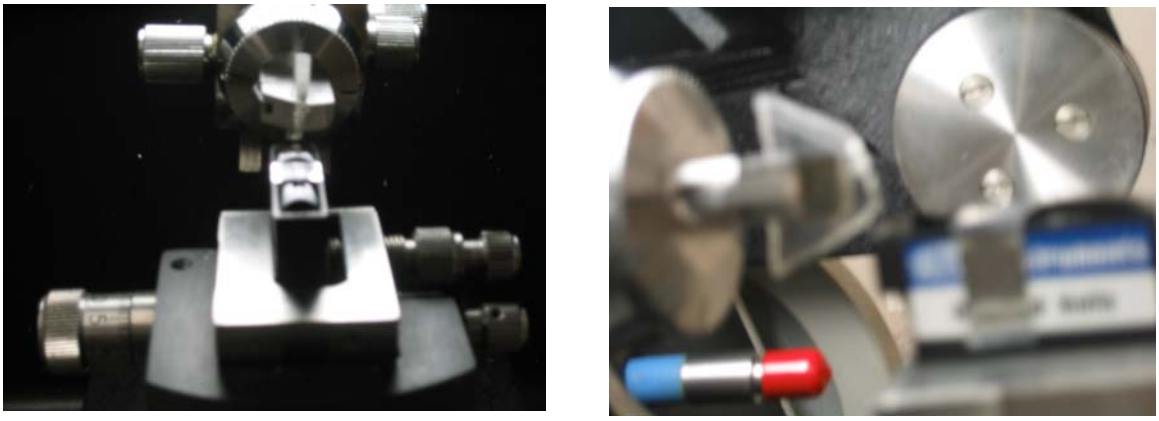

Figure 6-3 MT 5000 Vltramicrotome used for cutting micropost sample

(a)

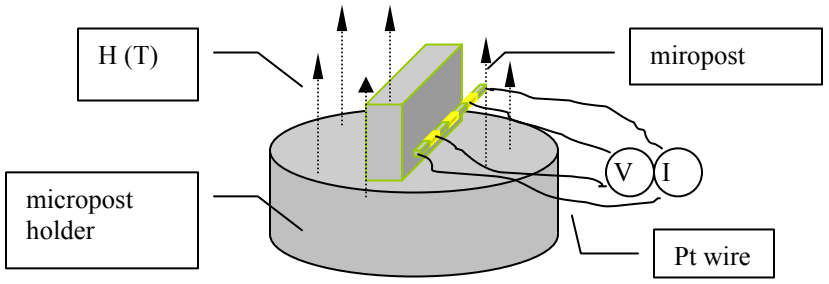

(b)

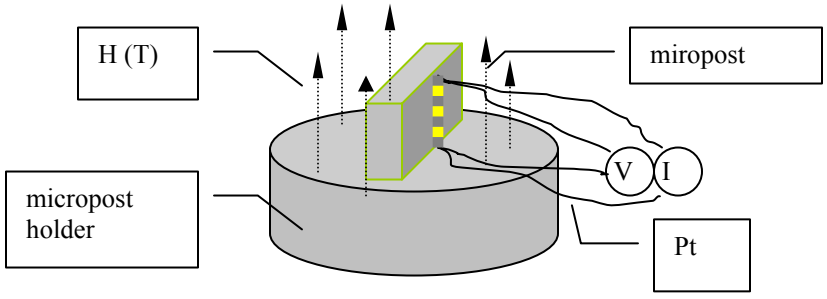

Figure 6-4 (a) A schematic of the transverse GMR(b) A schematic of the longitudinal GMR

6.3 Electrochemical Characterization

Figure 6-5 shows a polarization curve obtained with a pattern of deep recessed electrodes. Regions where copper and cobalt are deposited are evident from the curves; the plateau between -0.3 V and -0.65 V vs SCE corresponds to the limiting current for copper reduction and at more negative potentials cobalt is deposited. Cobalt started to deposit at more negative potential than -0.65 V vs SCE.

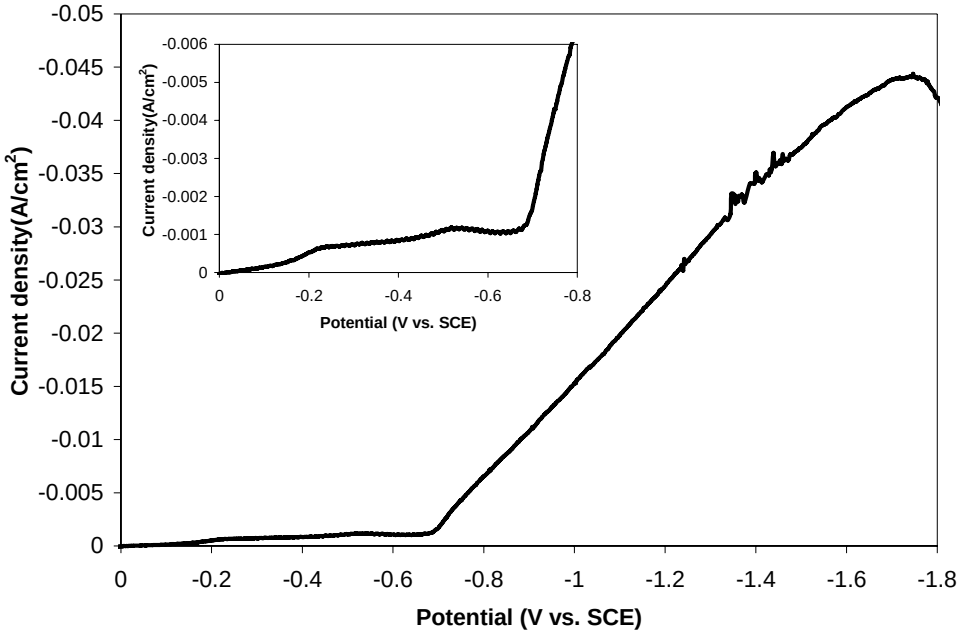

Figure 6-5 Polarization curve in the patterned microrecessed electrode

6.4 Co/Cu Multilayered Micropost Deposited by Potentialstatic Method

6.4.1 Layer Size

The multilayered microposts were obtained by applying a potential of -0.5 V for the copper layer deposition and -1.7 V for the cobalt layer deposition. Three micropost samples with different layer sizes were deposited. Figure 6-6(a) is a SEM of the array of deposited microposts containing thick multilayers. The sizes were determined by inspection of the layers. The copper and cobalt layer thicknesses were 473 ± 55 nm and

2633 ± 234 nm, respectively, visible without preferentially etching any one layer. GMR is not expected for such large layer sizes and thus, the magnetoresistance of a single micropost, shown in Figure 6-6(b), reflects the bulk, anisotropic magnetoresistance. When the magnetic field is perpendicular to the current, the transverse MR exhibited a negative -0.3 % value. When the magnetic field is parallel to the applied current, the longitudinal MR exhibited a positive value between 0.1 % and 0.2 %. These results indicate that the anisotropy magnetoresistance dominates in the micropost with larger size.

Figure 6-7(a) shows a representative SEM micrograph for a sample deposited with the same applied potential but with different deposition times; the copper and cobalt layers were deposited for 900 and 10 s, respectively. No clear layer structure was observed from the as-deposited sample, and therefore, the sample was etched in the H (a) solution before SEM analysis. A layered structure was evident and the characteristic waviness of the layers reflected columnar growth, as also reported in thin films.[16,17] The thicknesses of the copper and cobalt layers calculated from Figure 6-7 (a) were 168 ± 11 nm and 95 ± 17 nm, respectively. The corresponding transverse magnetoresistance was -0.7 % while the longitudinal magnetoresistance also exhibited a negative value of -0.45 % (Figure 6-7 (b)). This feature indicated that some GMR effect exists because both transverse and longitudinal magnetoresistance are negative. AMR also contributed to the magnetoresistance of the micropost because the magnitude of transverse GMR is larger than that of the longitudinal GMR. The layer thickness of this sample was used to determine the current efficiency and hence estimate the plating time for multilayers with nanometer size thicknesses.

(a)

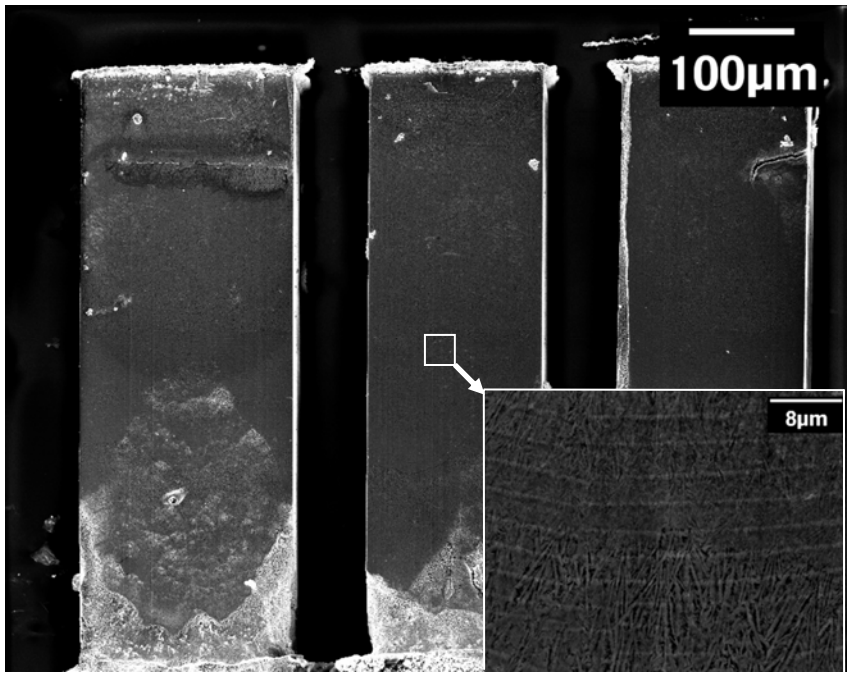

(b)

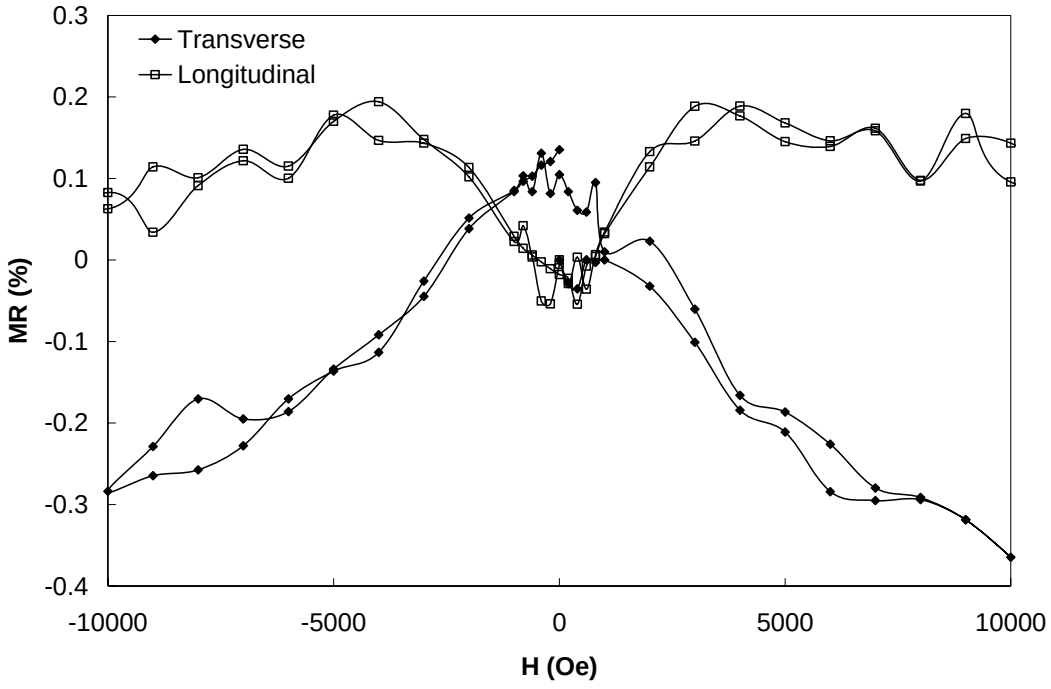

Figure 6-6 Multilayered micropost arrays with layer sizes of 473 nm for the copper layer and 2633 nm for the cobalt layer, (a) SEM, (b) magnetoresistance

(a)

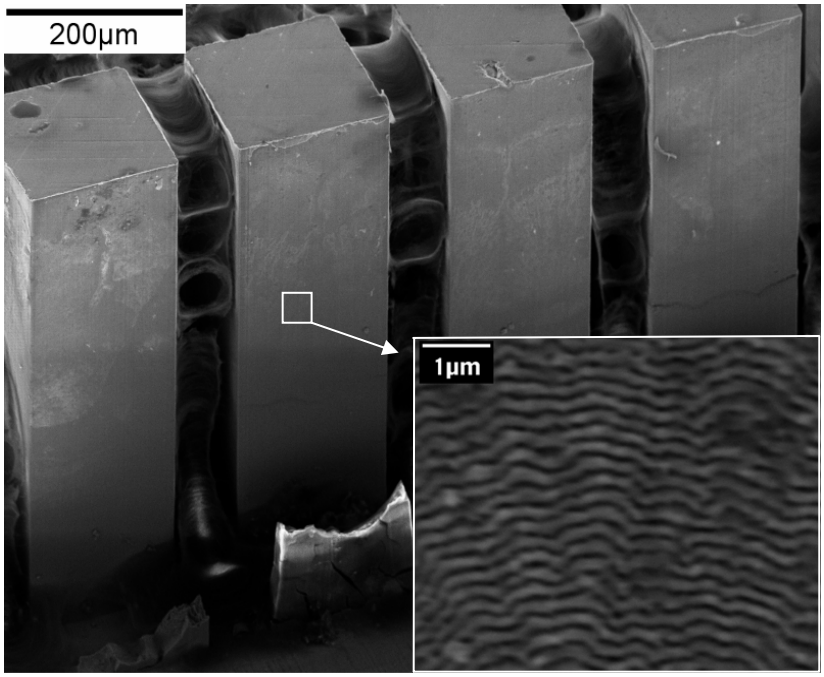

(b)

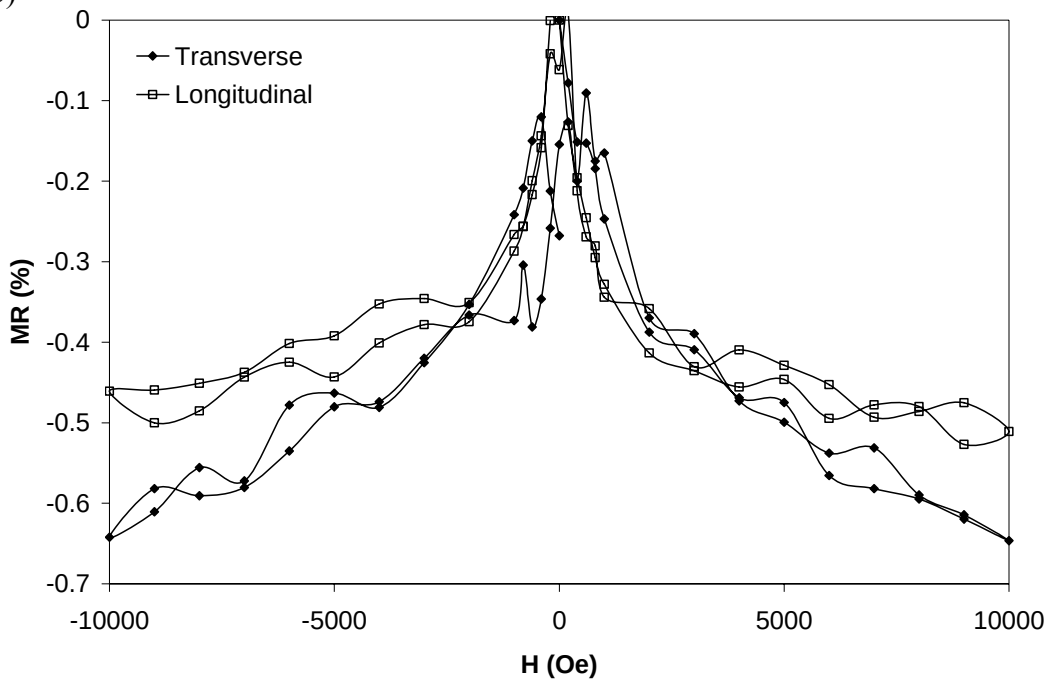

Figure 6-7 Multilayered micropost arrays with layer sizes of 168 nm for the copper layer and 95 nm for the cobalt layer (a) SEM, (b) magnetoresistance

Literature reports of nanowires with copper and cobalt layer thicknesses of both 10 nm achieved large GMR values (e.g. 15 %[18] and 20 %[19]) in nanowires, thus a similar layer thickness of copper and cobalt were also chosen to obtain giant magnetoresistance in the microposts. Keeping the pulse potential constant the copper plating time was reduced to 46 s and the cobalt plating time was reduced to 0.9 s. The bilayer number was 27777 when the micropost was plated to 500 μm tall. Magnetoresistance and a TEM micrograph of a small part of a micropost are shown in Figure 6.8. The change in resistance, Figure 6.8 (a), exhibits a maximum 'virgin state' at H_0. When the magnetic field was increased, the resistance decreased until it saturated at 0.5 kOe. When cycling the applied magnetic field to opposite polarity, the characteristic GMR behavior was observed with a decrease of resistance at H_M, reaching saturation with an increase in the magnetic field, and then returning to H_M when the field was removed. The room temperature 'virgin state' MR is about 6 % and after cycling it is reduced to 4 % under a saturation field less than 1 Tesla. This value is considerably larger than the value of 0.3 % GMR at low temperature of 4.2 K reported by Duvail *et al*,[14] who also employed an electrodeposition method to prepare pillar-like structures. TEM analysis is shown in Figure 6.8(b). The observed copper layer thickness, depicted as the white areas on the micrograph, was 9.4 ± 2 nm and the measured cobalt layer thickness was 13.5 ± 2 nm, both close to the estimated value. The TEM also established the long-range of the layers across the microposts. Some of the layers in the micropost are discontinuous, which may be responsible for the smaller value of GMR compared to electrodeposited thin films and nanowires and may contribute to the non-symmetric magnetoresistance behavior. The

heat treatment that was part of the TEM preparation may affect the structure, althought it was not large enough to destroy the layers through interdiffusion.

(a)

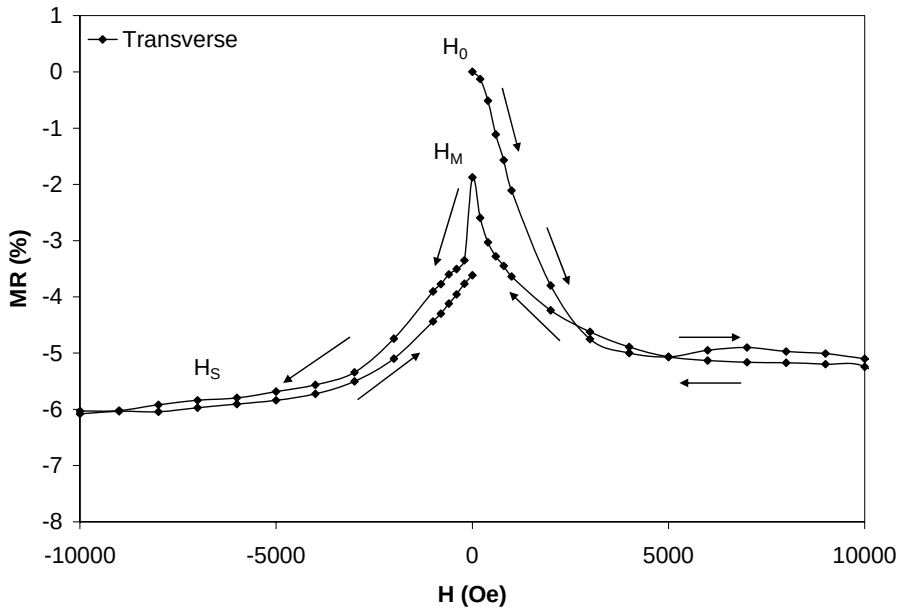

(b)

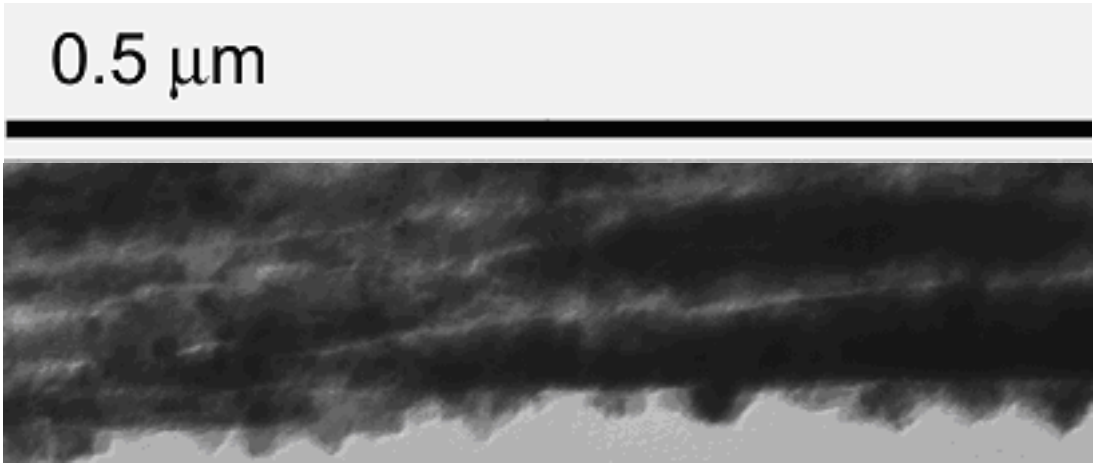

Figure 6-8 (a) Magnetoresistance, and (b) TEM of a single micropost Cu(9 nm)/Co(9 nm) deposited at E_{Cu}=-0.5 V, E_{Co}=-1.7 V (vs. SCE)

Since a giant magnetoresistance behavior was observed and the cobalt and copper layer thicknesses were important for the micropost magnetoresistance, two series of micropost samples were deposited in order to investigate the effect of the layer thickness

on magnetoresistance. The applied potential value for the copper layer and the cobalt layer were the same as those used for deposition of the micropost above. The first series of samples were deposited with different copper plating times of 15, 25, 46 and 61 s, while keeping the cobalt plating time constant at 0.9 s. The corresponding copper layer thicknesses were 3, 5, 9 and 12 nm, and the cobalt layer thickness was 9 nm. The total bilayer numbers were 41666, 35714, 27777 and 23809 with respect to the above copper layer thickness. The transverse magnetoresistance results were shown in Figure 6-9. A magnetoresistance of -0.2 % was obtained when the copper layer thickness was about 3 and 12 nm, and a magnetoresistance of -1.8 % with a symmetric curve was observed while the copper layer thickness was equal to 5 nm. However, the magnetoresistance of all of these three samples were lower than the -4.2 %, obtained with a copper layer thickness of 9 nm.

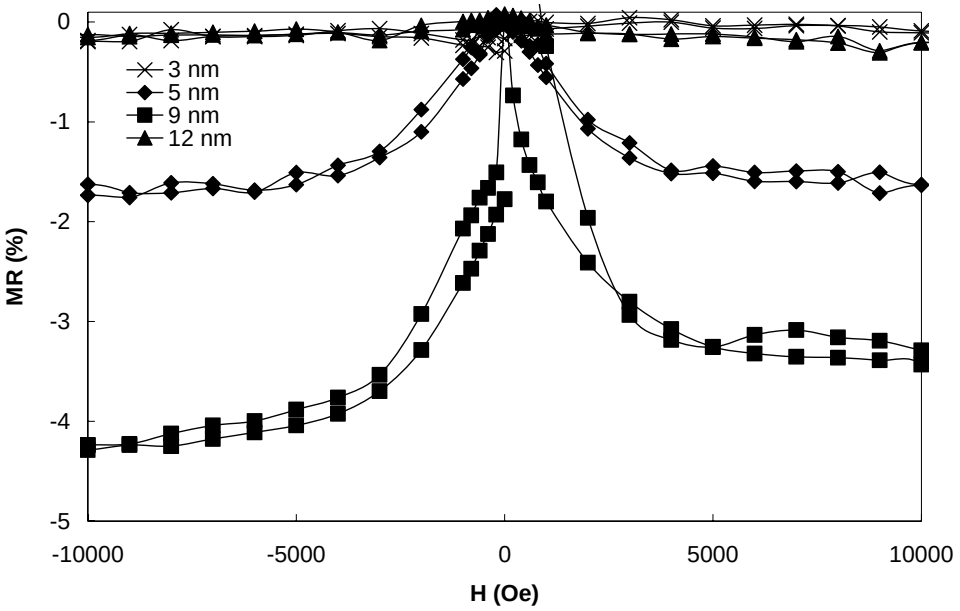

Figure 6-9 Transverse magnetoresistance of a single micropost Cu(x nm)/Co(9 nm) deposited at E_{Cu}=-0.5 V, E_{Co}=-1.7 V (vs. SCE)

Another series of samples were deposited with different cobalt plating time of 0.5, 0.7 and 0.9 s, while keeping the copper layer plating time constant at 46 s. The corresponding cobalt layer thicknesses were 5, 7 and 9 nm and the copper layer thickness was 9 nm. The bilayer numbers were 35714, 31250 and 27777 when the copper layer thicknesses varied from 5, 7 to 9 nm. The transverse magnetoresistance results were shown in Figure 6-10. A magnetoresistance of -0.7 % was obtained for the sample with a copper layer thickness of 5 nm. When the copper layer thickness was increased to 7 nm, the magnetoresistance increased to -1 %, and the sensitivity of the magnetoresistance decreased considerally. The saturated magnetoresistance was near 10000 Oe, much larger than the magnetic field needed to saturate the samples with a copper layer thickness of 5 nm and 9 nm. Therefore, the cobalt layer thickness not only had effect on the magnetoresistance value, but also influenced the sensitivity.

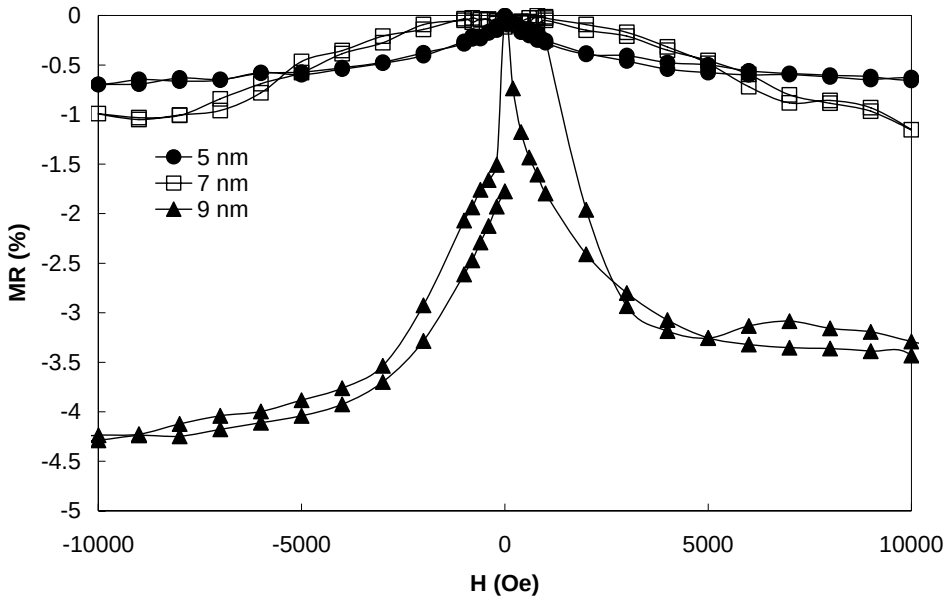

Figure 6-10 Transverse magnetoresistance of a single micropost Cu(9 nm)/Co(x nm) deposited at E_{Cu}=-0.5 V, E_{Co}=-1.7 V (vs. SCE)

6.4.2 Pulse Train Electrodeposition of Micropost

As discussed in Chapter 4 and Chapter 5, the pulse train control electrodeposition has the capability to enhance the magnetoresistance of the multilayered thin films and microdevices at certain duty cycleS Therefore, this deposition method was also applied to the potentiostatic deposition of Co/Cu multilayered microposts, where the cobalt rich layers were plated by a series of pulses with an on time of 0.15 s and a zero potential for 0.1 s. The total plating on time was equal to 0.9 s, the cycle number was 6. The total plating time of the Co rich layer was the same as that obtained by regular pulse deposition. The copper layers were plated by a constant potential at -0.5 V vs. SCE for 46 s similar to that used in the regular pulse scheme. And the cobalt layers were deposited at -1.7 V vs. SCE. The magnetoresistance of the pulse Co rich layer train is also shown in Figure 6-11. A 1 % magnetoresistance was obtained by the pulse train control deposition, having a saturation field of 2000 Oe. Compared to the sample plated by regular pulse, the magnetoresistance value was not enhanced, but the sensitivity was improved through a reduction of the saturation field by 2000 Oe.

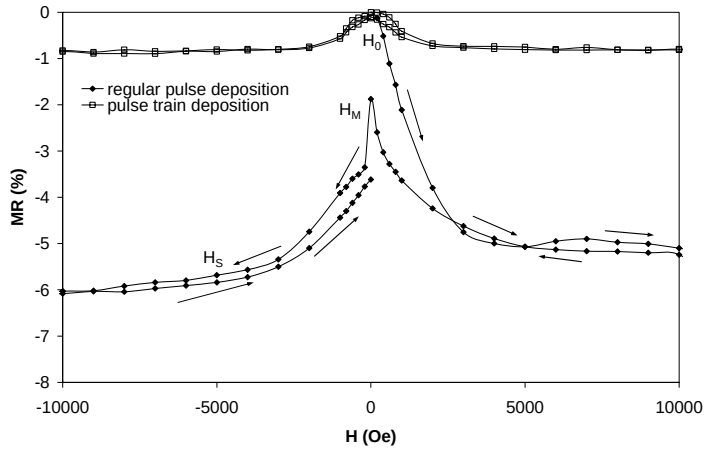

Figure 6-11 Transverse magnetoresistance of a single micropost Cu(9 nm)/Co(9 nm) deposited with pulse train control electrodeposition at E_{Cu}=-0.5 V, E_{Co}=-1.7 V (vs. SCE)

6.4.3 Potential Effect

The applied potential values were critical for deposition of discrete cobalt and copper layers and the realization of magnetoresistance of the micropost. A low over potential for the copper layer deposition in theory should help to enhance the copper purity and improve the magnetoresistance, but too low of an overpotential has the disadvantage of a longer plating time, especially for the deposition of 500 μm tall microposts. A higher overpotential for the cobalt layer deposition can increase its deposition reate but can also result in side reaction. (e.g. hydrogen evolution and water dissociation) lower overpotential, however, may produce cobalt layers with a higher copper component. Therefore, the potential effect on the magnetoresistance of the micropost was investigated. Since a symmetric magnetoresistance behavior was obtained when the copper and cobalt layer thicknesses were 5 nm and 9 nm, respectively, these layer thicknesses were employed to evaluate the potential effect on magnetoresistance of micropost. When the copper potential was lower than -0.5 V (vs. SCE), it was hard to obtain tall micropost in two weeks, therefore, higher values of -0.5 V and -0.6 V (vs. SCE) were chosen to deposit the copper layer with the same plating time of 23 s for copper layer thickness of 5 nm. For cobalt layer plating, two potential values of -1.7 V and -1.5 V was applied for the same plating time of 0.9 s. Figure 6-12 shows the transverse and longitudinal magnetoresistance behavior of the micropost sample plated at -0.5 V (vs. SCE) for the copper layer and -1.7 V (vs. SCE) for the cobalt layer. A transverse magnetoresistance of -1.7 % was obtained with a saturation field around 5000 Oe, and a longitudinal value of -1.3 % was observed with a saturation field less than 3000 Oe. Both transverse and longitudinal magnetoresistance were negative, which indicated

that this micropost sample had a giant magnetoresistance behavior. The difference between the transverse and longitudinal values verified an anisotropy magnetoresistance contributed to the transverse magnetoresistance behavior as well.

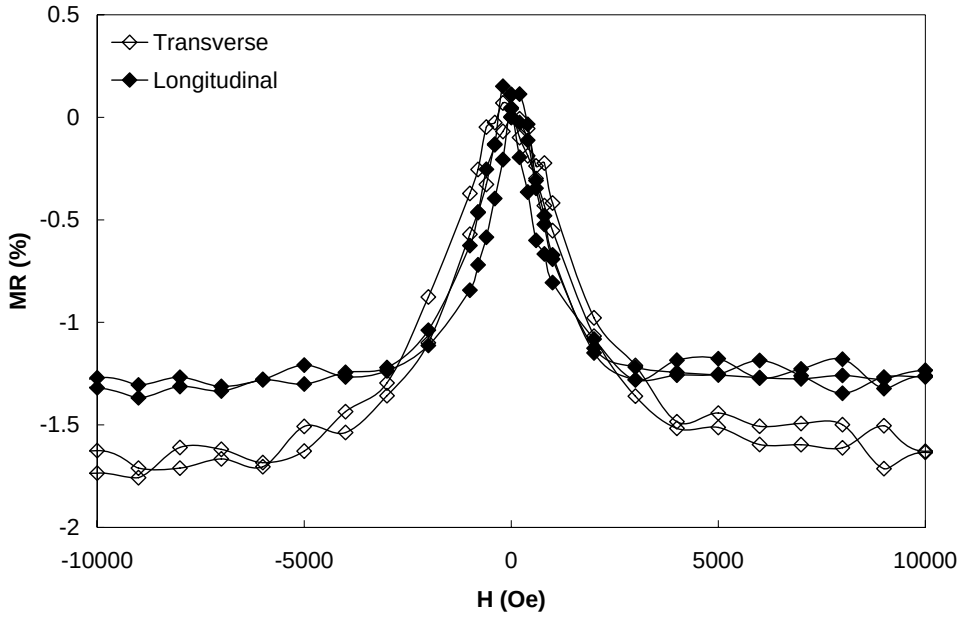

Figure 6-12 Magnetoresistance of a single micropost Cu (5 nm)/Co (9 nm) deposited with pulse train control electrodeposition at E_{Cu}=-0.5 V, E_{Co}=-1.7 V (vs. SCE)

Figure 6-13 showed the magnetoresistance of another micropost sample plated at higher potential of -0.6 V (vs. SCE) with plating time of 46 s. A virgin state behavior was observed for the transverse magnetoresistaance, A -3 % room temperature virgin state magnetoresistance was obtained when the magnetic field increased from 0 to 10000 Oe. After cycling back to 0 Oe, the magnetoresistance was kept at -1.5 %, without saturation until 10000 Oe. A longitudinal magnetoresistance of -0.5 was obtained without a virgin state. The saturation field was between 2000-3000 Oe, lower than the transverse saturation field. Both transverse and longitudinal magnetoresistance were negative, indicating a giant magnetoresistance behavior. The lack of a virgin state in the

longitudinal magnetoresistance was probably due to the different magnetization state from those in the transverse measurement. The copper potential effect on magnetoresistance can be observed by comparing Figure 6-12 and Figure 6-13. Larger magnetoresistance with better sensitivity was obtained when a -0.5 V (vs. SCE) was applied. The expected reason is probably due to the different copper layer composition. Purer copper layers should be obtained at lower potential of -0.5 V than at higher potential of -0.6 V. And a slight difference between these two copper layer thicknesses may also contribute to the different magnetoresistance behavior. Although the copper layer thicknesses were assumed to be equal to each other at 5 nm, the different copper potential of -0.5 V and -0.6 V may have resulted in a slightly different copper layer thickness.

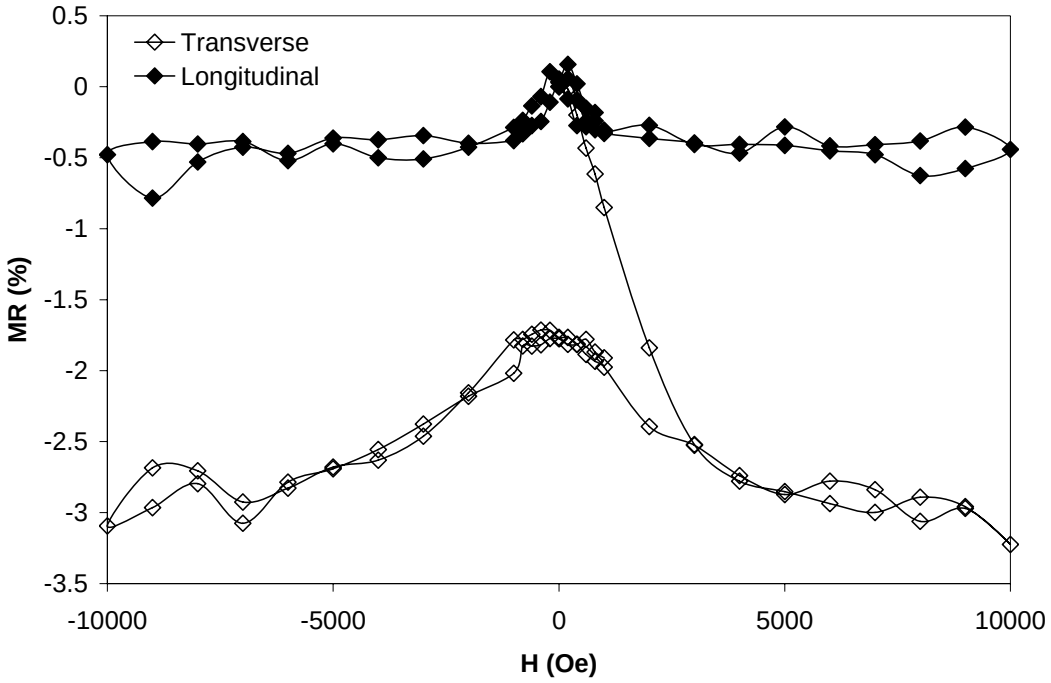

Figure 6-13 Magnetoresistance of a single micropost Cu(5 nm)/Co(9 nm) deposited with pulse train control electrodeposition at E_{Cu}=-0.6 V, E_{Co}=-1.7 V (vs. SCE)

The cobalt potential effect was also investigated by deposition of another sample at -1.5 V for 0.9 s, while the copper potential was kept at -0.5 V for 23 s. The magnetoresistance was shown in Figure 6-14. A -0.8 % transverse magnetoresistance was obtained without saturation until 10000 Oe, The longitudinal magnetoresistance showed a positive value of 1 % under 10000 Oe. The different sign of the transverse and longitudinal indicated that the anisotropy magnetoresistance dominated in the micropost plated at potential of -1.5 V for 23 s. The reasons were mainly due to two aspects. The first aspect was that more copper was deposited into the magnetic cobalt-rich layer when a low potential value of -1.5 V was applied. The second aspect was that the cobalt layer thickness was decreased at lower potential, which may have resulted in incomplete layers in some regions. Both of these effects make the multilayered micropost lose the giant magnetoresistance behavior. In general, the copper plating at -0.5 V for 23 s and -1.7 V for 0.9 s were the most appropriate parameters for the giant magnetoresistance property. Another sample deposited with conditions of the copper plating overpotential at -0.6 V for 23 s and the cobalt plating overpotential at -1.5 V for 0.9 s showed a poor symmetric and small positive value further verified the conclusion above. (the magnetoresistance of this sample was not shown here)

6.5 Summary*

A CoCu/Cu multilayered micropost was fabricated in a citrate electrolyte. To the best of our knowledge, this is the first demonstration of a CoCu/Cu multilayered micropost in a 500 μm deep recess. Both transverse and longitudinal magnetoresistance was measured on the micropost with different cobalt and copper layer thicknesses. A 4 %

* A part of the work presented in this chapter was presented at the 208th meeting of the Electrochemical Society, Oct. 2005.

transverse giant magnetoresistance at room temperature was obtained when both the cobalt and copper layer thickness were equal to 9 nm. Both the copper potential and the cobalt potentials affected the magnetoresistance behaviors. The recommended conditions for obtaining micropost that exhibit GMR are -0.5 V (vs. SCE) copper potential for 46 s and -1.7 V (vs. SCE) cobalt potential for 0.9 s.

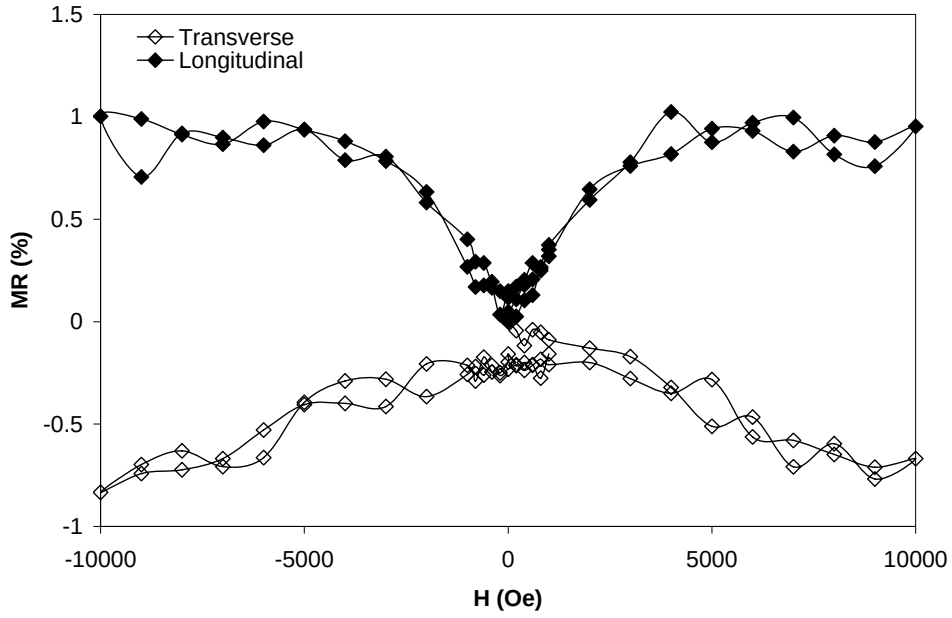

Figure 6-14 Magnetoresistance of a single micropost Cu(5 nm)/Co(9 nm) deposited with pulse train control electrodeposition at E_{Cu}=-0.5 V, E_{Co}=-1.5 V (vs. SCE)

6.6 References

1. W. Schwarzacher and D. Lashmore, *IEEE Transactions on Magnetics*, **32**, 3133 (1996).

2. M. Alper, in *Nanostructured Magnetic Materials and Their Applications*, D. Shi, B. Aktas, L. Pust and F. Mikailov, Editors, p. 111, Springer, Berlin, (2002).

3. W. P. Pratt, Jr., S. F. Lee, J. M. Slaughter, R. Loloee, P. A. Schroeder, and J. Bass, *Physical Review Letter,* **66**, 3060 (1991).4. S. Zhang and P. Levy, *Journal of Applied Physics,* **69**, 4786 (1991).

5. T. Valet and A. Fert, *Physical Review B*, **48**, 7099 (1993).

6. A. Fert and L. Piraux, *Journal of Magnetism and Magnetic Materials,* **200**, 338 (1999).

7. S. Dubois, J. Beuken, L. Piraux, J. Duvail, A. Fert, J. George, and J. Maurice, *Journal of Magnetism and Magnetic Materials,* **165**, 30 (1997).

8. M. A. M.Gijs, S. K. J. Lenczowski, and J. B. Giesbers, *Physical Review Letters*, **70**, 3343 (1993).

9. M. Gijs, S. K. J. Lenczowski, R. J. M. Vandeveerdonk, J. B. Giesbers, M. T. Johnson, *Physical Review B*, **50**, 16733 (1994).

10. M. Gijs and G. Bauer, *Advances in Physics*, **46**, 285 (1997).

11. J. Spallas, M. Mao, B. Law, F. Grabner, D. Okane, and C. Cerjan, *IEEE Transactions Magnetics,* **33**, 3391 (1997).

12. J. Spallas, Y. Huai, S. Vernon, B. Fuchs, B. Law, D. Kania, D. Kroes, M. Thomas, D. Okane, and Z. Tan, *IEEE Transactions on Magnetics,* **32**, 4710 (1996).

13. W. Schwarzacher, O. Kasyutich, P. Evans, M. Darbyshire, G. Yi, V. Fedosyuk, F. Rousseaux, E. Cambril, and D. Decanini, *Journal of Magnetism and Magnetic Materials,* **199**, 185 (1999).

14. J. Duvail, S. Dubois, L. Piraux, A. Vaures, A. Fert, D. Adam, M. Champagne, F. Rousseaux, and D. Decanini, *Journal of Applied Physics,* **84**, 6359 (1998).

15. C. Bonhote and D. Landolt, *Electrochemical Acta,* **42**, 2407 (1997).

16. A. Cziraki, M. Koteles, L. Peter, Z. Kupay, J. Padar, L. Pogany, I. Bakonyi, M. Uhlemann, M. Herrich, B. Arnold, J. Thomas, H. D. Bauer, and K. Wetzig, *Thin Solid Films,* **433**, 237 (2003).

17. C. Lim, Q. Huang, X. Xie, A. Safir, S. Harfenist, R. Cohn, and E. Podlaha, *Journal of Applied Electrochemistry,* **34**, 857 (2004).

18. L. Piraux, J. George, J. Despres, C. Leroy, E. Ferain, R. Legras, K. Ounadjela, and A. Fert, *Applied Physical Letters,* **65**, 2484 (1994).

19. T. Ohgai, X. Hoffer, A. Fabian, L. Gravier, and J.-P. Ansermet, *Journal of Materials Chemistry,* **13**, 2530 (2003).

CHAPTER 7. CONCLUSIONS

The magnetoresistance behavior of electrodeposited CoCu/Cu multilayers on silicon wafers was significantly influenced by the cobalt and copper layer thicknesses. Both the magnetoresistance value and sensitivity of the multilayers at a cobalt layer thickness of 2.5 nm were higher than those at 1.25 nm and 19 nm, due to a balance between having a complete coverage of the cobalt on the copper layer and minimizing the cobalt layer thickness. When the copper layer thickness varied from 0.5 nm to 3.5 nm, the GMR behavior depended on the cobalt layer thickness. In the regular pulse electrodeposition method, the best GMR result, with over 5 % magnetoresistance, was observed for the multilayer with a copper layer thickness of 3 nm and a cobalt layer thickness of 2.5 nm. The saturation field was less than 2000 Oe. While the value of GMR was not higher than most literature reports the sensitivity was considerably improved.

Many factors affect the magnetoresistance behavior of the electrodeposited multilayers. The electrolyte pH was very important to obtain the high sensitivity value of magnetoresistance. In the electrolyte pH range between 2.8 and 3.2, the pH of 3.0 was the the best value observed, if the magnetoresistance value and the deposition quality were considered. The bilayer number was another factor. Larger bilayer number was favorable because the total continuity of the thin film on the silicon wafers was improved. In addition, there was a seed layer effect. A seed layer on the silicon wafer was important to achieve a higher GMR. It is expected that the seed layer reduces the diffusion of the copper or cobalt atoms into the silicon wafer, and it may affect the nucleation of the deposit in a favorable way. The influence of nickel ions into the electrolyte on the

resulting deposit magnetoresistance depended on the nickel ion source. Nickel sulphamate was better than nickel sulfate, however, the magnetoresistance of the multilayers was not improved by adding a small amount of either nickel sulfate or nickel sulphamate.

A pulse train control deposition of the cobalt layer during the fabrication of CoCu/Cu multilayers can improve magnetoresistance over the conventional square-wave pulse. A maximum 7-8 % magnetoresistance can be obtained with a decrease of duty cycle. Pulse train control deposition on the copper layer has a slight effect on the magnetoresistance value. WDS analysis indicated that the copper concentration in the thin films increased with a decrease of duty cycle when the cobalt layer was deposited with pulse train current. At low duty cycle, there is a loss of magnetoresistance associated with an increase of the pulse limiting Cu current density and an enhancement of the displacement reaction during the off time.

A GMR micro-sensor patterned using a UV-lithography technique was successfully electrodeposited. The resistance of the microdevice was increased by manipulating the wire width and length. The geometry of the microdevice played a significant role in the magnetoresistance behavior. The magnetoresistance was increased with the enlargement of line width, affected by the contribution of the plating edge effect. The increase of bilayer number also improved the magnetoresistance values of the microdevice. The thickness of the photoresist had little effect on the magnetoresistance property of the microdevice. Pulse train deposition also improved the magnetoresistance of the microdevice at a cycle number of 0.33.

Deep recess multilayer electrodeposition was also carried out with the use of X-ray lithography. Sodium citrate was critical in the electrodeposition of CoCu components into the deep recesses because it has the capability to decrease the displacement reaction between cobalt and copper elements, and acts as a buffering agent. The CoCu/Cu multilayered microposts were successfully obtained in the citrate electrolyte by a pulsed potentiostatic method. This is the first demonstration of a CoCu/Cu multilayered micropost in a 500 μm deep recess. Both transverse and longitudinal magnetoresistance measurements were conducted on a single micropost at different cobalt and copper layer thicknesses. The cobalt and copper layer thicknesses influenced the micropost magneoresistance behavior. At larger layer thicknesses, anisotropic magnetoresistance dominated and at smaller layer thickness, giant magnetoresistance was observed. To date, a 4 % transverse giant magnetoresistance with saturation field less than 5,000 Oe at room temperature was obtained when both the cobalt and copper layer thickness were equal to 9 nm. Both the copper and cobalt applied potential were two important factors in order to obtain giant magnetoresistance behaviors. The best suggested conditions to obtain giant magnetoressistance are: copper applied potential = -0.5 V (vs. SCE) for 46 s, and a cobalt applied potential = -1.7 V (vs. SCE), for 0.9 s.

APPENDIX A. THIN FILMS ON NON-SILICON SUBSTRATES

1. Introduction

In this Appendix conditions for layered and unlayered CoCu alloy thin films electrodeposits are presented onto non-ideal substrates. The conditions that affected the alloy deposition and GMR have been used to develop the preferred conditions presented in the dissertation.

2. Experimental

2.1 Electrolyte

The electrolyte for thin film plating is listed in Table 1. Analytical grade reagents from Fisher were used in the preparation of the solutions in distilled-DI water. A stir bar provided bulk mixing. The pH value was adjusted to 2.0 with sulfuric acid and sodium hydroxide at room temperature and was measured using a Orion® Model 420A pH meter. The electrolyte was sparged with nitrogen for 1 hour before deposition.

Table 1 Electrolyte Compositions for Thin Film Plating

Component	Concentration
Copper Sulfate	0.005 M
Cobalt Sulfate	0.5 M
Boric Acid	0.543 M
Triton X-100	0.4 g/L

2.2 Substrate preparation

Stainless steel, gold or copper disks, having a diameter of 6 ±0.1 mm were employed as a cathode. The stainless steel surface was polished using 500, 1500, 2000 and 4000 silicon carbon papers and then polished using diamond and aluminium oxide

pastes in order to obtain a mirror finishing. When gold substrates were desired, the stainless steel was electroplated with gold. Gold plating utilized an acid gold strike (Technic Inc.) pretreatment. Techni gold 25 E (Technic Inc.) solution was used to plate about 100 nm layer gold on the stainless steel disk using an IM6e Zahner® Impedance Measurement/Potentiostat/Galvanostat system with currents –3.7 mA/cm^2 and –1 mA/cm^2, respectively for the strike and plating solution. Copper disks, with the same diameter were also used as cathode substrates. The polishing process for the surface was same as that for stainless steel.

Polycrystalline copper foil with preferred orientation (100) was also used as a substrate (cathode), with the surface polished using 4000 silicon carbon papers. Subsequently, the foil was cut into a 2.5×2.5 cm square plate and deionized water was employed to clean its surface before it was put into the sample holder.

2.3 Cell Design and Operation

Figure 1 is a schematic of the experimental setup for multilayer deposition. Two types of cell setup were used. The first one is for the multilayer deposition on disk electrodes with agitation. The second one is the multilayer deposition on copper foil without agitation. In the first setup as shown in Figure 1(a) a 1000 ml two-compartment cell was used to avoid the mixing of the anodic Co^{3+} products into the cathodic region. A Pine MSRX high precision speed control rotator provided the electrode agitation. A piece of platinum mesh was used as the anode. For the polarization and ohmic correction experiments, a saturated calomel electrode (SCE) was placed next to the substrate surface as reference electrode.

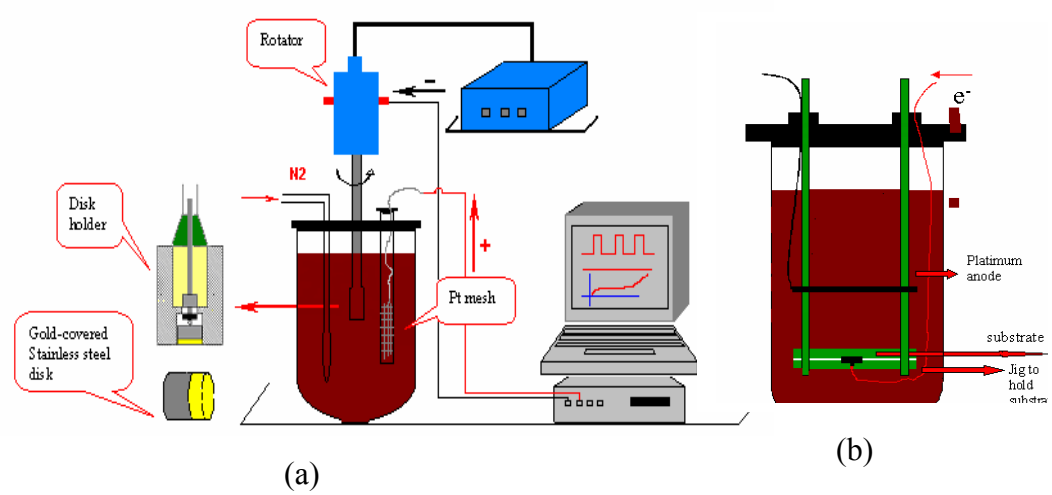

Figure 1 Schematic of the cell used for multilayer deposition

In the second setup, a jig was used as shown in Figure 1(b). The jig has two cylindrical disks, which are held together using screws. The bottom disk has a copper plate recessed to seat the copper foil substrate. A copper wire soldered to the bottom of the recessed plate served as the cathode connection. The top disk has a 1.5 cm diameter exposed area that enables the electrolyte solution to reach the substrate. The side of the jig was also protected from the electrolyte by insulation tape.

2.4 Deposition with Agitation

Polarization curves were carried out with a Pine Instruments bipotentiostat, at a scan rate of 5 mV/s and the potential was corrected for ohmic drop, which is measured by impedance analysis with a Bas-Zahner IM6 Zahner® unit. The same unit can also serve as the power supply to generate direct current for deposition. All experiments were carried out at atmospheric pressure and at room temperature.

Different constant current densities from –0.71 mA/cm^2 to –200 mA/cm^2 were applied to plate CuCo alloys on the gold-covered stainless steel rotating disk. In order to calculate the current efficiency and the partial current density during alloy deposition, the

mass of the deposit film was obtained by a stripping method. A sulfuric acid electrolyte, 0.1 M H_2SO_4, was employed for the stripping experiments. Copper foil served as the anode and a saturated calomel electrode (SCE) was placed next to the stainless steel disk as reference electrode.

After deposition, the multilayers on the disk was quickly taken out from the electrolyte and rinsed with water. Subsequently, the film was peeled off by scotch tape as shown in Figure 2. The tape was applied to the front surface of the multilayer deposit. When the tape was removed, adhesion of the multilayer deposit was greater on the tape than on the deposit.

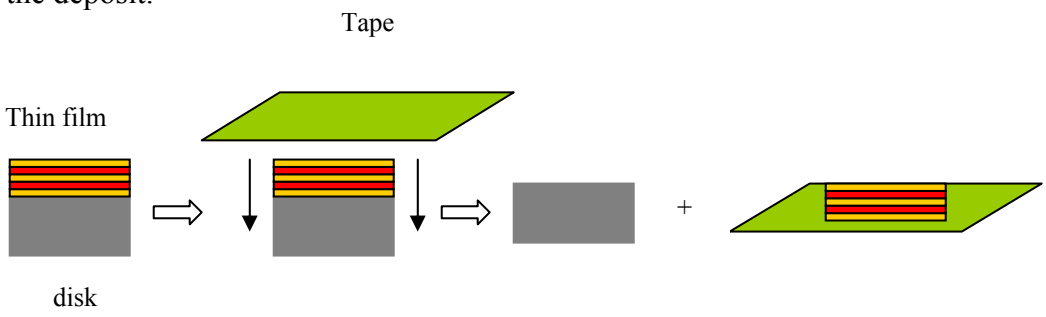

Figure 2 A schematic to peel off thin film(alloy or multilayer) from disk.

2.5 Deposition without Agitation

Some experiments were carried out without agitation. In this case, a polished copper foil was put into the jig holder, shown in Figure 1. A Pt mesh was used as an anode in a separate compartment. The bipotentiostat (Model AFCBP1) and programmable function generator (Amel Model 568) were set to control the pulse current and required deposition time. After deposition, the copper foil and multilayer was quickly rinsed with DI water.

3. Deposit Analysis

3.1 SEM and GMR

The morphology of the deposits was obtained from a Scanning Electron Microscope (SEM) (Joel JSM-840A), The posts were analyzed using a Superprobe 733-electron microprobe (JEOL company) with wavelength dispersive x-ray spectrometer for chemical composition of Cu and Co along the length of the micropost.

For GMR measurements, the multilayers were cut into small pieces and mounted in a GMR holder. The holder consisted of four platinum wires and was connected to the deposit in a straight line. When the magnetic field is parallel to the current in the film plane, the measured magnetoresistance is called longitudinal GMR. When the magnetic field is perpendicular to the current in the film plane, the magneto resistance is called transverse GMR. In the present works the in-plane transverse giant magnetoresistance (GMR) of the multilayers was measured at room temperature with a 9T quantum design physical properties measurement system (PPMS), using the standard four-point probe ac technique at 27 Hz with an excitation current of 1mA. The GMR is then defined according to $\Delta R/R=(R(H)-R(0))/R(0) \times 100$, where R(0) is the resistance at zero magnetic field, and R(H) is the resistance in external field H.

4. Electrolyte Characterization

Co-Cu alloys and multilayers were electrodeposited at a constant dc or a pulse control of current density from an aqueous sulfate electrolyte. Figure 3 shows the polarization curves obtained with different electrode rotation rates. Regions where copper and cobalt are deposited are evident from the curves. The copper partial current density is apparent from the flat regions of the curve followed by the rise of the cobalt partial current densities at potentials more negative than –0.78 V. Copper ions are in a much lower electrolyte concentration compared to cobalt and thus it is expected that Cu reaches

its limiting current density at low current densities. Confirmation that this is indeed the mass transport limited rate is evidenced by the linear increase in the flat portion of the curve with the square root of rotation rate. (See inset in Figure 3). The copper diffusion coefficient determined from the Levich equation is 4.8×10^{-6} cm^2/s, which is similar to values reported in the literature. For example, Qiang *et al.*[1] reported a value of 3×10^{-6} cm^2/s in sulfate electrolytes containing boric acid, Chassaing *et al.*[2] reported a value of 5 x 10^{-6} cm^2/s in a citrate electrolyte with nickel, Quickenden *et al.*[3] obtained a value of 7 x 10^{-6} cm^2/s and Bradley *et al.*[4] report a value of 5.92×10^{-6} cm^2/s in the electrolyte containing nickel sulfate and copper sulfate.

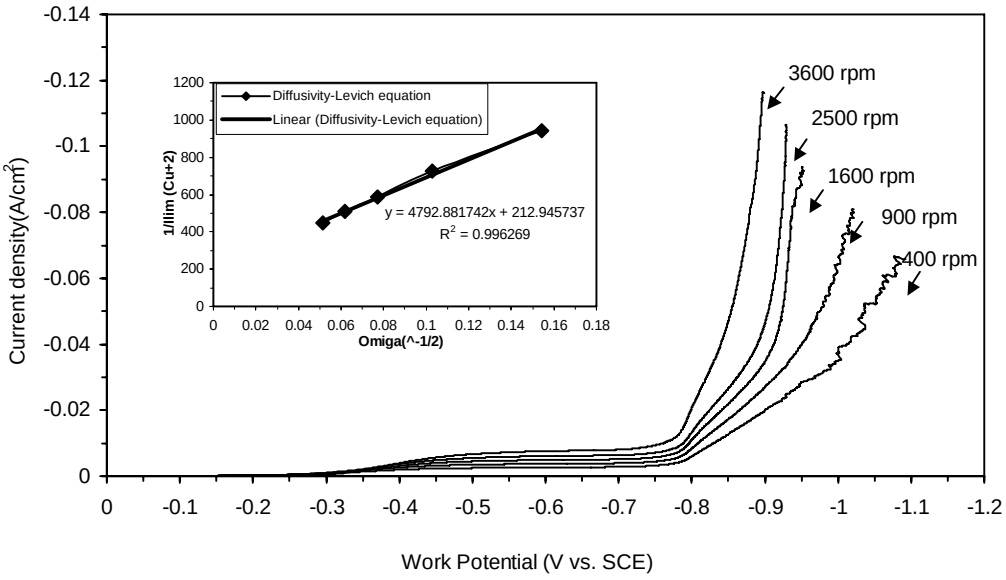

Figure 3. Total current polarization curves; inset diffusivity-Levich relation of limiting current density of Cu with agitation.

Figure 4 (a) shows the concentration of Co in the film as a function of current density, for a constant, unmodulated current density at rotation rate of 400 rpm. As expected, a Co-rich alloy is deposited at high current densities, with a small amount of copper. The Co content of the film increases from 0.39 to 94 wt. % with an increase in

current density from -0.71 to -60 mA/cm^2. Current efficiency, shown in Figure 4.2(b), was obtained by a stripping method. It is over 90 % at low current densities, where Cu is plated, goes through a minimum, and then increases again approaching a value of about 60 % at high current densities where Co-rich alloys are obtained. Both the efficiency and composition were used in the determination of partial current densities of each reactant.

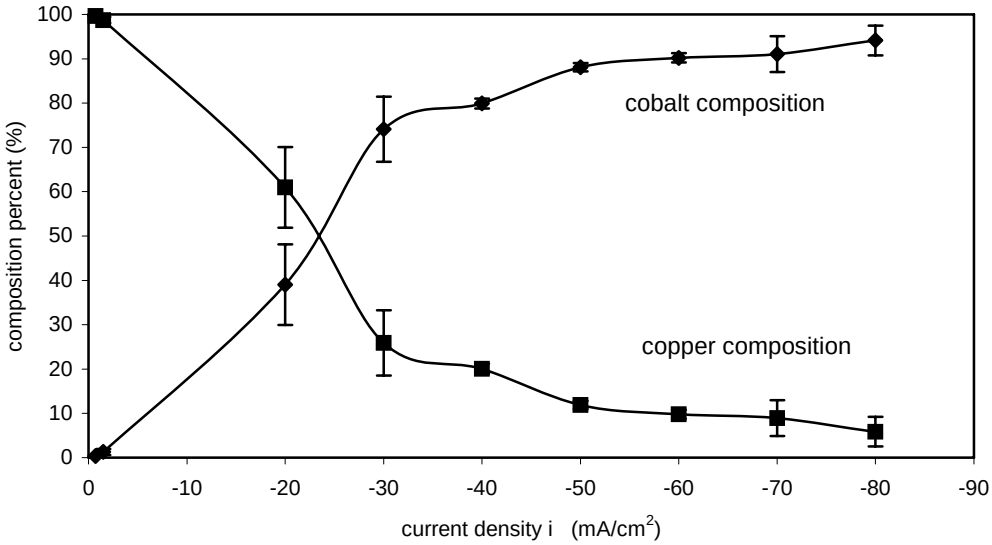

Figure 4 (a) Mass percent composition of cobalt and copper in dc electrodeposited Alloys.

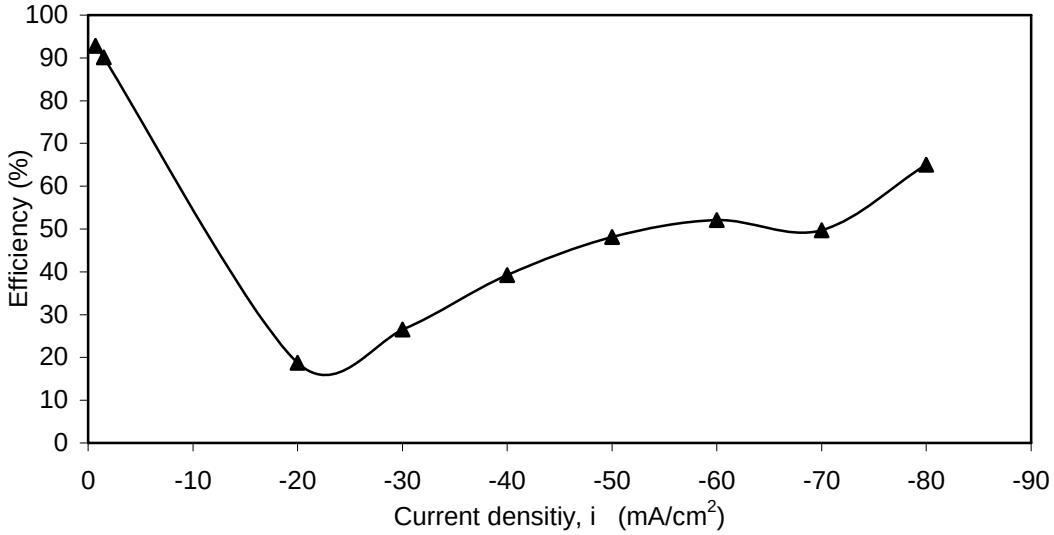

Figure 4 (b) Current efficiency in dc electrodeposited alloys

Figure 5 is the cobalt, copper and side reaction partial current density at an electrode rotation rate of 400 rpm. The copper partial current density is constant because of the mass transport limit. The cobalt partial current density increases with an increase of applied potential. The Co Tafel slope is 210 mV, which is a little larger than the value of 125 mV reported by Zhuang *et al.*[5] in the single sulfate cobalt electrolyte. The side reaction includes the evolution of hydrogen by proton and water reduction.

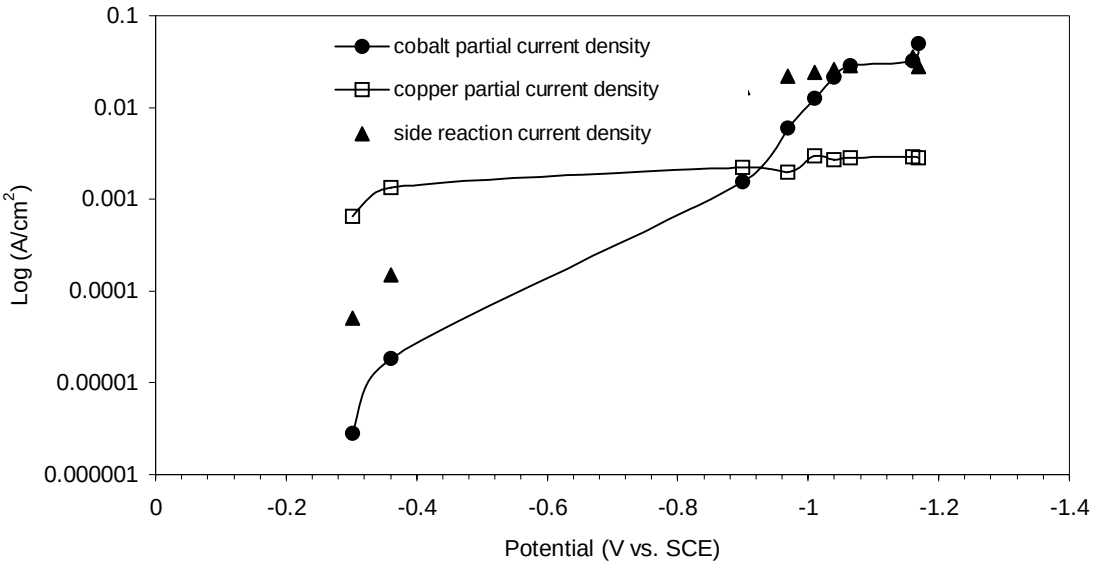

Figure 5 Cobalt and copper partial current density at a rotation rate of 400 rpm

Figure 6 is the polarization curve for the electrolyte without agitation. This curve is used to choose the plating currents for the multilayer deposited without agitation, on the square plate in the jig holder. It is observed that the Cu limiting current density is about -0.4 mA/cm^2, lower than when the electrode is rotated. Therefore, the current density values that were selected without electrode agitation were -0.2 mA/cm^2 to ensure copper plating lies in the kinetic region, and -15 mA/cm^2 for Co. Figure 7 (a) is the composition in the alloy deposited at constant current density. The composition for the alloys plated at

-0.2 mA/cm^2 and -15 mA/cm^2 contained 0.4 wt. % and 95.5 wt. % Co, respectively, with the corresponding current efficiency of 77 % and 61.7 %, shown in Figure 7 (b).

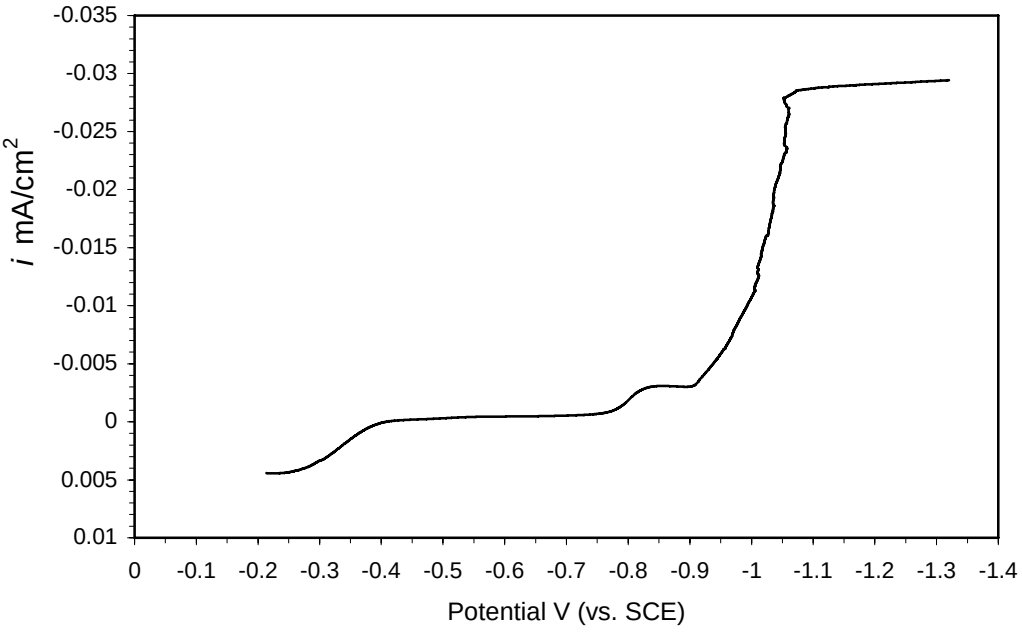

Figure 6. Polarization curves for electrolyte without agitation.

(a)

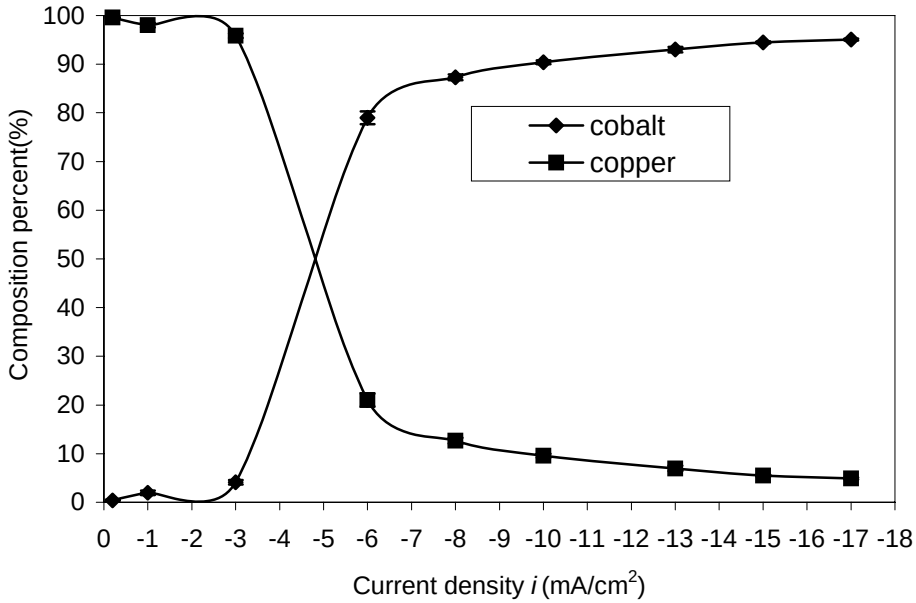

(b)

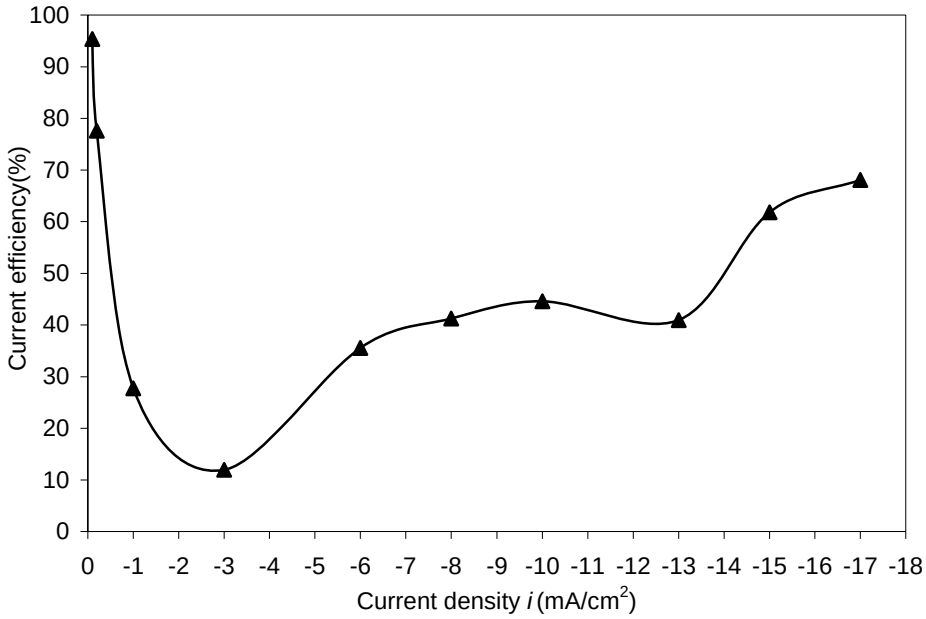

Figure 7 (a) Composition and (b) current efficiency for the thin film electrolyte without agitation.

5. Effect of Triton X-100 on Thin Film Morphology

Figure 8 shows SEM micrographs of 12 μm thick alloys and 1.3 μm thick multilayers, with and without Triton X-100. The alloys were plated at –60 mA/cm^2 for 900 s. The multilayers were deposited at -1.42 mA/cm^2 for 3.793 s and -424 mA/cm^2 for 0.0263 s. It is noted that Triton X-100 plays a role on the film quality. For samples plated without Triton X-100 (Figure 8 a,c) pinholes result from the evolution of hydrogen, whether the deposits were alloys or multilayers. Samples deposited with Triton X-100 (Figure 8 b,d) show no obvious pinholes. Thus, even though Lenczowski *et al*.[6] have reported a loss of GMR with Triton X-100, a trade-off between realizing a pit-free surface morphology for thick films and loss of GMR must be considered.

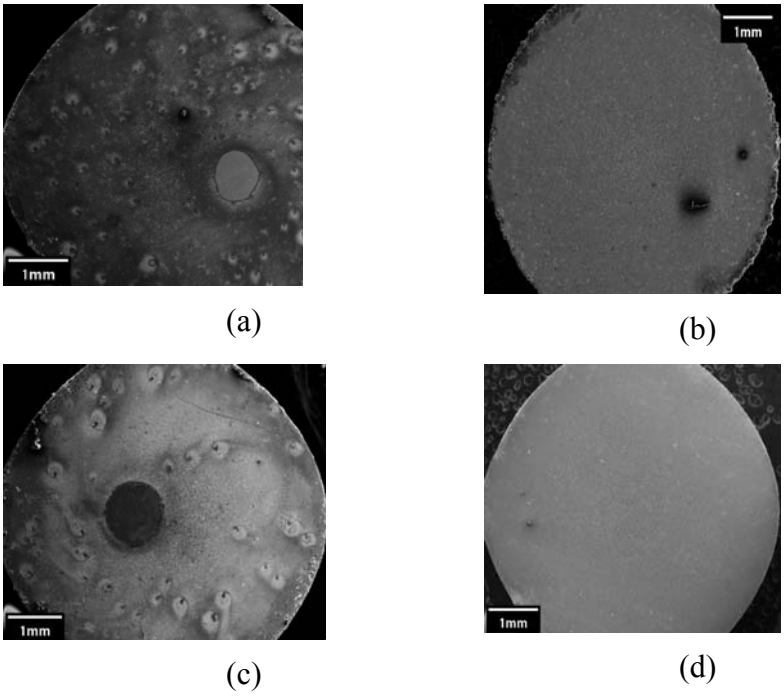

Figure 8 SEM of alloy and multilayers plated on stainless steel RDE, 400 rpm

(a). alloy plated without Triton x-100 at current density of –60mA/cm^2

(b) alloy plated with Triton x-100 at current density of –60mA/cm^2

(c) multilayer [Cu(1.7nm)/Co(1nm)]$_{500}$ plated without Triton x-100

(d) multilayer [Cu(1.7nm)/Co(1nm)]$_{500}$ plated with Triton x-100

6. Multilayer GMR

6.1 Agitation

The in-plane transverse giant magnetoresistance (GMR) of the multilayers was measured at room temperature. The plating current densities and times for each bilayer were: -0.71 mA/cm^2 or -1.42 mA/cm^2 for 3.793 s, and -424 mA/cm^2 for 0.0263 s. Figure 4.9 shows the change in resistance due to the transverse magnetic field at room temperature for the multilayer [Cu (x nm)/Co(1nm)]$_{500}$ plated on gold-covered stainless steel. A GMR of approximately –5 % at saturation was noted when the calculated Cu-rich

layer thickness was 1.7 nm and a Co-rich layer of 1 nm. However, when the Cu-rich layer is reduced in size to 0.9 nm, the anhysteretic behavior is lost, although MR was exhibited. In granular alloys, a resistance dependent history is observed, which may indicate the loss of the multilayer structure, similar to a granular-like film.

Figure 10 shows the MR measurement of a $[Co(1nm)/Cu(1.7nm)]_{500}$ multilayer plated on stainless steel, without the Au. The maximum MR is about -2.5 % at a magnetic field of 9 T when Triton X-100 is present and is slightly lower than the value obtained when the substrate had a gold layer, Figure 9. Since Triton X-100 has been observed to decrease GMR,[6] a sample was plated from a solution without the Triton X-100. The GMR was 1 % higher, although not largely improved.

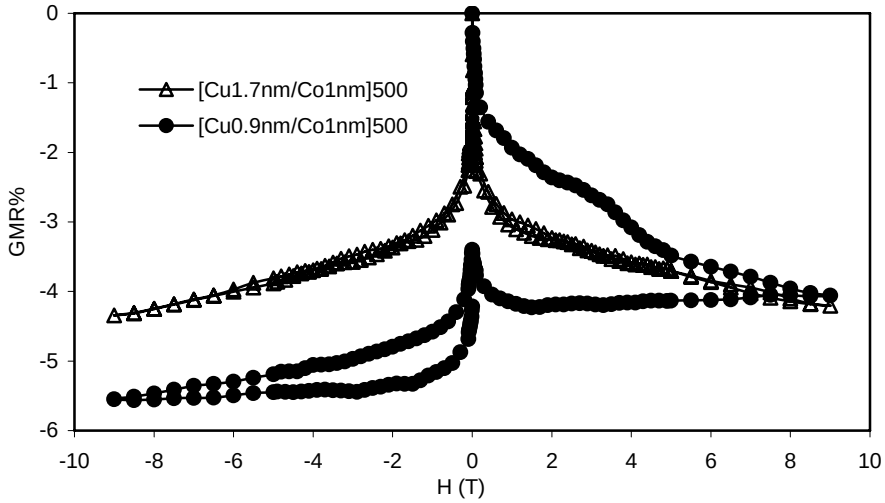

Figure 9 Measurement of GMR in the transverse direction for a film with 1 nm of Co- rich layer thickness, 1.7 nm and 0.9 nm of Cu-rich layer thickness.

The multilayers were also plated onto copper RDEs. The plating condition was the same as those plated on stainless steel. But because it is difficult to peel off the multilayer

from the copper disk, the bilayer number of the multilayer was enlarged to 9500. The measurement of GMR was shown in Figure 11. The GMR shows a good anhysteresis behavior except the value is lower. The reason for low GMR may be that the enlarged bilayer number increases the interfacial roughness, decreasing the GMR.

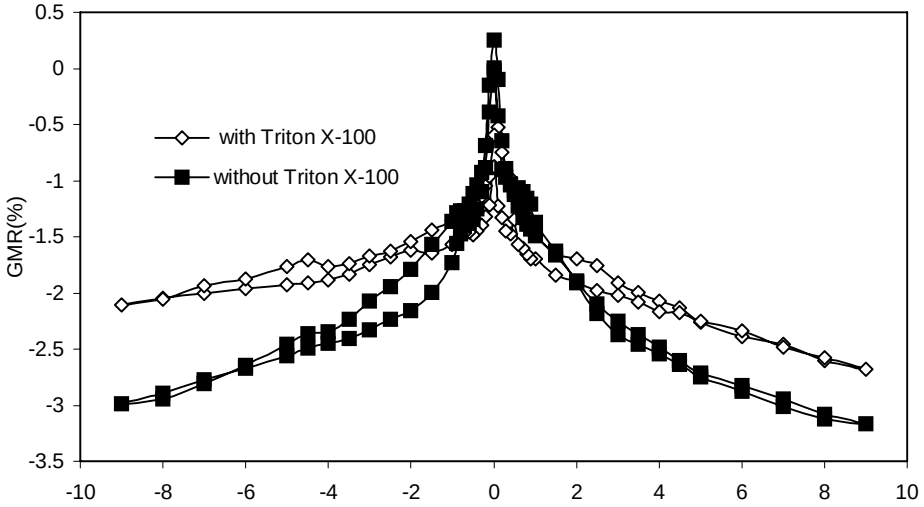

Figure 10 GMR in the transverse direction for a film plated with Triton X-100, and without Triton X-100, with 1 nm of Co-rich layer thickness and 1.7 nm of Cu-rich layer thickness.

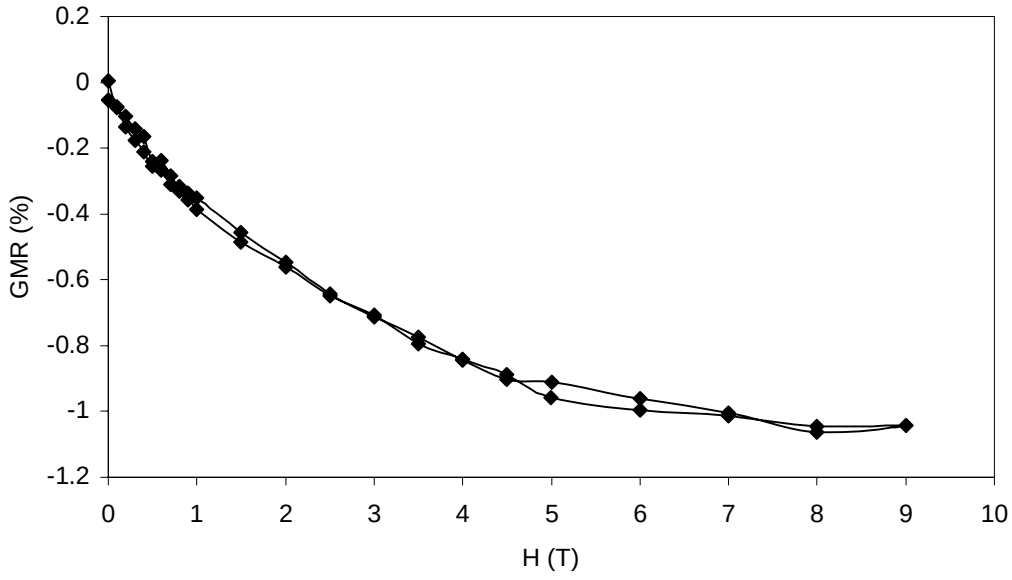

Figure 11 GMR in the transverse direction for multilayer[Cu(1.7nm)/Co(1nm)]$_{9500}$ plated on copper disk

The polycrystalline Cu disk exhibited a preferred (111) orientation. Polycrystalline copper foil with preferred (200) orientation was also employed to plate the multilayers. But because it is difficult to directly peal off the multilayer from the foil, multilayer GMR was measured with the copper foil together. Obviously copper foil will effect the GMR measurement, as shown in Figure 12, most of the current will be short circuited away to the copper foil, which results in very low resistance at the order of 10^{-4} ohm. The higher field is necessary to observe GMR results from the shunting of current due to the Cu substrate. With the quoted equipment sensitivity being 1 nV for 1 kHz and 20 nV for 1 Hz, the resistance measurement sensitivity, at 27 Hz and 10 mA, is believed to be smaller than 2×10^{-6} Ω, equivalent to an error of 2 % for a resistance of 10^{-4} Ω. As the applied magnetic field increases the resistance of the multilayer falls lower than that of copper. Therefore, the current passed in the experiment at low fields is directed through Cu, while at high fields it is expected to also go through the multilayer.

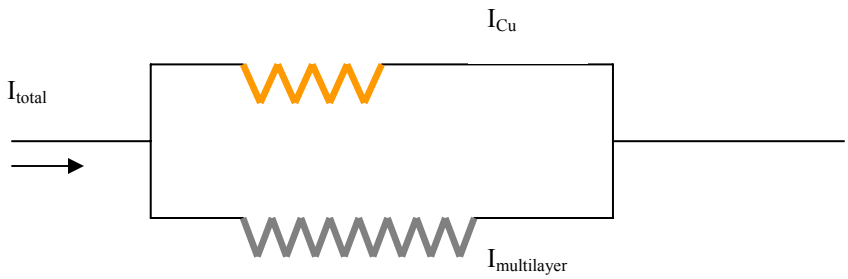

Figure 12 schemes for effect of copper foil on GMR measurement

In Figure 13 the RDE stainless steel substrate was replaced with a (200) Cu foil. Two different multilayer films were deposited onto the foil at 400 rpm with similar conditions as in Figure 6. One multilayer film was plated with a Cu current density of –1.6 mA/cm^2 for 3.793 s, and Co current density of –167.7 mA/cm^2 for 0.0263 s. The second film was deposited with a lower Cu current density of –0.79 mA/cm^2 for the same

time (3.793 s), keeping the Co current density and plating time the same. Both multilayer films contained 500 bilayers and the GMR was measured directly on the Cu foil substrate. The sample with the smaller copper current density exhibited a large GMR at high fields, where the resistance of the multilayer becomes smaller than the resistance of the Cu foil substrate. The GMR exceeds 18 %, which is an order of magnitude larger than what was obtained without the Cu foil.

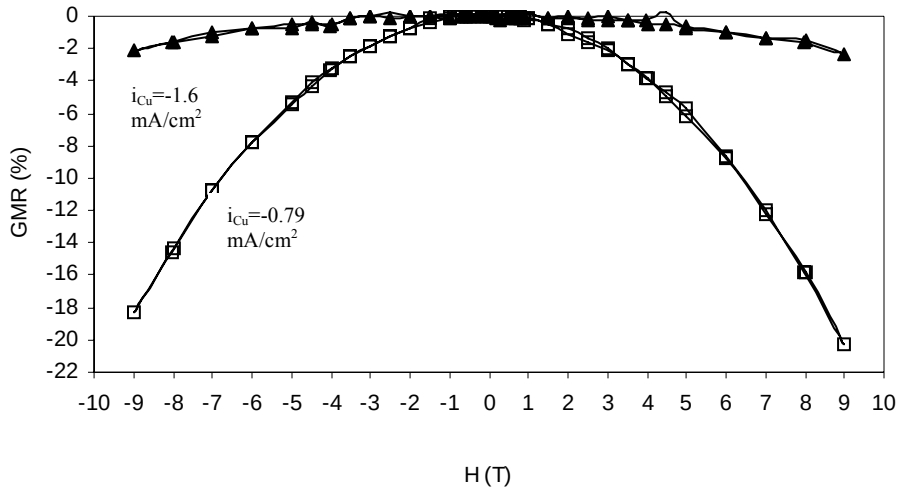

Figure 13 GMR of multilayer films on Cu foil substrate composites, bilayer number 500 at 400 rpm.

6. 2 Without Agitation

Figure 14 shows the magnetoresistance measurement for multilayers plated on copper foil, but without solution agitation and with a larger number of bilayers. The copper plating current density was lowered due to the decrease in the limiting current density. The current density was –0.2 mA/cm^2 and the plating time was 28.34 s, which yields a copper layer thickness of 1.6 nm, with a current efficiency of 77 % and a composition of 99.6 wt % Cu (Figure 7). The cobalt plating current density was –15 mA/cm^2, and the plating time varied from: 0.291, 0.314, 0.485 and 0.582 s. The

corresponding calculated cobalt thicknesses were: 1.2, 1.5, 1.9 and 2.2 nm based on the current efficiency of 61.7%. (Containing 5.54 wt. % Cu). The number of bilayers was 1500. The GMR varied with the Co layer thickness, and more than 25 % GMR was observed at a magnetic field of 9 T for the sample $[Cu1.6nm/Co1.1nm]_{1500}$. There was no MR at low field due to the shunting of the current through the copper substrate, as expected. When the Cu substrate is eliminated, by etching the backside of the film, then the MR drops an order of magnitude. This behavior may suggest that internal stress plays a role as suggested by Chassaing.[7]

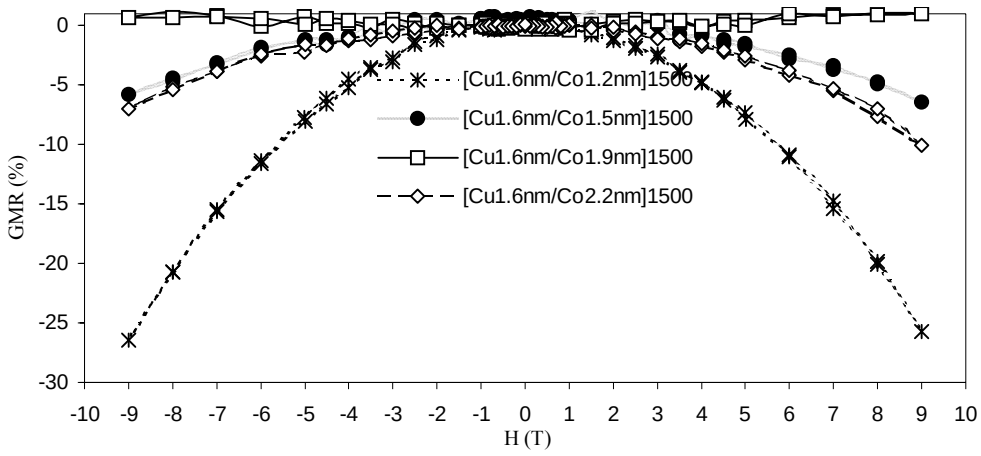

Figure 14 GMR of multilayer films on Cu foil substrate composites, bilayer number 1500.

Figure 15 is a multilayer plated on copper foil with the electrolyte similar to the previous one, Table 3.1, but without the Triton X-100. The plating current densities for the copper and cobalt layers were –0.1 mA/cm^2 and –15 mA/cm^2, respectively. The plating time was 21.48 s for the copper layer and 0.436 s for cobalt layer, respectively. The total bilayer number was 1500. A 40 % GMR was observed from this sample, which

exceeds most other reports of electrodeposited GMR except for the often criticized report of Bird *et al.*[8]

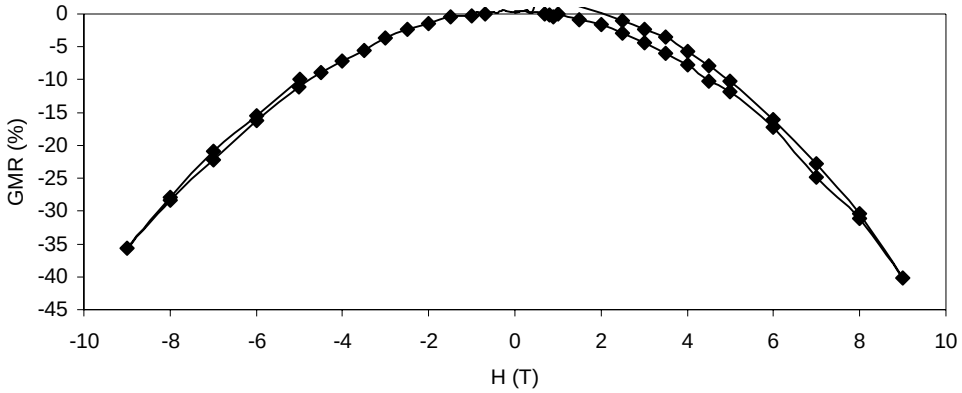

Figure 15 GMR of multilayer films on Cu foil substrate composites from electrolyte without Triton X-100, bilayer number 1500.

7. Conclusions*

Cu-Co alloy thin films have been successfully obtained by direct current electrodeposition in order to produce compositionally modulated multilayered structures. Triton X-100 has a great influence on the film quality, but didn't increase GMR. Different substrates were employed to deposit multilayers. The results show that substrate also plays a big role in the multilayer structure and GMR behavior. The copper foil with preferred (200) orientation showed a large enhancement in GMR. A large GMR enhancement > 25 % and up to 40 % was found when the multilayer was deposited on a (200) copper foil

8. References

1. Q. Huang and E. J. Podlaha, *Journal of the Electrochemical Society*, **151**, C119 (2004).

* A part of the work presented in this chapter was presented at the 204th meeting of the Electrochemical Society, Oct. 2003

2. E. Chassaing, K. V. Quang, and R. Wiart, *Journal of Applied Electrochemistry* **17**, 1267 (1987).

3. T. I. Quickenden and X. Jiang, *Electrochimica Acta*, **29**, 693 (1984).

4. P. Bradley, S. Roy and D. Landolt, *Journal of the Chemical Society-Faraday Transactions*, **92**, 4015 (1996).

5. Y. Zhuang and E. J. Podlaha, *Journal of the Electrochemical Society*, **147**, 2231 (2000).

6. S. Lenczowski, C. Schonenberger, M. Gijs, and W. Dejonge, *Journal of Magnetism and Magnetic Materials*, **148**, 455 (1995).

7. E. Chassaing, A. Morrone and J. Schmidt, *Journal of the Electrochemical Society*, **146**, 1794 (1999).

8. K. Bird, & M. Schlesinger, *Journal of the Electrochemical Society*, **142**, L65 (1995).

APPENDIX B. CoCu ALLOY DEEP RECESS DEPOSITION

1. Influence of Sodium Citrate on Deep Recesses Deposition

Table 1 summarizes three electrolytes used in deep recess alloy deposition. Electrolyte #1 and Electrolyte #2 were used for CoCu alloy micropost deposition. A pulse current density of -20 mA/cm^2 with a plating time of 10 s, and zero current with relaxation time of 70 s were applied. Figure 1 shows the SEM micrographs of the CoCu deposits obtained from these two different electrolytes. The height of the deposit (Figure 1a) obtained from Electrolyte #1 was very short, less than 50 micrometer with a rough topography. A considerable amount of red-black precipitation blocked the mouth of the deep recesses. In contrast, the deposit obtained from Electrolyte #2 (Figure 1b) has a very good quality with a full growth to 500 μm tall. Therefore, sodium citrate played a critical role in the successful deposit of CoCu alloy into 500 μm deep recesses.

Table 1. Electrolyte components

Electrolyte	$CoSO_4.7H_2O$ (M)	$CuSO_4.5H_2O$(M)	H_3BO_4(M)	$Na_3C_6H_5O_7.2H_2O$(M)	pH
#1	0.75	0.005	0.543	0	3.5
#2	0.75	0.005	0.543	0.1	3.5
#3	0.75	0.005	0.543	0.1	6.0

Sodium citrate influenced the growth of the deposits in two aspects. The first was to reduce displacement current between the cobalt deposit and copper ion during the off time, which can be verified from the polarization curve analysis, as shown in Figure 2. Figure 2 shows the oxidation of a solid cobalt deposit and the reduction of copper ions with and without sodium citrate. The cathodic or anodic current density that is found when the magnitude of the cobalt oxidation rate equals the copper ion reduction rate determines the displacement reaction rate. At this point $|i_c| = |i_a|$ and $i_c + i_a = 0$. A straight line is indicated

in Figure 2 to show where these two values are equal. When there is an addition of citrate there is a small enhancement in the displacement reaction that occurs during the off-time when the total current density equals zero. The second role of citrate is to act as a buffer. It is known that hydrogen evolution and water reduction in deep recesses leaded to local a pH increase. The pH increase can generate precipitation in the worst case, which could block the mouth of the recess and interrupt the micropost growth process. It is expected that the electrolyte with sodium citrate should have a better buffering effect than that without sodium citrate, and therefore help to circumvent the local pH increase, subsequently reduce the precipitation in the deep recesses.

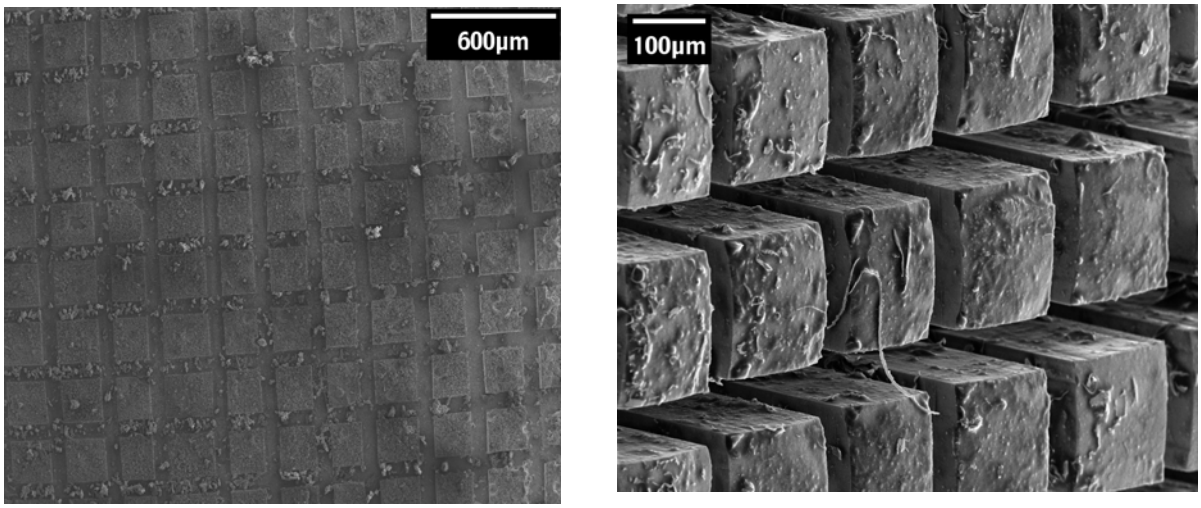

Figure 1. SEM of micropost deposited at current density –20mA/cm^2 with on time of 10 s and an off time 80 s, (a) with Electrolyte #1, (b) with Electrolyte #2

2. Composition Analysis

Figure 3 is a schematic of the metal partial current densities when the boundary layer changes. The copper transport limiting current density is expected to increase with time in the micropost as the geometry of the recess changes. A decrease in the recess

height results in a decrease in the boundary layer thickness. This leads to the graded copper concentration along the height of the micro-post, which is shown in Figure 4. This micropost is obtained with the electrolyte #2 and shown in Figure 3. Copper concentration is lower near the substrate side, while it is higher near the electrolyte side.

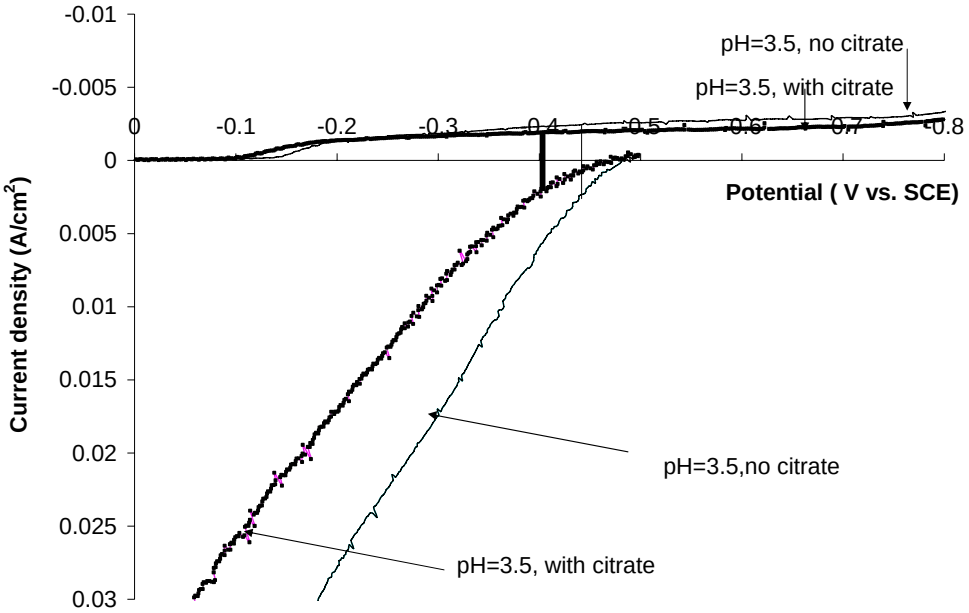

Figure 2. Polarization curve for Electrolyte #1 and Electrolyte #2

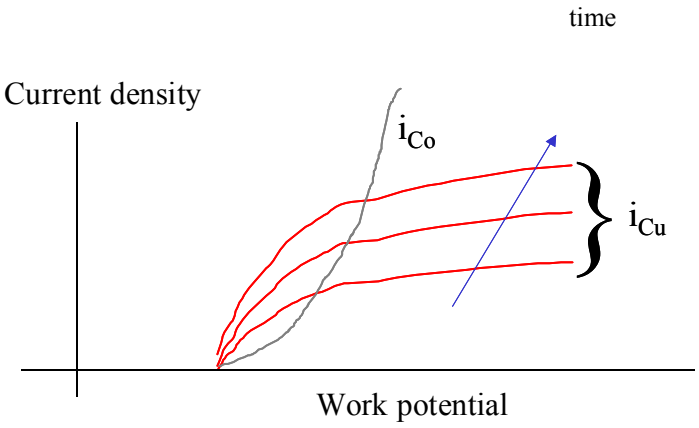

Figure 3 Schematic of copper and cobalt partial current densities as the deposit grows in the recess. The arrows indicate an increase of the copper limiting current density with time

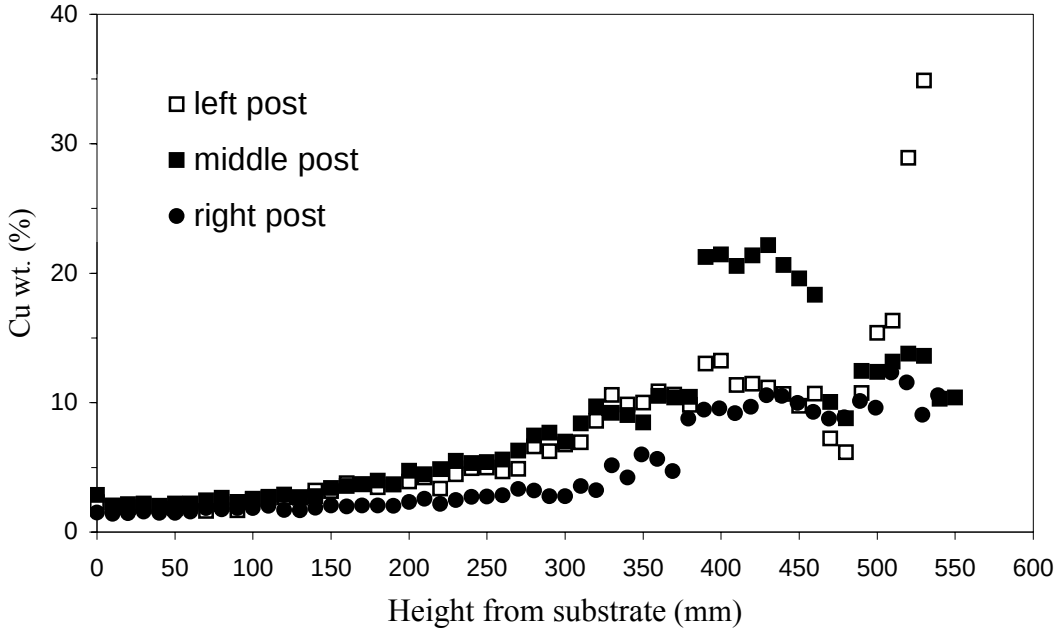

Figure 4 WDS analysis of micro-posts plated at a current density of –20 mA/cm^2 with on time 10 s and off time 80 s.

3. Chemical Equilibrium

Since citrate species were complexed with the metal ions in the electrolyte, a simulation of the electrolyte component was important, in order to determine the micropost deposition in the deep recesses. The simulation of the processes was listed in the following steps. The equilibrium equations and their equilibrium constants were obtained from the metal complex handbooks.

3.1 Copper Species Equilibrium

The different copper species chemical equilibrium, equilibrium equation and the equilibrium constants are listed on Table 1. There are a total of 9 equilibrium reactions and 10 copper species.

Table 1. Copper species equilibrium

Chemical Equilibrium	Equilibrium equation	Constants	Eq. No.
$2Cu^{+2} + 2Cit^{-3} \Leftrightarrow Cu_2(Cit)_2^{-2}$	$K1 = \frac{[Cu_2Cit_2^{-2}]}{[Cu^{+2}]^2[Cit^{-3}]^2}$	K1=$10^{14.43}$	(1)
$Cu^{+2} + Cit^{-3} + H^+ \Leftrightarrow CuHCit$	$K2 = \frac{[CuHCit]}{[Cu^{+2}][Cit^{-3}][H^+]}$	K2=$10^{9.55}$	(2)
$2Cu^{+2} + 2Cit^{-3} \Leftrightarrow Cu_2Cit_2^{-4} + 2H^+$	$K3 = \frac{[Cu_2Cit_2^{-4}][H^+]^2}{[Cu^{+2}]^2[Cit^{-3}]^2}$	K3=$10^{5.87}$	(3)
$2Cu^{+2} + 2Cit^{-3} \Leftrightarrow Cu_2Cit_2H_{-1}^{-3} + H^+$	$K4 = \frac{[Cu_2Cit_2H_{-1}^{-3}][H^+]}{[Cu^{+2}]^2[Cit^{-3}]^2}$	K4=$10^{10.85}$	(4)
$2Cu^{+2} + Cit^{-3} \Leftrightarrow Cu_2CitH_{-1} + H^+$	$K5 = \frac{[Cu_2Cit_2H_{-1}][H^+]}{[Cu^{+2}]^2[Cit^{-3}]}$	K5=$10^{4.92}$	(5)
$Cu^{+2} + OH^- \Leftrightarrow CuOH^+$	$K6 = \frac{[CuOH^+]}{[Cu^{+2}][OH^-]}$	K6=$10^{6..3}$	(6)
$Cu^{+2} + 2OH^- \Leftrightarrow Cu(OH)_2$	$K7 = \frac{[Cu(OH)_2]}{[Cu^{+2}][OH^-]^2}$	K7=$10^{12.8}$	(7)
$Cu^{+2} + 3OH^- \Leftrightarrow (Cu(OH)_3)^-$	$K8 = \frac{[Cu(OH)_3^-]}{[Cu^{+2}][OH^-]^3}$	K8=$10^{14.5}$	(8)
$Cu^{+2} + 4OH^- \Leftrightarrow (Cu(OH)_4)^{-2}$	$K9 = \frac{[Cu(OH)_4^{-2}]}{[Cu^{+2}][OH^-]^4}$	K9=$10^{15.6}$	(9)

3.2 Cobalt Species Equilibrium

The different cobalt species chemical equilibrium, equilibrium equation and the equilibrium constants are listed on Table 2. There are a total of 3 equilibrium reactions and 4 cobalt species.

3.3 Citrate Acid Species Equilibrium

The different citrate species chemical equilibrium, equilibrium equation and the equilibrium constants are listed on Table 3. There are a total 3 equilibrium reaction and 4 citrate species

Table 2. Cobalt species equilibrium

Chemical Equilibrium	Equilibrium equation	Constants	Eq. No.
$Co^{+2} + H_3Cit \Leftrightarrow CoH_2Cit^{+} + H^{+}$	$K10 = \frac{[CoH_2Cit^{+}][H^{+}]}{[Co^{+2}][H_3Cit]}$	K10=$10^{-1.44}$	(10)
$CoH_2Cit^{+} \Leftrightarrow Co(H_{-1})Cit^{2-} + 3H^{+}$	$K11 = \frac{[CoH_{-1}Cit^{-2}][H^{+}]^3}{[CoH_2Cit^{+}]}$	K11=$10^{-12.9}$	(11)
$Co^{+2} + 2HCit^{-2} \Leftrightarrow Co(HCit^{-2})_2^{-2}$	$K12 = \frac{[Co(HCit^{-2})_2^{-2}]}{[Co^{+2}][HCit^{-2}]^2}$	K12=$10^{2.57}$	(12)

Table 3. Citrate species equilibrium

Chemical Equilibrium	Equilibrium equation	Constants	Eq. No.
$HCit^{-2} \Leftrightarrow H^{+} + Cit^{-3}$	$K13 = \frac{[H^{+}][Cit^{-3}]}{[HCit^{-2}]}$	K13=$10^{-5.69}$	(13)
$H_2Cit^{-} \Leftrightarrow H^{+} + HCit^{-2}$	$K14 = \frac{[H^{+}][HCit^{-2}]}{[HCit^{-}]}$	K14=$10^{-4.34}$	(14)
$H_3Cit \Leftrightarrow H^{+} + H_2Cit^{-}$	$K15 = \frac{[H^{+}][H_2Cit^{-}]}{[H_3Cit]}$	K15=$10^{-2.92}$	(15)

3.4 Water Equilibrium

The water equilibrium is listed in Table 4.

3.5 Boric Acid Equilibrium

The boric acid equilibrium is listed in Table 5.

Table 4. Water equilibrium

Chemical Equilibrium	Equilibrium equation	Constants	Eq. No.
$H_2O \Leftrightarrow H^+ + OH^-$	$K16 = [H^+][OH^-]$	K16=10^{-14}	(16)

Table 5. Boric acid equilibrium

Chemical Equilibrium	Equilibrium equation	Constants	Eq. No.
$3B(OH)3 \Leftrightarrow H^+ + B_3O_3(OH)_4^- + 2H_2O$	$K17 = \frac{[B_3O_3(OH)_4^-][H^+]}{[H_3BO_3]^3}$	K17=$10^{-6.8}$	(17)

3.6 Conservation of Mass for *Cu*

A mass balance for copper species is shown in equation 18.

$[Cu_{total}]$

$=[\ Cu^{+2}\ ]+2[\ Cu_2(Cit)_2^{-2}\ ]+[\ CuHCit\ ]+2[\ Cu_2(Cit)_2^{-4}\ ]+2[\ Cu_2(Cit)_2^{-3}\ ]+2[\ Cu_2CitH_{-}\ ]$

$+[CuOH^+]+[Cu(OH)_2]+[(Cu(OH)_3)^-]+[(Cu(OH)_4)^{-2}]$ (18)

3.7 Conservation of Mass for *Co*

Mass balance for cobalt species was shown in equation 19.

$[Co_{total}]= [\ Co^{+2}\ ] +[CoH_2Cit^+]+ [\ Co(H_{-1})Cit^{2-}\ ] + [\ Co(HCit^{-2})_2{}^{-2}\ ]$ (19)

3.8 Conservation of Mass for Citrate

Mass balance for citrate species was shown in equation 20.

$[Citrate_{total}]=2[\ Cu_2(Cit)_2^{-2}\ ]+[\ CuHCit\ ]+2[\ Cu_2(Cit)_2^{-4}\ ]+2[\ Cu_2(Cit)H_{-1}^{-3}\ ]+[\ Cu_2Cit\ ]+[$

$CoH_2Cit^+]+[Co(H_{-1})Cit^{2-}]+2[Co(HCit^{-2})_2{}^{-2}]+[Cit^{-3}]+[HCit^{-2}]+[H_2Cit^-]+[H_3Cit]$

(20)

3.9 Conservation of Mass for Na^+

Mass balance for Na species was shown in equation 21.

$$[Na^{+}_{total}]=3[\text{Citrate}_{total}] \quad (21)$$

3.10 Conservation of Mass for SO_4^{-2}

Mass balance for SO_4^{-2} species was shown in equation 22.

$$[SO_4^{-2}{}_{total}]=[\text{Cu}_{total}]+[\text{Co}_{total}] \quad (22)$$

3.11 Conservation of Mass for Boric Acid

Mass balance for boric species was shown in equation 23.

$$[\text{Boric acid}_{total}] =[[H_3BO_3]+3[B_3O_3(OH)_4^-] \quad (23)$$

3.12 Unknowns

The total unknowns and their code used in a Fortran program are listed in Table 6. The number of total equations is 23 and the total unknowns is also 23.

Table 6. Unkowns

Species #	unknowns	Unknowns Code
1	Cu^{+2}	C1
2	$Cu_2(Cit)_2^{-2}$	C2
3	$CuHCit$	C3
4	$Cu_2(Cit)_2^{-4}$	C4
5	$Cu_2(Cit)H_{-1}^{-3}$	C5
6	Cu_2CitH_{-1}	C6
7	$CuOH^{+}$	C7
8	$Cu(OH)_2$	C8
9	$(Cu(OH)_3)^{-}$	C9
10	$(Cu(OH)_4)^{-2}$	C10

11	Co^{+2}	C11
12	CoH_2Cit^{+}	C12
13	$Co(H_{-1})Cit^{2-}$	C13
14	$Co(HCit^{-2})_2^{-2}$	C14
15	Cit^{-3}	C15
16	$HCit^{-2}$	C16
17	H_2Cit^{-}	C17
18	H_3Cit	C18
19	OH^{-}	C19
20	Na^{+}	C20
21	SO_4^{-2}	C21
22	H_3BO_3	C22
23	$B_3O_3(OH)_4^{-}$	C23

3.13 FORTRAN Program

The algebraic equations are cast into FORTRAN code below. The equations are in the form where the function, F, is equal to zero.

F(1)=0=K1*(C1**2)*(C15**2)-C2

F(2)=0=K2*(C1)*(C15)*10(**-pH)-C3

F(3)=0=K3*(C1**2)*(C15**2)-(C4**2)*[(10**-pH)**2

F(4)=0=K4*(C1**2)*(C15**2)-(C5)*(10**- pH)

F(5)=0=K5*(C1**2)*(C15)-(C6)*(10**- pH)

F(6)=0=K6*(C1)*(C19)-C7

F(7)=0=K7*(C1)*(C19)-C7

F(8)=0=K8*(C1)*(C19**3)-C9

F(9)=0=K9*(C1*(C19**4)-C10

F(10)=0=K10*(C11)*(C18)-(C12)*(10**- pH)

F(11)=0=K11*(C12)-(C13)*[(10**-pH)**3]

F(12)=0=K12*(C11)**(C16**20)-C14

F(13)=0=K13*(C16)-(10**-pH)*(C15)

F(14)=0=K14*(C17)-(10**-pH)*(C16)

F(15)=0=K15*(C18)-(10**-pH)*(C17)

F(16)=0=K16-(10**-pH)*(C19)

F(17)=0=K17*(C22)-C(23)* (10**-pH)

F(18)=0=C1+2*C2+C3+2*C4+2*C5+2*C6+C7+C8+C9+C10-Cu_{total}

F(19)=0=C11+C12+C13+C14-Co_{total}

F(20)=0=2*C2+C3+2*C4+2*C5+C6+C12+C13+2*C14+C15+C16+C17+C18-$Citrate_{total}$

F(21)=0=3* $Citrate_{total}$

F(22)=0= Cu_{total}+Co_{total}

F(23)=0=C22+C23-boric $acid_{total}$

The equations are solved with a Crank-Nicholson method. The FORTRAN code is attached in Appendix C.

3.13 Simulation Results

The simulation results for the copper species are shown in Figure 5. All of the concentrations of the main copper species Cu^{+2}, $Cu_2(Cit)_2^{-2}$, $Cu_2(Cit)_2^{-4}$, $Cu_2(Cit)H_{-1}^{-3}$ and Cu_2CitH_{-1} varied with the electrolyte pH. The copper species were almost completely complexed with the citrate species. In the electrolyte pH of 6, the main copper

species was $Cu_2(Cit)_2^{-4}$. Therefore the copper deposition was mainly obtained by reduction of $Cu_2(Cit)_2^{-4}$.

The concentration of the cobalt species at different pH values were shown in Figure 6. The cobalt ions were complexed a little with the citrate species at higher electrolyte pH. Therefore, the cobalt deposit was obtained by mainly reduction of Co^{+2}.

The concentration of the citrate species at different pH values were shown in Figure 7. The main species were H_3Cit and H_2Cit^- at middle electrolyte pH. At higher pH values, the citrate species were almost completely complexed with the copper metal ions. The concentration of boric acid species was shown in Figure 8. Boric acid was the main component in the electrolyte.

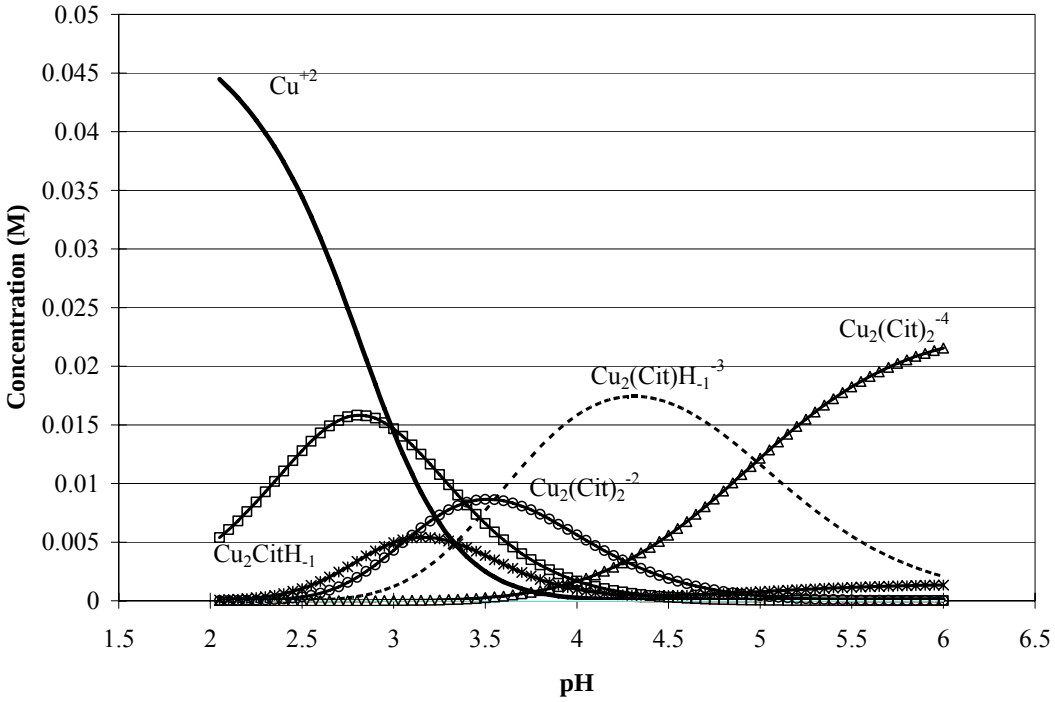

Figure 5. Copper species in the electrolyte equilibrium

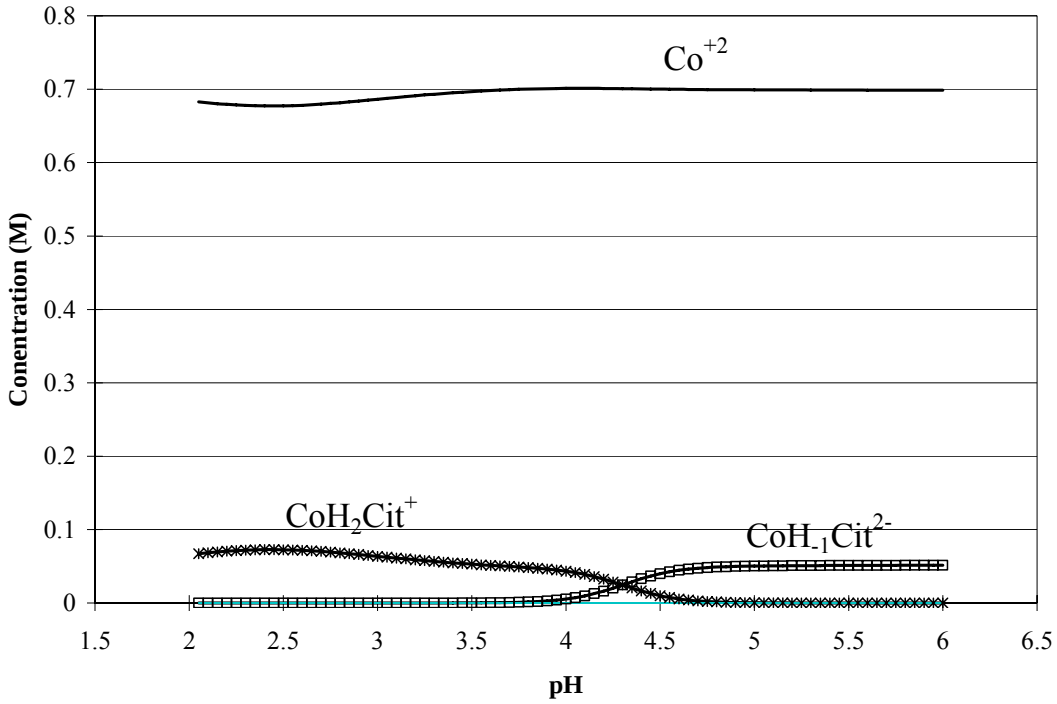

Figure 6. Cobalt species in the electrolyte equilibrium

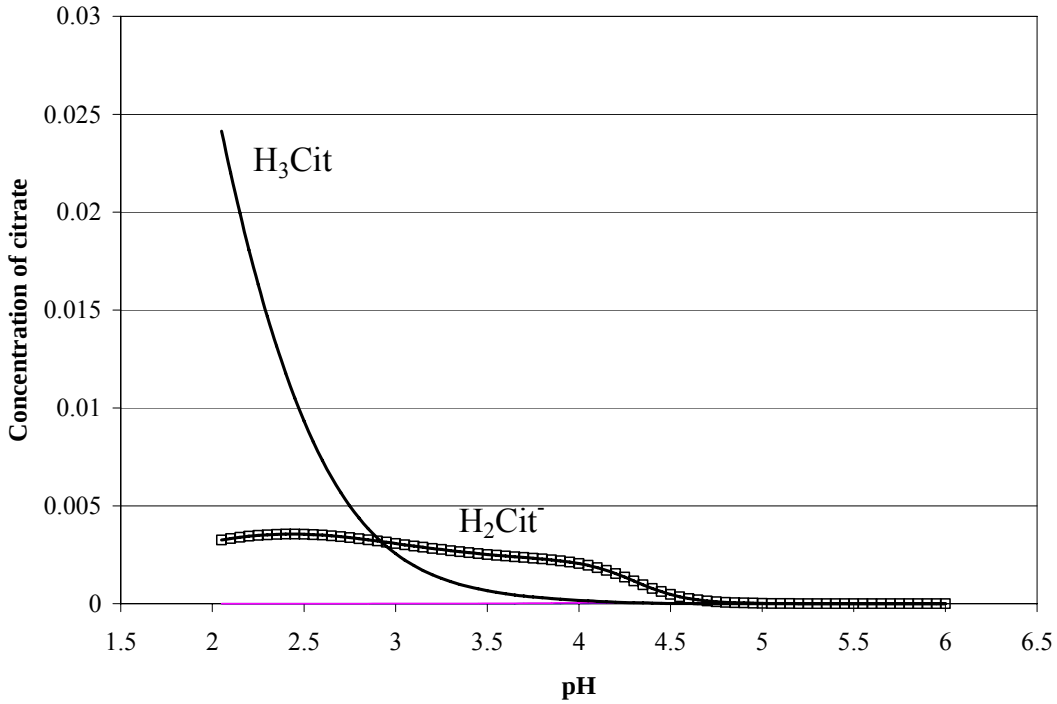

Figure 7. Citrate species in the electrolyte equilibrium

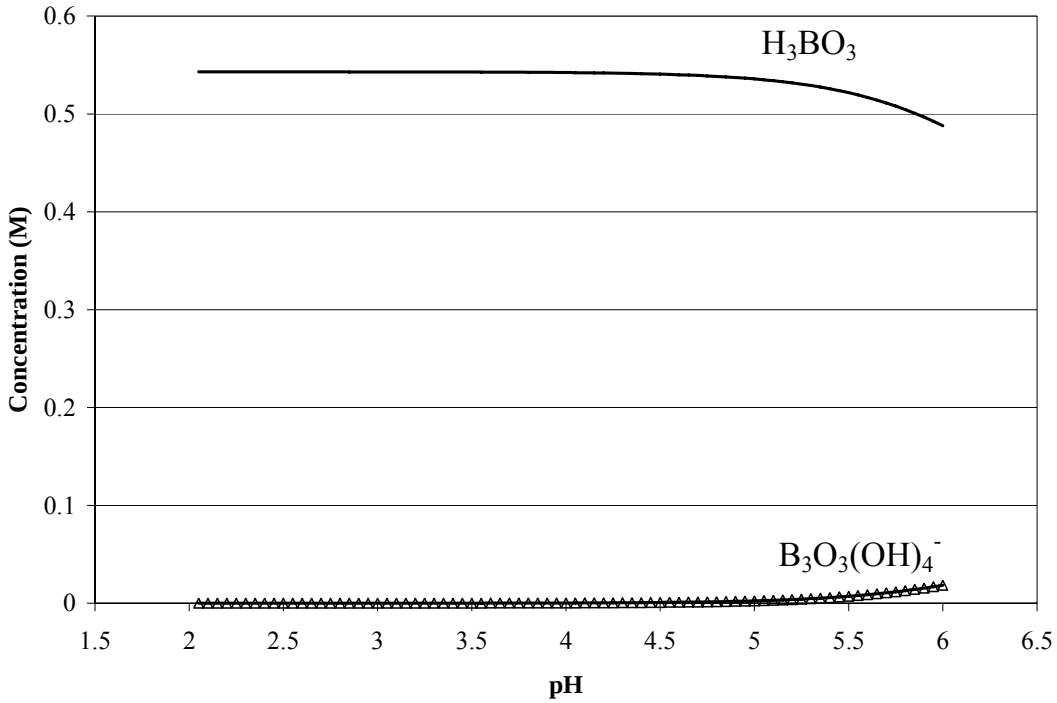

Figure 8. Boric acid species in the electrolyte equilibrium

APPENDIX C. FORTRAN PROGRAM

```
C*****************************************************************C
C          Cu-Co-citrate complexes Alloy Simulation in FORTRAN
C                    --> still need to look up.
C                 - Steady State Model
C                  -Finite Differences in the Spatial Direction

C
================================================================
=====C
c____X_____________________________________________________________c
      IMPLICIT DOUBLE PRECISION(A-H,O-Z)

       DIMENSION CC(24,50),A(24,24),B(24,24),C(24,50),D(24,160),G(24),
     1 X(24,24),Y(24,24),F(24),DIST(50),ZC(24,50),
     2 X1(24,24),X2(24,24),Y1(24,24),Y2(24,24),
     3 cb(24), DC(24)

       COMMON /INARRAY/ cb, DC
       COMMON /INREAL/ XkA, XkB, XkC, XkD, alfA, alfB, alfC, alfD,
     1      Xnu, deptime, Dlim, TEMP,
     2     R, F1,Xkw,VAPP,VINC, XMWCu, XMWNi, dencu, denni, xheight
       COMMON /ININTEGER/ NTOP,N,NJ

       COMMON /CALC/ del, H1, bA, bB, bC, bD
       COMMON /BLOCKA/ CC,A,B,C,D,G,X,Y,X1,X2,Y1,Y2
       COMMON /BLOCKB/ F,DIST,ZC

       COMMON /BLOCKM2/ TIME,CU,DELT, pH
            COMMON /ph/ pH0, pHstart
      OPEN (UNIT=30,FILE='yudata.dat',STATUS='UNKNOWN')

      CALL DATAIN   !gets all inputs from subroutine
C ********** STUFF NOT NEEDED...KEEP FOR LATER **********
C          high aspect ratio geometry:
            del = xheight           !bounday layer thickness

C*************************************************.....
       H1=del/FLOAT(NJ-1)  !step size for finite differences

      CALL ECHOPRINT        !echo printing input

C .....................................MORE CONSTANTS.....................

 210   CU=1.0001
```

```
      PI=3.141596
      TIME=0.0
         pH=pHstart
          DO 214 J=1,NJ          !Initial Guess for finite differences
          DIST(J)=(J-1)*H1
                          DO 214 J1=1,N
                         C(J1,J)=0.00001*J1
214                CC(J1,J)=0.0001*J1

         WRITE(30,110)
 110  FORMAT(/,'Cu Concentrations',/,2X,'pH',5X,'C1',7X,'C2',
    1  5X,'C3',6X,'C4',5X,'C5',3X,'C6',5X,
    1  'C7',7X,'C8',7X,'C9',5X,'C10',5X,'C11',
    1  5X,'C12',5X,'C13',3X,'C14',4X,'C15',5X,
    1  'C16',6X,'C17',7X,'C18'7X,'C19',7X,'C20', 9X,
    1   'C21',10X, 'C22', 9X,'C23')


                    DO 288  jloop =1, NTOP

                    pH= pH0 +pH
                   cb(5)=10**(-pH)

                     CALL DIFEQ    !Subroutine which calls equation
                             ! subroutine (Begin),linearizes,
                       ! calls BAND to solve and then checks
                       ! convergence criterion ....change only
                       ! convergence criterion at bottom of DIFEQ

C    SAVE INITIAL SOLUTION

     DO 401 J=1,NJ
     DO 401 I=1,N
 401   C(I,J)=CC(I,J)

     WRITE(30,111) pH,C(1,1),C(2,1),C(3,1),C(4,1),C(5,1),C(6,1),C(7,1),
    1     C(8,1),C(9,1),C(10,1),C(11,1),C(12,1),C(13,1),C(14,1),
    1    C(15,1),C(16,1),C(17,1),C(18,1),
    1C(19,1),C(20,1),C(21,1),CC(22,1),CC(23,1)

 288    CONTINUE
C.....output.....

 111   FORMAT(F6.2,23G12.4)

        END
```

```
      SUBROUTINE DATAIN
      IMPLICIT DOUBLE PRECISION(A-H,O-Z)
      COMMON /INARRAY/ cb(24), DC(24)
      COMMON /INREAL/ XkA, XkB, XkC, XkD, alfA, alfB, alfC, alfD,
     1         Xnu, deptime, Dlim, TEMP, R, F1,  Xkw,
     3         VAPP,VINC, XMWCu, XMWNi, dencu, denni,xheight
      COMMON /ININTEGER/ NTOP,N,NJ
           COMMON /ph/ pH0, pHstart

C.............Numerical things
       VAPP =-0.2        ! applied potential minus ohmic drop {V}
       VINC =0.02        ! increment potential to produce polarization curves
       NTOP =40          ! maximum number of increments
       N=23              ! number of equations or unknows
       NJ=100         ! maximum number of node point >>should be atleast 100

C.............Bulk Concentrations.....................................................
      cb(1) =0.05     ! TOTAL Cu bulk concentration     {mol/l3}
      cb(2) =0.1      ! TOTAL Citrate bulk concentration   {mol/l3}
           cb(3) =0.75   !TOTAL Co bulk concentation {mol/l3}
           cb(4) = 0.543 !boric acid

      pH0 = 0.05  ! pH increment
           pHstart= 2.5 ! pH starting point >6
           Xkw=(1.00e-14) !kw for water equilibrium


C.............Rate Constants.....................................................

            xheight = 500./1.0e+4     ! High apect ratio height   {cm}

      RETURN
      END

       SUBROUTINE ECHOPRINT
       IMPLICIT DOUBLE PRECISION(A-H,O-Z)
       COMMON /INARRAY/ cb(24), DC(24)
       COMMON /INREAL/ XkA, XkB, XkC, XkD, alfA, alfB, alfC, alfD,
     1               Xnu, deptime, Dlim, TEMP, R, F1, Xkw,
     2               VAPP,VINC, XMWCu, XMWNi, dencu, denni,xheight
       COMMON /ININTEGER/ NTOP,N,NJ
        COMMON /CALC/ del, H1, bA, bB, bC, bD

        write(30,70)
        write(*,70)
```

```
70    format('~~~ Cu Compositions ~~~~')
1010  format(/,'**************************************************
     **********',/,
     *'*                                          *',/,
     *'*    MODEL DESCRIPTION: This model solves for the       *',/,
     *'*                    Concentration of Cu            *',/,
     *'*                    Concentration of citrate       *',/,
     *'*                   Concentration of ammonia species    *',/,
     *'*                   Concentration of OH-           *',/,
     *'*************************************************************',//)

      RETURN
      END

      SUBROUTINE BEGIN(J)
      IMPLICIT DOUBLE PRECISION(A-H,O-Z)
       COMMON /INARRAY/ cb(24), DC(24)
        COMMON /INREAL/ XkA, XkB, XkC, XkD, alfA, alfB, alfC, alfD,
     1          Xnu, deptime, Dlim, TEMP, R, F1, Xkw,
     2          VAPP,VINC, XMWCu, XMWNi, denxcu, denni,xheight
       COMMON /ININTEGER/ NTOP,N,NJ
       COMMON /CALC/ del, H1, bA, bB, bC, bD
       COMMON/BLOCKA/CC(24,50),A(24,24),B(24,24),C(24,50),D(24,160),
     1  G(24),X(24,24),Y(24,24),X1(24,24),X2(24,24),Y1(24,24),Y2(24,24)

       COMMON /BLOCKB/ F(24),DIST(50),ZC(24,50)

                    If(J.GE.1.AND.J.LT.NJ) THEN
          !C1: Cu+2
          !C2: Cu2Cit2-2
          !C3: CuHCit
          !C4: Cu2Cit2-4 ??? same as c2?
          !C5: Cu2Cit2(H-1)-3
          !C6: CuCitH-1
          !C7: CuOH+
          !C8: Cu(OH)2
          !C9: Cu(OH)3-
          !C10:Cu(OH)4-2
          !C11:Co+2
          !C12:CoH2Cit
          !C13:Co(H-1)Cit-2
          !C14:Co(HCit-2)2-2
          !C15:Cit-3
          !C16:HCit-2
          !C17: H2Cit-
```

```
      !C18:H3Cit
      !C19:OH-
      !C20:Na+
      !C21:So4
      !C22:B(OH)3
      !C23:B3O3(OH)4

          !Chemical Equilibria
    F(1)=10**(14.4)*((CC(1,J)**2)*(CC(15,J)**2)) - CC(2,J) !2Cu+2 + 2Cit-3 =
Cu2(Cit2)-2
    F(2)=10**(9.55)*(CC(1,J)*CC(15,J)*cb(5)) - CC(3,J)!Cu+2 + Cit-3+H+ = CuHCit
      F(3)=10**(5.87)*((CC(1,J)**2)*(CC(15,J)**2)) - CC(4,J)*(cb(5)**2)!Cu+2 +
2Cit-3 = Cu2(Cit2)-4 +2H+
      F(4)=10**(10.8)*((CC(1,J)**2)*(CC(15,J)**2)) - CC(5,J)*cb(5)!2Cu+2 + 2Cit-3
= Cu2Cit2(H-1)-3 +H+
      F(5)=10**(4.92)*((CC(1,J)**2)*CC(15,J)) - CC(6,J)*cb(5)!2Cu+2 + Cit-
3=CuCit(H-1) +H+

    F(6)=10**(6.3)*(CC(1,J)*CC(19,J)) - CC(7,J)!Cu+2+ OH-=CuOH+
      F(7)=10**(12.8)*(CC(1,J)*(CC(19,J)**2))- CC(8,J)!Cu+2 +2OH-=Cu(OH)2
    F(8)=10**(14.5)*(CC(1,J)*(CC(19,J)**3)) - CC(9,J)!Cu+2 +3OH-=Cu(OH3)-
      F(9)=10**(15.6)*CC(1,J)*(CC(19,J)**4)-CC(10,J)  !Cu+2 +4OH-= Cu(OH4)-2

      F(10)=10**(-1.44)*(CC(11,J)*CC(18,J)) - CC(12,J)*cb(5)!Co+2 + H3Cit
=CoH2Cit+ +H+
      F(11)=10**(-12.9)*CC(12,J)-(CC(13,J)*(cb(5)**3))!CoH2Cit+ +Co(H-1)Cit-2
+3H+
      F(12)=10**(2.57)*CC(11,J)*(CC(16,J)**2)- CC(14,J)!Co+2 + 2HCit-2
=Co((HCit-2)2)-2

    F(13)=10**(-4.34)*CC(16,J)-cb(5)*CC(15,J)!HCit-2 =H+ +Cit-3
      F(14)=10**(-5.69)*CC(17,J)-(CC(16,J)*cb(5))!H2Cit-=H+ +HCit-2
      F(15)=10**(-2.92)*CC(18,J)-(CC(17,J)*cb(5))!H3Cit=H+ +H2Cit-

      F(16) =10**(-14.0)/cb(5)-CC(19,J) !!!!!10**(-14.0)/cb(5)-CC(16,J) !water
equilibrium

      F(17)=10**(-6.8)-(CC(23,J)*cb(5))/(CC(22,J)**3)! 3B(OH)3=H+
+B3O3((OH)4)-

          !Adding constraint of electroneutrality
      zero =-(2*CC(2,J)+4*CC(4,J)+3*CC(5,J)+ CC(9,J)+2*CC(10,J)
     1  +2*CC(13,J)+2*CC(14,J)+3*CC(15,J)+2*CC(16,J)+CC(17,J)+CC(19,J)
    2+2*CC(21,J)+CC(23,J))+(cb(5)+CC(7,J)+2*CC(11,J)+CC(12,J)+
    3  CC(20,J)+2*CC(1,J))
```

```
                cj1 =0.5*((2*CC(2,J)+4*CC(4,J)+3*CC(5,J)+ CC(9,J)+2*CC(10,J)
     1  +2*CC(13,J)+2*CC(14,J)+3*CC(15,J)+2*CC(16,J)+CC(17,J)+CC(19,J)
    2+2*CC(21,J)+CC(23,J))-
    3 (cb(5)+CC(7,J)+2*CC(11,J)+CC(12,J)+CC(20,J)))
              !Electroneutrality, all anions = all cations in solution

                  !Mass balances

C         F(18)= cj1+2*CC(2,J)+CC(3,J)+2*CC(4,J)+2*CC(5,J)
C     1    +2*CC(6,J)+CC(7,J) +CC(8,J) +CC(9,J)+CC(10,J)-cb(1) !Cu mass balance

          F(18)= CC(1,J)+2*CC(2,J)+CC(3,J)+2*CC(4,J)+2*CC(5,J)
    1    +2*CC(6,J)+CC(7,J) +CC(8,J) +CC(9,J)+CC(10,J)-cb(1) !Cu mass balance

     F(19)=CC(11,J)+CC(12,J)+CC(13,J)+CC(14,J)-cb(3) !Co mass balance

           F(20)= 2*CC(2,J)+CC(3,J)+2*CC(4,J)+2*CC(5,J)+CC(6,J)+
    1       CC(12,J)+CC(13,J)+2*CC(14,J)+CC(15,J)+CC(16,J)+
    2       CC(17,J)+CC(18,J)-cb(2)
          !citrate mass balance

          F(21)=CC(20,J)-3*cb(2)!Na+ mass balance

          F(22)=CC(21,J)-(cb(1)+cb(3))         !SO4-2 mass balance

     F(23)=CC(22,J)+3*CC(23,J)-cb(4)        !Boric acid mass balance

     ELSEIF(J.EQ.NJ) THEN
               Do 55 IJK = 1, N
55       F(IJK)= CC(IJK,J)-CC(IJK,J-1)

     ENDIF

           RETURN
    END

    SUBROUTINE DIFEQ
C*****************************************************************
*
C     IMPROVED TO INCLUDE 5-PT FINITE DIFFERENCE
C     BAND CSUBROUTINE OUTLINED BY WHITE.
C*****************************************************************
       IMPLICIT DOUBLE PRECISION(A-H,O-Z)
       DIMENSION AA(24,24),SUM(24),COLD(24,50)

       COMMON /INARRAY/ cb(24), DC(24)
```

```
      COMMON /INREAL/ XkA, XkB, XkC, XkD, alfA, alfB, alfC, alfD,
     1        Xnu, deptime, Dlim, TEMP, R, F1,Xkw,
     3        VAPP,VINC, XMWCu, XMWCo, dencu, denCo, xheight
      COMMON /ININTEGER/ NTOP,N,NJ

      COMMON /CALC/ del, H1, bA, bB, bC, bD

     COMMON/BLOCKA/CC(24,50),A(24,24),B(24,24),C(24,50),D(24,160),
     1   G(24),X(24,24),Y(24,24),X1(24,24),X2(24,24),Y1(24,24),Y2(24,24)

      COMMON /BLOCKB/ F(24),DIST(50),ZC(24,50)

       COMMON /BLOCKM2/ TIME,CU,DELT,pH

      CU=1.0001
 110   CD=2.0-CU
     ITCNT=0
 10    CONTINUE
     DO 15 K=1,N
       DO 15 J=1,NJ
         COLD(K,J)=CC(K,J)
 15    CONTINUE
     SWITCH=0.
     J=0
     JCHECK=0
     IF(ITCNT.GT.10) THEN
            CU=1.00001
         CD=2.0-CU
      ELSE
      END IF
     IF(ITCNT.GT.50) THEN
          WRITE(6,1) pH
          WRITE(30,1) pH
 1      FORMAT(' CONVERGENCE UNATTAINABLE',E10.4)
c          DO 1111 J6=1,NJ
c 1111      WRITE(30,1010) (CC(J5,J6), J5=1,N)
        GO TO 50
 1010 FORMAT(6E12.5)
      ELSE
      ENDIF
     ITCNT=ITCNT+1
 20    CONTINUE
             DO 21 II=1,N
             DO 21 I=1,N
              X1(II,I)=0.
              X2(II,I)=0.
```

```
            X(II,I)=0.
            A(II,I)=0.
            B(II,I)=0.
            D(II,I)=0.
            Y(II,I)=0.
            Y1(II,I)=0.
21          Y2(II,I)=0.
    J=J+1
    L=J-5
    DO 25 I=1,N
      SUM(I)=0.0
25  CONTINUE
    IF(J.EQ.1) MM=5
    IF(J.EQ.1) MM1=4
    IF(J.EQ.2) MM=4
    IF(J.EQ.2) MM1=5
    IF(J.GT.2.AND.J.LT.NJ-1) MM=3
    IF(J.GT.2.AND.J.LT.NJ-1) MM1=4
    IF(J.EQ.NJ-1) MM=1
    IF(J.EQ.NJ-1) MM1=5
    IF(J.EQ.NJ) MM1=4
    IF(J.EQ.NJ) MM=1
    DO 35 M=MM,MM+MM1
      DO 35 K=1,N
        SAVEC=CC(K,L+M)
        IF (DABS(SAVEC).LT.1.0D-100) CC(K,L+M)=1.0D-100
        CC(K,L+M)=CC(K,L+M)*CU
665       CALL BEGIN(J)
155       DO 30 I=1,N
          AA(I,K)=F(I)
30        CONTINUE
        CC(K,L+M)=SAVEC
        IF (DABS(SAVEC).LT.1.0D-100) CC(K,L+M)=1.0D-100

        CC(K,L+M)=CC(K,L+M)*CD
160       CALL BEGIN(J)
165       CC(K,L+M)=SAVEC
        DO 35 I=1,N
        IF (DABS(SAVEC).LT.1.0D-100) CC(K,L+M)=1.0D-100
          AA(I,K)=(AA(I,K)-F(I))/((CU-CD)*CC(K,L+M))
          CC(K,L+M)=SAVEC
          SUM(I)=SUM(I)+AA(I,K)*CC(K,L+M)
           IF (L+M.EQ.J-4) Y2(I,K)=AA(I,K)
           IF (L+M.EQ.J-3) Y1(I,K)=AA(I,K)
        IF (L+M.EQ.J-2) Y(I,K)=AA(I,K)
        IF (L+M.EQ.J-1) A(I,K)=AA(I,K)
```

```
          IF (L+M.EQ.J)   B(I,K)=AA(I,K)
          IF (L+M.EQ.J+1) D(I,K)=AA(I,K)
          IF (L+M.EQ.J+2) X(I,K)=AA(I,K)
             IF (L+M.EQ.J+3) X1(I,K)=AA(I,K)
             IF (L+M.EQ.J+4) X2(I,K)=AA(I,K)
 35     CONTINUE
170     CALL BEGIN(J)
 177     DO 40 I=1,N
       G(I)=-F(I)+SUM(I)
 40     CONTINUE
       CALL BAND(J)
65      IF (J.LT.NJ) GO TO 20
       DO 45 K=1,N
       DO 45 J=1,NJ
            IF (DABS(CC(K,J)).LT.1.0D-100) GO TO 45
       IF (DABS((CC(K,J)-COLD(K,J))/CC(K,J)).GT.1.0D-4) GO TO 10
 45     CONTINUE
 50     RETURN
       END

C**********************************************************************
***********
C*******    Five point Finite Boundary Value Tridiagonal Solver
C****          (theory given in: "Electrochemical Cell Design",
C****         ed. by White, R.;
C****       'Extension of Newman's Numerical Technique
C****      to Pentadiagonal Systems of Equations', Plenum Press, NY    p.377, 1984.
C**********************************************************************
***********


      SUBROUTINE BAND(J)
      IMPLICIT DOUBLE PRECISION(A-H,O-Z)
      DIMENSION E(30,145,401)
      COMMON/BLOCKA/CC(24,50),A(24,24),B(24,24),C(24,50),D(24,160),
     1  G(24),X(24,24),Y(24,24),X1(24,24),X2(24,24),Y1(24,24),Y2(24,24)
      COMMON /ININTEGER/ NTOP,N,NJ
      COMMON /BLOCKM2/ TIME,CU,DELT, pH
 101  FORMAT(' 0DETERM=0 AT J=',I4)
 1010 FORMAT(6E12.5)

      IF (J-2) 1,6,8
 1     DO 2 I=1,N
       D(I,4*N+1)=G(I)
       DO 2 L=1,N
        D(I,L+N)=X(I,L)
```

```
      D(I,L+2*N)=X1(I,L)
2     D(I,L+3*N)=X2(I,L)
     CALL MATINV(N,4*N+1,DETERM,B,D)
     IF (DETERM) 4,3,4
3     WRITE(6,101) J
      WRITE(30,101) J
          DO 1111 J6=1,NJ
1111      WRITE(30,1010) (CC(J5,J6), J5=1,N)
          STOP
4     DO 5 K=1,N
      E(K,4*N+1,1)=D(K,4*N+1)
     DO 5 L=1,N
      E(K,L,1)=-D(K,L)
      E(K,L+N,1)=-D(K,L+N)
      E(K,L+2*N,1)=-D(K,L+2*N)
5     E(K,L+3*N,1)=-D(K,L+3*N)
     RETURN
6    DO 61 I=1,N
61       D(I,4*N+1)=-G(I)
     DO 7 I=1,N
     DO 7 L=1,N
      D(I,4*N+1)=D(I,4*N+1)+ A(I,L)*E(L,4*N+1,1)
     DO 7 K=1,N
      D(I,K)=D(I,K)+A(I,L)*E(L,K+N,1)
      D(I,K+N)=X(I,K)+A(I,L)*E(L,K+2*N,1)
      D(I,K+2*N)=X1(I,K)+A(I,L)*E(L,K+3*N,1)
      D(I,K+3*N)=X2(I,K)
7     B(I,K)=B(I,K)+A(I,L)*E(L,K,J-1)
     CALL MATINV(N,4*N+1,DETERM,B,D)
       IF (DETERM) 41,31,41
31       WRITE(6,101) J,TIME
        WRITE(30,101) J,TIME
          DO 1112 J6=1,NJ
1112      WRITE(30,1010) (CC(J5,J6), J5=1,N)
          STOP
41   DO 51 K=1,N
       E(K,4*N+1,2)=-D(K,4*N+1)
     DO 51 L=1,N
       E(K,L,2)=-D(K,L)
       E(K,L+N,2)=-D(K,L+N)
       E(K,L+2*N,2)=-D(K,L+2*N)
51      E(K,L+3*N,2)=-D(K,L+3*N)
      RETURN
8    IF (J.GT.3) GOTO 83
82    DO 72 I=1,N
       D(I,3*N+1)=-G(I)
```

```
      DO 72 K=1,N
      DO 72 L=1,N
 72     A(I,K)=A(I,K)+Y(I,L)*E(L,K,1)
      DO 71 I=1,N
      DO 71 L=1,N
       D(I,3*N+1)=D(I,3*N+1)+ A(I,L)*E(L,4*N+1,2)
     .       +   Y(I,L)*E(L,4*N+1,1)
      DO 71 K=1,N
       D(I,K)=D(I,K)+A(I,L)*E(L,K+N,2)+Y(I,L)*E(L,K+2*N,1)
       D(I,K+N)=X(I,K)+A(I,L)*E(L,K+2*N,2)+
     .          Y(I,L)*E(L,K+3*N,1)
       D(I,K+2*N)=A(I,L)*E(L,K+3*N,2)
 71    B(I,K)=B(I,K)+A(I,L)*E(L,K,J-1)+Y(I,L)*E(L,K+N,1)
     CALL MATINV(N,3*N+1,DETERM,B,D)
     IF (DETERM) 411,311,411
 311     WRITE(6,101) J,TIME
         WRITE(30,101) J,TIME
          DO 1113 J6=1,NJ
 1113     WRITE(30,1010) (CC(J5,J6), J5=1,N)
          STOP
 411    DO 511 K=1,N
        E(K,3*N+1,3)=-D(K,3*N+1)
       DO 511 L=1,N
        E(K,L,3)=-D(K,L)
        E(K,L+N,3)=-D(K,L+N)
 511     E(K,L+2*N,3)=-D(K,L+2*N)
     RETURN
 83   IF (J-(NJ-1)) 9,11,11
 9     DO 711 I=1,N
          D(I,2*N+1)=-G(I)
       DO 711 K=1,N
       DO 711 L=1,N
 711       A(I,K)=A(I,K)+Y(I,L)*E(L,K,J-2)
      DO 712 I=1,N
      DO 712 L=1,N
         IF (J.EQ.4) D(I,2*N+1)=D(I,2*N+1)+
     .  A(I,L)*E(L,3*N+1,J-1)+ Y(I,L)*E(L,4*N+1,J-2)
         IF (J.EQ.5) D(I,2*N+1)=D(I,2*N+1)+
     .  A(I,L)*E(L,2*N+1,J-1)+ Y(I,L)*E(L,3*N+1,J-2)
         IF (J.GE.6) D(I,2*N+1)=D(I,2*N+1)+
     .  A(I,L)*E(L,2*N+1,J-1)+ Y(I,L)*E(L,2*N+1,J-2)
       DO 712 K=1,N
         IF (J.EQ.4.OR.J.EQ.5) D(I,K)=D(I,K)+A(I,L)*E(L,K+N,J-1)
     .                 +Y(I,L)*E(L,K+2*N,J-2)
         IF (J.GE.6) D(I,K)=D(I,K)+A(I,L)*E(L,K+N,J-1)
         IF (J.EQ.4) D(I,K+N)=X(I,K)+A(I,L)*E(L,K+2*N,J-1)+
```

```
     .          Y(I,L)*E(L,K+3*N,J-2)
           IF (J.GE.5) D(I,K+N)=X(I,K)
712        B(I,K)=B(I,K)+A(I,L)*E(L,K,J-1)+Y(I,L)*E(L,K+N,J-2)
      CALL MATINV(N,2*N+1,DETERM,B,D)
      IF (DETERM) 4111,3111,4111
3111      WRITE(6,101) J,TIME
         WRITE(30,101) J,TIME
            DO 1114 J6=1,NJ
1114        WRITE(30,1010) (CC(J5,J6), J5=1,N)
            STOP
4111       DO 5111 K=1,N
           E(K,2*N+1,J)=-D(K,2*N+1)
         DO 5111 L=1,N
           E(K,L,J)=-D(K,L)
5111        E(K,L+N,J)=-D(K,L+N)
      RETURN
11    DO 1001 I=1,N
              D(I,N+1)=-G(I)
      DO 1001 L=1,N
      DO 1001 M=1,N
1001          Y1(I,L)=Y1(I,L)+Y2(I,M)*E(M,L,J-4)
      DO 1002 I=1,N
      DO 1002 L=1,N
            DO 1002 M=1,N
1002          Y(I,L)=Y(I,L)+Y1(I,M)*E(M,L,J-3)+Y2(I,M)*E(M,N+L,J-4)
      DO 1003 I=1,N
      DO 1003 L=1,N
      DO 1003 M=1,N
1003          A(I,L)=A(I,L)+Y(I,M)*E(M,L,J-2)+Y1(I,M)*E(M,N+L,J-3)
      DO 1004 I=1,N
      DO 1004 M=1,N
            IF (J.EQ.NJ) THEN
         D(I,N+1)=D(I,N+1) + A(I,M)*E(M,N+1,J-1)+
     .          Y(I,M)*E(M,2*N+1,J-2) +Y1(I,M)*E(M,2*N+1,J-3)+
     .          Y2(I,M)*E(M,2*N+1,J-4)
            ELSE
         D(I,N+1)=D(I,N+1) + A(I,M)*E(M,2*N+1,J-1)+
     .          Y(I,M)*E(M,2*N+1,J-2) +Y1(I,M)*E(M,2*N+1,J-3)+
     .          Y2(I,M)*E(M,2*N+1,J-4)
            END IF
      DO 1004 L=1,N
            IF (J.EQ.NJ-1)    D(I,L)=D(I,L)+A(I,M)*E(M,N+L,J-1)
         B(I,L)=B(I,L)+A(I,M)*E(M,L,J-1)+Y(I,M)*E(M,L+N,J-2)
1004  CONTINUE
      CALL MATINV(N,N+1,DETERM,B,D)
      IF (DETERM) 410,310,410
```

```
310    WRITE(6,101) J,TIME
       WRITE(30,101) J,TIME
         DO 1115 J6=1,NJ
1115     WRITE(30,1010) (CC(J5,J6), J5=1,N)
         STOP
410  DO 15 K=1,N
     DO 15 M=1,N+1
15     E(K,M,J)=-D(K,M)
     IF (J-NJ) 20,16,16
16   DO 181 K=1,N
       CC(K,J)=E(K,N+1,J)
       CC(K,J-1)=E(K,N+1,J-1)
       CC(K,3)=E(K,3*N+1,3)
       CC(K,2)=E(K,4*N+1,2)
       CC(K,1)=E(K,4*N+1,1)
     DO 181 M=4,NJ-2
       CC(K,M)=E(K,2*N+1,M)
181  CONTINUE
     DO 18 K=1,N
     DO 18 L=1,N
18     CC(K,J-1)=CC(K,J-1)+E(K,L,J-1)*CC(L,J)
     DO 182 JJ=2,NJ-4
       M=NJ-JJ
     DO 182 K=1,N
     DO 182 L=1,N
       CC(K,M)=CC(K,M)+E(K,L,M)*CC(L,M+1)+E(K,L+N,M)*CC(L,M+2)
182    CONTINUE
     DO 185 K=1,N
     DO 185 L=1,N
185    CC(K,3)=CC(K,3)+E(K,L,3)*CC(L,4)+E(K,L+N,3)*CC(L,5)+
    .       E(K,2*N+L,3)*CC(L,6)
     DO 19 JK=1,2
     DO 19 K=1,N
     DO 19 L=1,N
       M=3-JK
19     CC(K,M)=CC(K,M)+E(K,L,M)*CC(L,M+1)+ E(K,L+N,M)*CC(L,M+2)
    .      +E(K,L+2*N,M)*CC(L,M+3)+E(K,L+3*N,M)*CC(L,M+4)
20   RETURN
     END

C
**********************************************************************
**
C  CALLED AT EACH MESH POINT TO SOLVE THE SET OF LINEARIZED
EQUATIONS.
C  THESE ARE DEVELOPED BY NEWMAN. (EXPANDED TO INCLUDE 5-PTS)
```

```
C
**********************************************************************
*

      SUBROUTINE MATINV(N,M,DETERM,B,D)
      IMPLICIT DOUBLE PRECISION(A-H,O-Z)
      DIMENSION ID(24),B(24,24),D(24,160)

*
      DETERM=1.0
      DO 1 I=1,N
    1 ID(I)=0
      DO 18 NN=1,N
      BMAX= 0.0
      DO 6 I=1,N
      IF (ID(I)) 2,2,6
    2 DO 5 J1=1,N
      IF (ID(J1)) 3,3,5
    3 B2=B(I,J1)
      SUBT=DABS(B2)-BMAX
      IF (SUBT) 5,5,4
    4 BMAX=DABS(B2)
      IROW= I
      JCOL= J1
    5 CONTINUE
    6 CONTINUE
      IF (BMAX) 7,7,8
    7 DETERM= 0.0
      RETURN
    8 ID(JCOL)= 1
      IF (JCOL-IROW) 9,12,9
    9 DO 10 J1=1,N
      SAVE= B(IROW,J1)
      B(IROW,J1)= B(JCOL,J1)
   10 B(JCOL,J1)= SAVE
      DO 11 K=1,M
      SAVE= D(IROW,K)
      D(IROW,K)= D(JCOL,K)
   11 D(JCOL,K)= SAVE
   12 F= 1.0/B(JCOL,JCOL)
      DO 13 J1=1,N
   13 B(JCOL,J1)= B(JCOL,J1)*F
      DO 14 K=1,M
   14 D(JCOL,K)= D(JCOL,K)*F
      DO 18 I=1,N
      IF (I-JCOL) 15,18,15
```

```
15  F= B(I,JCOL)
    IF (DABS(F).LE.1.D-100) F=0.0
    DO 16 J1=1,N
16  B(I,J1)= B(I,J1) - F*B(JCOL,J1)
    DO 17 K=1,M
17  D(I,K)= D(I,K) - F*D(JCOL,K)
18  CONTINUE
    RETURN
    END
```

APPENDIX D. LIST OF SYMBOLS

A,	Effective Surface area, cm^2
a,	A diffusion parameter, $a = \pi^2 D/4\delta^2$ (s^{-1})
C,	Concentration, mol/l
D,	Diffusion coefficient of the metal ion, cm^2/sec
E,	Potential, V
F,	Faraday's constant, 96485 coulomb/equiv
I,	Current, A
$(i_{p\text{-}c})_{lim}$, $(i_{d\text{-}c})_{lim}$,	Limiting current density for p-c plating and for d-c plating, A/cm^2
M_{Cu}, M_{Co}	Molecular weight for copper and cobalt, g/mol
$(i_{p\text{-}c})_{lim}$, $(i_{d\text{-}c})_{lim}$,	Limiting current density for p-c plating and for d-c plating, A/cm^2
M_{Cu}, M_{Co}	Molecular weight for copper and cobalt, g/mol
Q,	Electronic charge passed through the cathode, C
x_{Cu},x_{Co}	Weight fractions of Cu and Co in the deposits,
δ,	Steady state diffusion layer thickness, μm
θ_2, θ,	On time and period in one cycle, s
i_{Cu}, i_{Co},	Plaiting current density for copper layer and cobalt layer, A/cm^2
t_{Cu}, t_{Co},	Plating time for copper layer and cobalt layer, s
ρ,	Density of metal species, g/cm^3
ε,	Current efficiency

VITA

Yutong Li was born in 1973 to Yanhua Liu and Jianzhang Li, in Hebei Province, China. He completed his high school education in Shijiazhuang. He was accepted by Hebei University of Science and Technology, China, in to the chemical engineering program and earned a Bachelor of Science degree in 1996. Then he earned his Master of Science degree from the chemical engineering program, Beijing University of Chemical Technology, China, in 1999. Two years later he came to the United States of America to pursue a Doctor of Philosophy degree in the Department of Chemical Engineering at Louisiana State University. He hopes to pursue a career in the emerging fields of microfabrication and nanotechnology.